Two-pion exchange for coupled-channel scattering of two heavy mesons

J. T. Chacko,[1] V. Baru,[2] C. Hanhart,[1] and S. L. Krug[1,3,*]

[1]*Institute for Advanced Simulation, Institut für Kernphysik and Jülich Center for Hadron Physics, Forschungszentrum Jülich, D-52425 Jülich, Germany*

[2]*Institut für Theoretische Physik II, Ruhr-Universität Bochum, D-44780 Bochum, Germany*

[3]*Machine Learning Group, Technische Universität Berlin, 10587 Charlottenburg, Germany*

(Received 8 December 2024; accepted 25 January 2025; published 27 February 2025)

To improve the theoretical understanding of multiquark states like $Z_b(10610)$ and $Z_b(10650)$, we calculate the heavy-meson heavy-(anti)meson scattering potential up to next-to-leading order, $\mathcal{O}(Q^2)$, within chiral effective field theory (χEFT) employing a power counting scheme that explicitly keeps track with the large momentum scale $Q \sim \sqrt{2\mu\delta}$ (where $\delta = m_V - m_P$ is the vector-pseudoscalar mass difference and μ their reduced mass) introduced by the coupled channel dynamics. We provide expressions for the two-pion exchange (TPE) terms up to $\mathcal{O}(Q^2)$ and their partial-wave decomposition. We show that these potentials are well approximated by contact terms at $\mathcal{O}(Q^2)$, with minor residual nonanalytic TPE contributions, supporting χEFT convergence in the theoretical predictions for $Z_b(10610)$ and $Z_b(10650)$, as well as their spin partners. These findings are also relevant for $D^{(*)}D^{(*)}$ scattering, especially for the T_{cc} state, for both physical and lattice quantum chromodynamics (QCD) data with moderately larger pion masses. We further demonstrate that the differences between isovector and isoscalar potentials for heavy mesons are naturally explained by the TPE contributions.

DOI: 10.1103/PhysRevD.111.034042

I. INTRODUCTION

Understanding exotic hadrons within quantum chromodynamics (QCD) holds the promise for deeper insights into the strong force. In addition to the well-established quark model states, that describe mesons as quark-antiquark and baryons as three-quark systems, exotic hadrons encompass a large variety of states, including multiquark configurations, glueballs, hybrids, etc., as documented in a large number of review articles [1–10]. Exotic mesons with heavy quarks, often denoted as XYZ states, challenge the predictions of the conventional quark model, giving rise to intriguing questions about their internal structure. Some of these states are manifestly exotic—notable examples include the charged states of the Z family, namely, $Z_b^{\pm}(10610)$, $Z_b^{\pm}(10650)$ [11], $Z_c^{\pm}(3900)$ [12,13], $Z_c^{\pm}(4020)$ [14], $Z_c^{\pm}(4430)$ [15–18], which decay into final states containing a heavy quarkonium accompanied by a single light hadron.

The states $Z_b(10610)$ and $Z_b(10650)$ discovered by the Belle Collaboration [19], commonly denoted as Z_b and Z_b' for brevity, provide an excellent playground for gaining deeper insights into exotic states. Both have $J^{PC} = 1^{+-}$ [19] and manifest themselves as two narrow peaks, separated by approximately 45 MeV, in the invariant mass distributions of the $\pi^{\pm}\Upsilon(nS)$ ($n = 1, 2, 3$) and $\pi^{\pm}h_b(mP)$ ($m = 1, 2$) subsystems in the dipion transitions from the vector bottomonium $\Upsilon(10860)$ [11] (hereafter referred to as inelastic channels). Moreover, these states have been observed in the $B\bar{B}^*$[1] and $B^*\bar{B}^*$ invariant mass distributions (hereafter referred to as elastic channels) in the decays $\Upsilon(10860) \to \pi B^{(*)}\bar{B}^*$ with dominant branching fractions [20,21]. The proximity of $Z_b(10610)$ and $Z_b(10650)$ to the $B\bar{B}^*$ and $B^*\bar{B}^*$ thresholds, respectively, along with the predominance of the open-flavor branching fractions, strongly support their molecular interpretation [22]. However, despite this observation, the two primary explanations for the Z_b states, consistent with the data, are a tetraquark model and a hadronic molecule picture, see, e.g., Refs. [2–4,7,23] for review articles and references therein.

*Present address: Department of Chemistry and Applied Biosciences, ETH Zurich, 8093 Zurich, Switzerland.

[1]Here, a properly normalized C-odd combination of the $B\bar{B}^*$ and $\bar{B}B^*$ components is understood.

Understanding the nature of near-threshold exotic states hinges on accurately extracting their properties from data, typically found in the pole position and residue of the elastic scattering amplitude or probed using low-energy hadronic parameters like scattering length and effective range. Then, Weinberg's compositeness criterion can be employed to assess their internal structure. This criterion establishes a relationship between the pole position and residue of a state and the molecular component within its complete wave function. Although originally formulated for shallow bound states [24–26], it was recently extended to virtual states and resonances [26–37], provided their constituents are narrow [38]. Since the states of interest are located very close to the production thresholds of particle pairs to which they couple strongly, systematic theoretical analyses, respecting analyticity and unitarity principles, are compulsory. Especially, simplistic Breit-Wigner parameterizations are to be avoided for the parameters extracted in this way are reaction dependent. An effective field theory (EFT) approach serves as a suitable framework for this purpose, offering model independence in the relevant energy range. Furthermore, it enables the formulation of testable predictions for various observables, facilitating the observation of potential molecular candidates and their heavy-quark (HQ) partner states.

Recently, a chiral EFT-based approach was formulated to address experimental data for all measured production and decay channels of the bottomoniumlike states $Z_b(10610)$ and $Z_b(10650)$ [39,40]. The EFT approach is constructed based on an effective Lagrangian that respects both chiral and heavy-quark spin symmetry (HQSS) of QCD. The essential aspects of this approach can be summarized as follows:

(i) The coupled-channel hadron-hadron EFT is formulated using the Weinberg counting [41], initially designed for treating few-nucleon systems. Furthermore, it was demonstrated in [42] that at least in channels where the pion tensor force is operative, a nonperturbative treatment of the one-pion exchange is necessary—for a modern discussion on the subject see Ref. [43]. The potential is built to a specific order in the chiral expansion Q/Λ_χ, with the hard scale of the chiral EFT being represented by $\Lambda_\chi \approx 1$ GeV, and then nonperturbatively resummed through Lippmann-Schwinger type equations.

(ii) Simultaneously with the chiral expansion, the potential undergoes an expansion around the spin symmetry limit. At the leading order, this involves incorporating the mass difference of the spin partners B-B^* along with all interaction vertices constructed in accordance with HQSS. In the loops at next-to-leading order the B-B^* mass difference can be dropped.

(iii) The binding momenta, pion mass, and the momentum scale resulting from the splitting between open-flavor partner thresholds $B\bar{B}^{(*)}$ and $B^*\bar{B}^*$ are considered as soft scales of the system, collectively denoted as Q. The explicit inclusion of the coupled-channel scale extends the energy range, where the theory is applicable. This is crucial for analyzing experimental data around the two elastic thresholds and in between. Note that for energies near the $B^*\bar{B}^*$ threshold, the on-shell relative momentum in the $B\bar{B}^*$ channel can be as large as $p_{\rm typ} = \sqrt{m_B\delta} \simeq 500$ MeV, where $\delta = m_{B^*} - m_B$, with m_{B^*} and m_B being the B^* and B meson mass, respectively. The expansion parameter can be therefore as large as

$$\chi = Q/\Lambda_\chi \sim p_{\rm typ}/\Lambda_\chi \simeq 1/2. \tag{1}$$

Thus the convergence of the chiral expansion needs to be investigated.

(iv) The elastic coupled-channel effective potential V constructed in chiral EFT up to $\mathcal{O}(Q^2)$ reads

$$V_{\rm EFT} = V^{(0)}_{\rm OPE} + V^{(0)}_{\rm cont} + V^{(0)}_{\rm OEE} + V^{(2)}_{\rm cont} + V^{(2)}_{\rm TPE} + \mathcal{O}(\chi^4). \tag{2}$$

The potential at leading order (LO) includes two momentum-independent, $\mathcal{O}(Q^0)$, contact interactions, consistent with HQSS, while its long-ranged component is attributed to the pseudoscalar Goldstone boson exchange represented here by the one-pion (OPE) and the one-η-meson (OEE) exchanges. Note that the Goldstone-boson exchange potential is well defined in the sense of an EFT only in combination with the pertinent contact operators [44]. To tame the strong regulator dependence arising from higher-momentum OPE contributions, especially when multiple open-flavor coupled channels are considered, a formally $\mathcal{O}(Q^2)$ S-wave-to-D-wave counterterm is promoted to leading order, as detailed in [39,40]. At next-to-leading order (NLO), two momentum-dependent $\mathcal{O}(Q^2)$ S-wave-to-S-wave contact terms appear. The intermediate range contributions are represented by the two-pion exchanges (TPE). However, the current calculations [39,40] have, until now, omitted the contribution from TPE. In this work we provide the potentials that are necessary to overcome this shortcoming.

(v) The potential incorporates the contributions of inelastic channels by enabling their coupling to the S-wave open-flavor thresholds. This inclusion results in effective elastic open-flavor potentials with imaginary components driven by unitarity. Meanwhile, the contributions to the real parts of the elastic potentials from inelastic channels can be absorbed through a redefinition of the momentum-independent $\mathcal{O}(Q^0)$ contact interactions [40,45].

(vi) All low-energy constants, including the two elastic couplings, effective couplings to inelastic channels, and the S-S and S-D contact interactions, are determined through a combined fit to all available experimental line shapes.

(vii) The leading contribution to the production operator typically comes from the open-flavor channels, unless notable structures in line shapes, like a dip near the threshold, suggest otherwise. If a dip is present, production might occur through more distant inelastic channels, as discussed in [46], see also [47] for a recent application to the $X(3872)$. Another possibility in this case is the existence of a Castillejo-Dalitz-Dyson (CDD) zero near the threshold, challenging the effective range expansion of the scattering amplitude [30,48,49]. For insights into the impact of triangle singularities on near-threshold line shapes, we refer to the review article [8]. However, none of these structures play a role in production of Z_b states from the decay of $\Upsilon(10860)$.

(viii) To be able to analyse data in the final states involving a quarkonium and two pions, namely the transitions $\Upsilon(10860) \to \pi\pi h_b(mP)$ and $\Upsilon(10860) \to \pi\pi\Upsilon(nS)$ $(n = 1, 2, 3)$, the $\pi\pi$ final state interaction (FSI) in an S-wave including its coupling to the $K\bar{K}$ channel has to be taken into account. This was achieved by employing dispersion theory in Refs. [50,51].

The EFT approach formulated above has been employed to analyze all available data from the decay of $\Upsilon(10860)$. Utilizing data on the decays of $\Upsilon(10860) \to \pi^{\pm} h_b(mP)$ $(m = 1, 2)$ and $\Upsilon(10860) \to \pi B^{(*)}\bar{B}^*$ to fix unknown low-energy constants from the best χ^2 fits, the approach revealed a very good understanding of these line shapes and resulted in the extraction of the pole positions and residues of the Z_b states [39,40]. Based on these results, the line shapes for the HQSS partner states of the Z_b's, namely the positive P- and C-parity states $W_{bJ}^{++}(J = 0, 1, 2)$ were predicted parameter free in the radiative decays $\Upsilon(10860) \to \gamma B^{(*)}\bar{B}^{(*)}$, $\Upsilon(10860) \to \gamma\pi\chi_{bJ}(mP)(m = 1, 2; J = 0, 1, 2)$, and $\Upsilon(10860) \to \gamma\pi\eta_{b0}(nS)(n = 1, 2)$ [40]. Furthermore, a version of the EFT amplitudes corresponding to a contact fit from Refs. [39,40], augmented with the $\pi\pi/K\bar{K}$ FSI, was used to show consistency with the two-dimensional Dalitz plots for the $\Upsilon(10860) \to \pi^+\pi^-\Upsilon(nS)$ $(n = 1, 2, 3)$, revealing the importance of these FSI effects especially for $\Upsilon(1S)$ and $\Upsilon(2S)$ final bottomonium states. On the other hand, $\pi\pi/K\bar{K}$ FSI in the process $\Upsilon(10860) \to \pi^{\pm} h_b(mP)$ $(m = 1, 2)$ was shown to be strongly suppressed by HQSS [51].

The effect of the OPE on the results of Refs. [39,40] can be formulated as follows. First, we stress once again that the OPE potential is well defined in the sense of an EFT only in connection with contact operators, which implies that the true effect of the OPE on observables can only be seen after the potential is renormalized. Second, the effect from the OPE depends on isospin and C-parity [52]. At large distances the OPE contribution to the Z_b's (isovector $B^{(*)}\bar{B}^*$ scattering with $C = -1$) is repulsive, and the OPE cannot go on shell since the decay $B^* \to B\pi$ is not possible at physical pion masses. Without the OPE, the $Z_b(10610)$ and $Z_b(10650)$ were found to be virtual states with respect to the nearby $B\bar{B}^*$ and $B^*\bar{B}^*$ thresholds, respectively [39,40]. However, the nontrivial interplay of the repulsive OPE and attractive contact potentials resulted in shifting poles into the complex plane, rendering them resonance states located just below the corresponding thresholds. The same pattern was also observed for their predicted HQSS partners that in some channels can even move above threshold. This picture is entirely consistent with recent findings for DD^* scattering at unphysically large pion masses in Ref. [53], where it was shown that the inclusion of the repulsive OPE in the analysis of lattice finite-volume spectra from Ref. [54] shifts the T_{cc} pole to the complex plane (see also Refs. [55,56] for related studies). As a result, the repulsion generated by the OPE has a pronounced effect on the T_{cc} pole trajectory as a function of the pion mass, by pushing it into the complex energy plane for $m_\pi \geq 230$ MeV [57].

In this work, we provide the contributions to the $B^{(*)}\bar{B}^{(*)}$ potential that are so far missing in the analysis to NLO. Those comprise two-pion exchange contributions to one loop. The inclusion of these contributions is necessary to test the convergence of the chiral EFT formalism (which is especially important given the rather large expansion parameter $\chi \sim 1/2$), provide a systematic uncertainty estimate of the theoretical results, and finally extract the pole positions reliably. It is worth noting that we are aiming at the calculation of the TPE terms in the so-called momentum counting scheme (MCS), which treats the momentum between $B\bar{B}^{(*)}$ and $B^*\bar{B}^*$ as a leading soft scale—see Eq. (1). As will become clear below, the MCS selects a specific subclass of the one-loop contributions, which are enhanced due to the presence of the large momentum scale p. This kind of power counting was introduced originally to provide a convergent EFT for pion production in nucleon-nucleon collisions near the threshold, where the large momentum scale, $p \simeq \sqrt{m_\pi M_N}$ with $m_\pi(M_N)$ being the pion(nucleon) mass, was introduced through the large momentum (relative to the pion mass) necessary in the initial state. This approach indeed led to a successful understanding of the nontrivial pion production mechanisms in $NN \to NN\pi$, which was not achievable within the original Weinberg's counting where momenta and the pion mass where treated at the same order—see Refs. [58,59] for reviews. The TPE contributions for pion production in two nucleon collisions were calculated in this power counting in Refs. [60–62].

It should be stressed that the rate of convergence of the chiral expansion is a crucial diagnostic tool to understand the nature of the multiquark states under investigation here: a compact state driving the experimental signals would call for a pole term in the scattering potential. Its presence should then lead to a bad convergence of the series of local

contact terms included in the EFT. After all, in a low-energy EFT organized according to an expansion in powers of the soft momenta, the presence of a compact state can only influence the rate of convergence of the expansion, or in other words, the power counting. However, it cannot modify the individual contributions as such, since those are built solely on the symmetries of the underlying theory. While the data existing up to date for the Z_b states can be well described with higher-order contact terms naturally suppressed in accordance with the power counting (up to the need to promote the S-D counterterm called for by renormalizability of the OPE in the presence of several coupled hadronic channels), data with improved statistics expected from the Belle II experiment will call for a refined theoretical effort.

As the results for TPE diagrams derived here up to order $\mathcal{O}(Q^2)$ do not depend on the heavy-meson mass, they can also be applied to other heavy-meson heavy- (anti)meson systems, such as $D^{(*)}D^* - D^{(*)}D^*$ scattering, particularly in the context of the T_{cc} and its possible partner states. It should be noted that for the physical pion mass, the three-body cuts in the TPE diagrams will provide some contributions to the T_{cc} width, which need to be included if one aims at the high-accuracy calculation of this quantity. On the other hand, the effect of the cuts on the real part of the TPE diagrams should be very small, and the TPE contributions can be still largely absorbed by the contact operators. This conclusion should also hold for not too large unphysical pion masses, $m_\pi^{\rm ph} < m_\pi < p_{\rm typ}$, in the context of lattice QCD data analyses.

The TPE contributions to heavy-mesonheavy-(anti)meson scattering have already been addressed in the literature. For instance, phenomenological calculations in Refs. [63,64] considered a particular subclass of TPE operators. Additionally, Refs. [65,66] (see also [67,68]) provide investigations within the framework of EFT. These TPE operators, however, were derived ignoring all coupled-channel transitions based on the original Weinberg's counting and no attempt was made to check for the renormalization of those to the given order. In this work we overcome those short comings. Moreover, we will provide a comparison of our results with the earlier EFT works.

The paper is organized as follows. In Sec. II, the Lagrangian and the vertices for our approach are provided. The power counting scheme is discussed in detail in Sec. III. In Sec. IV, the effective potential of one representative channel is presented at $\mathcal{O}(\chi^0)$ and $\mathcal{O}(\chi^2)$. Appendix C contains the effective potentials of all the channels. Section V provides the partial wave decomposed potentials with Appendix B containing a complete set of the relevant projection operators. Section VI summarizes the various checks conducted on our PWD potentials and Sec. VIII gives the comparison our potentials to those of previous works. Section IX gives a summary and outlook of this paper. Additionally, Appendix A provides details about the evaluation of the pertinent loop integrals of the TPE potentials.

II. LAGRANGIAN AND VERTICES

The effective Lagrangian describing $B^{(*)}\,\bar{B}^{(*)}$ scattering at low energies reads [39,40,69,70]

$$
\begin{aligned}
\mathcal{L} = {} & \mathrm{Tr}[H_a^\dagger (iD_0)_{ba} H_b] + \frac{\delta}{4}\mathrm{Tr}[H_a^\dagger \sigma^i H_a \sigma^i] + \mathrm{Tr}[\bar{H}_a^\dagger (iD_0)_{ab} \bar{H}_b] + \frac{\delta}{4}\mathrm{Tr}[\bar{H}_a^\dagger \sigma^i \bar{H}_b \sigma^i] - \frac{g_Q}{2}\mathrm{Tr}[\boldsymbol{\sigma}\cdot\mathbf{u}_{ab} H_a^\dagger H_b] \\
& + \frac{g_Q}{2}\mathrm{Tr}[\bar{H}_a \bar{H}_b^\dagger \boldsymbol{\sigma}\cdot\mathbf{u}_{ab}] - \frac{C_{10}}{8}\mathrm{Tr}[\bar{H}_a^\dagger \tau^A_{aa'} H^\dagger_{a'} H_b \tau^A_{bb'} \bar{H}_{b'}] - \frac{C_{11}}{8}\mathrm{Tr}[\bar{H}_a^\dagger \tau^A_{aa'} \sigma^i H^\dagger_{a'} H_b \tau^A_{bb'} \sigma^i \bar{H}_{b'}] \\
& - \frac{D_{10}}{8}\{\mathrm{Tr}[\nabla^i \bar{H}_a^\dagger \tau^A_{aa'} \nabla^i H^\dagger_{a'} H_b \tau^A_{bb'} \bar{H}_{b'}] + \mathrm{Tr}[\bar{H}_a^\dagger \tau^A_{aa'} H^\dagger_{a'} \nabla^i H_b \tau^A_{bb'} \nabla^i \bar{H}_{b'}]\} \\
& - \frac{D_{11}}{8}\{\mathrm{Tr}[\nabla^i \bar{H}_a^\dagger \tau^A_{aa'} \sigma^j \nabla^i H^\dagger_{a'} H_b \tau^A_{bb'} \sigma^j \bar{H}_{b'}] + \mathrm{Tr}[\bar{H}_a^\dagger \tau^A_{aa'} \sigma^j H^\dagger_{a'} \nabla^i H_b \tau^A_{bb'} \sigma^j \nabla^i \bar{H}_{b'}]\} \\
& - \frac{D_{12}}{8}\left\{\mathrm{Tr}\left[\left(\nabla^i \bar{H}_a^\dagger \tau^A_{aa'} \sigma^i \nabla^j H^\dagger_{a'} + \nabla^j \bar{H}_a^\dagger \tau^A_{aa'} \sigma^i \nabla^i H^\dagger_{a'} - \frac{2}{3}\delta^{ij}\nabla^k \bar{H}_a^\dagger \tau^A_{aa'} \sigma^i \nabla^k H^\dagger_{a'}\right) H_b \tau^A_{bb'} \sigma^j \bar{H}_{b'}\right]\right. \\
& \left. + \mathrm{Tr}\left[\bar{H}_a^\dagger \tau^A_{aa'} \sigma^i H^\dagger_{a'}\left(\nabla^i H_b \tau^A_{bb'} \sigma^j \nabla^j \bar{H}_{b'} + \nabla^j H_b \tau^A_{bb'} \sigma^j \nabla^i \bar{H}_{b'} - \frac{2}{3}\delta^{ij}\nabla^k H_b \tau^A_{bb'} \sigma^j \nabla^k \bar{H}_{b'}\right)\right]\right\} + \ldots,
\end{aligned}
\tag{3}
$$

1where a and b are isospin indices, σ's and τ's are the spin and isospin Pauli matrices, respectively. The isospin matrices are normalized as $\tau^A_{ab}\tau^B_{ba} = 2\delta^{AB}$ and the trace (Tr) is taken over spin space. The contact terms C_{1i} $(i = 0, 1)$ and D_{1i} $(i = 0, 1, 2)$ represent short-range interactions, while the ellipsis in Eq. (3) denotes similar terms C_{0i} and D_{0i} which are not shown explicitly and appear without the τ matrices. The terms proportional to $\delta = m_{B^*} - m_B \approx 45$ MeV are the leading terms that violate spin symmetry. To the order we are working (NLO in the chiral expansion and in the heavy quark expansion) they do not contribute to the loops in the potentials but only to the two-body propagators in the LS-equation.

The H_a and $\bar{H}_a$ are super-fields which contain the $B^{(*)}$ and $\bar{B}^{(*)}$ fields, respectively, with $H_a = B_a + B_a^{*i}\sigma^i$ and $\bar{H}_a = (\bar{B}\tau_2)_a - (\bar{B}^{*i}\tau_2)_a\sigma^i$, where $B_a(\bar{B}_a)$ and $B_a^{*i}(\bar{B}_a^{*i})$ are the pseudoscalar and vector B mesons (antimesons), respectively. The τ_2, acting as the charge conjugation matrix in isospin space, appears in the expressions for the anti-B-mesons, since they contain light antiquarks. H_1 contains B^0 and $(B^0)^*$ and H_2 contains B^+ and $(B^+)^*$, while $\bar{H}_1$ and $\bar{H}_2$ contain the respective antiparticles [70]. The zeroth component of the chiral covariant derivative is given by $D_0 = \partial_0 + \Gamma_0$ with

$$\Gamma_0 = \frac{i}{4f_\pi^2}(\boldsymbol{\pi} \times \partial_0\boldsymbol{\pi}) \cdot \boldsymbol{\tau} + \mathcal{O}(\boldsymbol{\pi}^4), \tag{4}$$

where $f_\pi = 92.4$ MeV denotes the pion decay constant. The spatial components of the axial current read

$$\mathbf{u} = -\boldsymbol{\nabla}(\boldsymbol{\tau} \cdot \boldsymbol{\pi})/f_\pi + \mathcal{O}(\boldsymbol{\pi}^3). \tag{5}$$

In both cases $\boldsymbol{\tau}$ and $\boldsymbol{\pi}$ are 3-dimensional vectors made of the Pauli matrices and the pions fields, respectively. Employing heavy quark spin symmetry, the pion-heavy meson coupling constant is fixed to

$$g_Q \approx g_b \approx g_c \approx g = 0.57,$$

extracted from the partial decay width $D^* \to D\pi$ provided in Ref. [71] (this value agrees within 10% with that extracted in lattice QCD for static sources [72]). The terms proportional to the low-energy constants (LECs) C_{10} and C_{11} correspond to the $\mathcal{O}(p^0)$ S-wave contact interactions, whereas the terms proportional to D_{10} and D_{11} correspond to $\mathcal{O}(p^2)$ S-wave contact interactions. The term D_{12} gives rise to S-D transitions—this is the counterterm formally appearing at NLO, however, promoted to LO as detailed above. As we are only interested in S-S and S-D transitions, terms proportional to $\nabla^i H^\dagger \nabla^j H$, leading to P-wave interactions, are ignored [39].

From the Lagrangian provided in Eq. (3) we now derive the vertex structures relevant for this work. The B-meson–pion interactions are

$$\mathcal{L}_{B^{(*)}B^{(*)}\pi} = \frac{g}{2f_\pi}\partial_i\boldsymbol{\pi}[B^\dagger\boldsymbol{\tau}B_i + B_i^\dagger\boldsymbol{\tau}B + i\epsilon_{jki}B_j^\dagger\boldsymbol{\tau}B_k], \tag{6}$$

where the indices i, j, k refer to the spacial index of the derivative or the B^* polarization vectors—summation over those is assumed. The factor of $(1/2)$ comes from the normalization of the heavy-meson field as shown in Appendix A of Ref. [73]. If we define $\boldsymbol{k}$, the momentum of the pion, as outgoing, we can replace the spacial derivative in Eq. (6) by $-i\boldsymbol{k}$ and get for the various vertices

$$\begin{aligned}
v_{B\to B\pi_a} &= 0,\\
v_{B^*\to B\pi_a} &= \frac{g}{2f_\pi}(\boldsymbol{\epsilon}\cdot\boldsymbol{k})\tau_a,\\
v_{B\to B^*\pi_a} &= \frac{g}{2f_\pi}(\boldsymbol{\epsilon}^*\cdot\boldsymbol{k})\tau_a,\\
v_{B^*\to B^*\pi_a} &= -i\frac{g}{2f_\pi}\tau_a(\boldsymbol{\epsilon}\times\boldsymbol{\epsilon}^*)\boldsymbol{k}.
\end{aligned}$$

In all expressions a denotes the isospin index of the pion. The corresponding vertices for the antimesons are near identical to the meson case with the exception that the charge-conjugated Pauli matrix, related to the antifundamental representation of the isospin group, is to be used which reads $\boldsymbol{\tau}^c = \tau_2\boldsymbol{\tau}^T\tau_2 = -\boldsymbol{\tau}$ [40].

The leading two-pion $B^{(*)}B^{(*)}$ couplings arise from the chiral covariant derivative acting on the heavy fields, namely the Weinberg-Tomozawa (WT) vertex. In particular we have

$$\mathcal{L}_{B^{(*)}B^{(*)}\pi\pi} = -\frac{1}{4f_\pi^2}\epsilon_{abc}\pi_a\partial_0\pi_b[B^\dagger\tau_c B + B^{*j\dagger}\tau_c B^{*j}]. \tag{7}$$

From this the pertinent vertices are

$$\begin{aligned}
v_{B\pi_a\to B\pi_b} &= \frac{1}{4f_\pi^2}\epsilon_{abc}\tau_c(k_0' + k_0),\\
v_{B^*\pi_a\to B^*\pi_b} &= \frac{1}{4f_\pi^2}\epsilon_{abc}\tau_c(\boldsymbol{\epsilon}\cdot\boldsymbol{\epsilon}^*)(k_0' + k_0),
\end{aligned}$$

where k_0 (k_0') denotes the zeroth component of the incoming (outgoing) pion four-momentum. Again, to switch to the corresponding vertices for the anti-B-mesons the τ matrices need to be replaced by their charge conjugate counterparts.

III. POWER COUNTING

The power counting of the pion loops for the $B^{(*)}\bar{B}^{(*)}$ potentials (and also the $B^{(*)}B^{(*)}$ potentials that we calculate as a byproduct) is dependent on the three dynamical scales of the system namely, the pion mass, m_π, the momentum scale $p_{\text{typ}} = \sqrt{m_B\delta} \simeq 500$ MeV and the difference of m_B and m_{B^*}, $\delta \approx 45$ MeV. The hard scale is the chiral symmetry breaking scale Λ_χ, but it may also include the heavy meson mass m_B. Since the binding energies of the Z_b states are generated dynamically through the solution of the LS equation, they do not need to be considered in the power counting for the potentials. As we aim to fit the available experimental data in the energy range that covers both Z_b states, we need an effective field theory that allows us to cover the energy range from the $B\bar{B}$ threshold up to the $B^*\bar{B}^*$ threshold, which spans 90 MeV. We therefore need to treat p_{typ} dynamically as a soft scale. It is therefore important to keep track of momentum scales, which dictate the pertinent contributions in the loops. Thus, the expansion parameters are

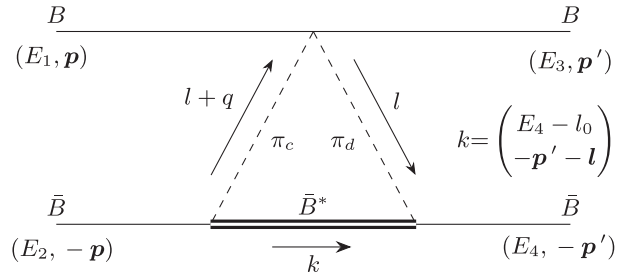

FIG. 1. Typical one loop diagram that appears at NLO in the momentum expansion as well as the standard power counting.

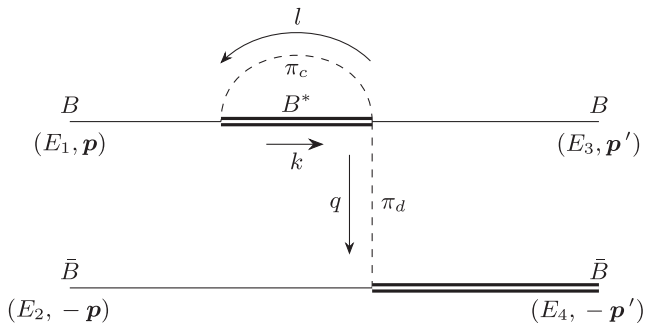

FIG. 2. Typical one loop diagram that appears at NNLO in the momentum expansion, but at NLO in the standard counting.

$$\chi_1 = \frac{p_{\rm typ}}{\Lambda_\chi}, \quad \chi_2 = \frac{m_\pi}{\Lambda_\chi}, \quad \chi_3 = \frac{p_{\rm typ}}{m_B}, \quad \chi_4 = \frac{\delta}{\Lambda_\chi}, \tag{8}$$

which numerically take values of about $1/2$, $1/7$, $1/10$, and $1/20$ in order. It should be noted, however, that in the charm system the mass splitting between the pseudoscalar and vector ground state mesons is of the order of the pion mass, making χ_2 and χ_4 similar. Because of this and to keep the scheme simple, one may combine the given parameters into a one-parameter expansion,

$$\chi \sim \chi_1, \qquad \chi^2 \sim \chi_1^2 \sim \chi_2 \sim \chi_3 \sim \chi_4. \tag{9}$$

In what follows we are only interested in the leading loop contributions. In particular we will use that $m_\pi/p_{\rm typ} \sim \mathcal{O}(\chi)$.

The implications of this power counting scheme for the order assignment of one-loop diagrams is now illustrated on two examples, namely one specific TPE contribution to the $B\bar{B} \to B\bar{B}$ potential seen in Fig. 1, and a one-loop vertex correction shown in Fig. 2. Since we are focusing on the leading loop corrections, in all cases the vertices are taken in leading order only.

The effective potential for the triangle diagram is written as,

$$\begin{aligned} iV_T = \sum_\lambda \int \frac{d^4l}{(2\pi)^4} \frac{1}{4f_\pi^2} ((2l_0 + q_0)\epsilon_{cdh}(\tau_1)_h) \frac{i}{(E_4 - l_0 - m_{B^*} - (\boldsymbol{p}' + \boldsymbol{l})^2/(2m_{B^*}))} \\ \times \left(\frac{g}{2f_\pi}(\epsilon_j(\lambda)(-l)_j)(\tau_2^c)_d\right) \frac{i}{(l+q)^2 - m_\pi^2} \left(\frac{g}{2f_\pi}(\epsilon_i^*(\lambda)(l+q)_i)(\tau_2^c)_c\right) \frac{i}{l^2 - m_\pi^2} \end{aligned} \tag{10}$$

where

$$q = (E_3, \boldsymbol{p}') - (E_1, \boldsymbol{p}) = (0, \boldsymbol{q}) + \mathcal{O}(\chi), \tag{11}$$

with $\boldsymbol{p}$ and $\boldsymbol{p}'$ as initial and final relative momenta of the heavy mesons, respectively, and E_1 (E_2) and E_3 (E_4) for the energies of the meson (antimeson) in the initial and final states, respectively. For this discussion we assume that the external states are on their mass shell and the total energy is at the $B^*\bar{B}^*$ threshold. Then $q \sim p_{\rm typ}$. Using

$$\epsilon_{cdh}(\tau_1)_h(\tau_2)_d(\tau_2)_c = -2i(\boldsymbol{\tau_1} \cdot \boldsymbol{\tau_2}), \tag{12}$$

and

$$\sum_\lambda \epsilon_i^*(\lambda)\epsilon_j(\lambda) = \delta_{ij} \tag{13}$$

we get,

$$V_T = \frac{g^2}{4f_\pi^4}(\boldsymbol{\tau_1} \cdot \boldsymbol{\tau_2}) I_{\rm tr} \tag{14}$$

where the pertinent integral is given by,

$$\begin{aligned} I_{\rm tr} = \frac{i}{2} \int \frac{d^4l}{(2\pi)^4} \left(\frac{2l_0 + q_0}{l_0 + \delta + (2\boldsymbol{p}'\boldsymbol{l} + \boldsymbol{l}^2)/(2m_{B^*})}\right) \\ \times \frac{(\boldsymbol{l} + \boldsymbol{q}) \cdot \boldsymbol{l}}{[(l+q)^2 - m_\pi^2 + i\epsilon][l^2 - m_\pi^2 + i\epsilon]} \end{aligned} \tag{15}$$

One observes that the pion propagators drive $l_0 \sim l \sim p_{\rm typ}$ [58,59]. Indeed, keeping the leading terms in the pion propagator, one finds

$$(l+q)^2 - m_\pi^2 + i\epsilon = l_0^2 - (\boldsymbol{l} + \boldsymbol{q})^2 + i\epsilon + \mathcal{O}(\chi^3), \tag{16}$$

which yields $l_0 \sim q \sim p_{\rm typ}$ as well as $|\boldsymbol{l}| \sim p_{\rm typ}$. Then, one observes that l_0 is the dominant term in the expression within the parentheses in the first line of Eq. (15). Because of this, we can drop all terms except l_0, since all other terms appear to be suppressed relative to l_0 either as

$\delta/p_{\rm typ} \sim \mathcal{O}(\chi)$ or $p_{\rm typ}/m_B$ which is counted as $\mathcal{O}(\chi^2)$ according to Eq. (9). Thus the integral to evaluate is

$$I_{\rm tr} = i\int \frac{d^4l}{(2\pi)^4}\frac{(\boldsymbol{l}+\boldsymbol{q})\cdot\boldsymbol{l}}{[(l+q)^2-m_\pi^2+i\epsilon][l^2-m_\pi^2+i\epsilon]}, \quad (17)$$

with the dominant contribution coming from $l \sim q \sim p_{\rm typ}$. As long as multiple scales enter the expansion, any given loop contributes at various orders simultaneously [58,59]. The lowest order at which the pion loops start to contribute to $B^{(*)}\bar{B}^{(*)}$ and $B^{(*)}B^{(*)}$ scattering is $\mathcal{O}(\chi^2)$. To derive results at $\mathcal{O}(\chi^2)$, all scales except for $q \sim p_{\rm typ}$ can be initially omitted in the loop expressions. But the same loops also contain contributions additionally suppressed by $(m_\pi^2/p_{\rm typ}^2)$, thus contributing at $\mathcal{O}(\chi^4)$. To illustrate this point, we use dimensional regularization to find for the integral in Eq. (17) the following expression

$$\begin{aligned} I_{\rm tr} &= -\frac{1}{16\pi^2}\left\{\left(\frac{5}{12}\boldsymbol{q}^2+\frac{3}{2}m_\pi^2\right)\mathcal{R} - \frac{13}{36}\boldsymbol{q}^2 - \frac{m_\pi^2}{3} \right. \\ &\quad \left. + \left(\frac{5}{6}\boldsymbol{q}^2+3m_\pi^2\right)\ln\left(\frac{m_\pi}{\mu}\right) + \left(\frac{5}{6}\boldsymbol{q}^2+\frac{4}{3}m_\pi^2\right)L(q)\right\} \\ &= -\frac{5\boldsymbol{q}^2}{96\pi^2}\left\{\frac{\mathcal{R}}{2} - \frac{13}{30} + \ln\left(\frac{m_\pi}{\mu}\right) + L(q)\right\} + \mathcal{O}(\chi^4), \end{aligned} \quad (18)$$

where μ is the renormalization scale in dimensional regularization,

$$\begin{aligned} L(q) &= \frac{\sqrt{4m_\pi^2+q^2}}{q}\ln\left(\frac{\sqrt{4m_\pi^2+q^2}+q}{2m_\pi}\right) \\ &= \ln\left(\frac{q}{m_\pi}\right) + \mathcal{O}(\chi). \end{aligned} \quad (19)$$

and

$$\mathcal{R} = -\frac{2}{\xi} + \gamma_E - 1 - \ln(4\pi) \quad (20)$$

with $\xi = 4 - D$ and $\gamma_E \approx 0.57$ denoting the Euler-Mascheroni constant. Thus, the dominant loop contribution, as evaluated in the last lines of Eqs. (18) and (19), corresponds to $\mathcal{O}(\chi^2)$, while in general, the loops [see the first lines in Eqs. (18) and (19)] also give rise to higher-order terms. Since the leading order potential for scattering of two heavy particles appears at $\mathcal{O}(\chi^0)$ and, as in the two-nucleon system, there are no contributions at $\mathcal{O}(\chi)$, the loops at $\mathcal{O}(\chi^2)$ are, by convention, associated with the next nonvanishing order, referred to as NLO.

For the vertex correction (seen in Fig. 2) the integration variable can always be chosen such that the pion propagator in the loop does not contain any external variable. Therefore, contrary to Eq. (16), the momentum $q \sim p_{\rm typ}$ does not enter the pion propagator in the loop. Hence, the energy scale l_0 in this case is given by either δ or m_π, since both are being counted at the same order. At the same time the momentum scale is also given by m_π. Combining all factors, we conclude that the vertex corrections are suppressed as compared to the TPE discussed above by a factor of $(m_\pi/p_{\rm typ})^2 = \chi^2$. Due to this observation, all the vertex correction terms can be ignored in this study, since they start to contribute only at order N^{3}LO.

IV. EFFECTIVE POTENTIALS

In this section the effective potentials of $B^{(*)}\bar{B}^{(*)} \to B^{(*)}\bar{B}^{(*)}$ and $B^{(*)}B^{(*)} \to B^{(*)}B^{(*)}$ are discussed—further details are provided in the appendices.

A. Leading-order diagrams for $B^{(*)}\bar{B}^{(*)} \to B^{(*)}\bar{B}^{(*)}$

1. LO contact terms

The relevant contact term (CTs) diagrams at leading order $[\mathcal{O}(\chi^0)]$ are shown in the left column of Fig. 3. The CTs contain the momentum independent terms proportional to the LECs C's from the Lagrangian in Eq. (3) as well as the S-D transition term, D_{12}, promoted to leading order as described in the introduction.

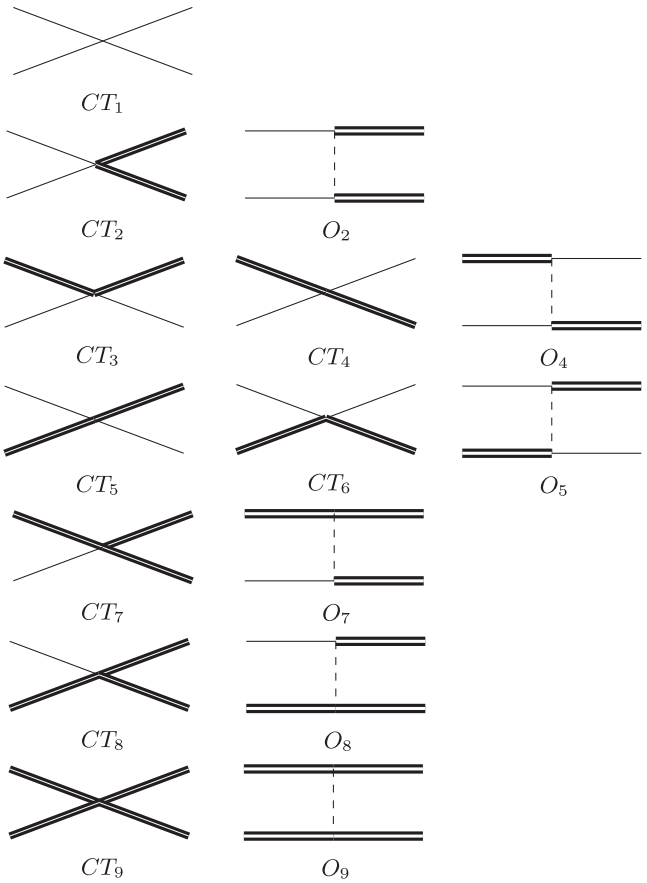

FIG. 3. LO contributions to the $B^{(*)}\bar{B}^{(*)} \to B^{(*)}\bar{B}^{(*)}$ scattering potential. Here single (double) solid lines denote B (B^*) mesons and dashed lines represent pions.

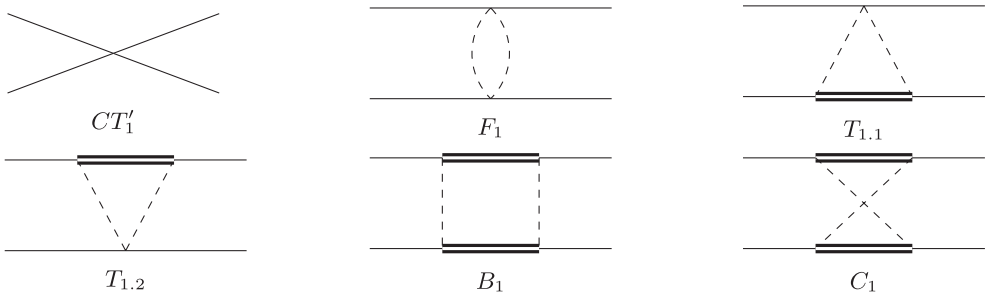

FIG. 4. NLO diagrams for $B\bar{B} \to B\bar{B}$.

2. LO one-pion exchange

The vertices for the one-pion exchange were derived in Sec. II with q as the pion momentum. Since the kinetic energies of the heavy mesons are suppressed by $p_{\text{typ}}/m_B \sim \mathcal{O}(\chi^2)$ relative to the momenta, we can safely set them to zero here. At the same time, using that $\delta/p_{\text{typ}} \sim \mathcal{O}(\chi)$ from Eq. (9), this implies that the energy transfer, $q^0 = E_p - E_{p'}$, can be dropped completely. Taking all this together, we get for the $B^*\bar{B} \to B\bar{B}^*$ potential

$$V_{O_4} = -\frac{g^2}{4f_\pi^2}(\boldsymbol{\tau_1}\cdot\boldsymbol{\tau_2^c})(\epsilon^*_{2',n}\epsilon_{1,i})\frac{q_i q_n}{\boldsymbol{q}^2+m_\pi^2}, \tag{21}$$

where the external polarization vectors for incoming and outgoing B^* meson ($\bar{B}^*$) are denoted as $\epsilon_{1,i}$ and $\epsilon^*_{1',k}$ ($\epsilon_{2,l}$ and $\epsilon^*_{2',n}$), respectively.

The isospin factor for heavy-meson heavy-antimeson scattering reads

$$\boldsymbol{\tau_1}\cdot\boldsymbol{\tau_2^c} = -\boldsymbol{\tau_1}\cdot\boldsymbol{\tau_2} = 3 - 2I(I+1), \tag{22}$$

which evaluates to 3 for isoscalar and -1 for isotriplet states.

B. Next-to-leading order diagrams

At next-to-leading-order, $\mathcal{O}(\chi^2)$, there are momentum-dependent contact interactions and the TPE diagrams. There are three types of TPE diagrams: triangle-diagrams, football-diagrams, and box-diagrams. In the main part of the paper we discuss general properties of these diagrams while the complete expressions are provided in the Appendix C.

1. Contact interactions at NLO

The relevant CTs at NLO, $\mathcal{O}(\chi^2)$, are the two momentum-dependent terms proportional to D_{10} and D_{11}, as seen in the Lagrangian in Eq. (3). The chiral expansion formally also generates momentum independent subleading contact terms proportional to m_π^2, which in the standard power counting would appear at the same order. In the momentum counting scheme imposed here, however, those are suppressed by $(m_\pi/p_{\text{typ}})^2 \sim \chi^2$ and thus start to contribute only at $\mathcal{O}(\chi^4)$. In addition, for a fixed pion mass, the m_π^2-dependent CT's only lead to a redefinition of the LO CT's.

2. Triangle and football diagrams

For the $B^{(*)}\bar{B}^{(*)}$ case, the sum of all triangle diagrams vanishes. In this section we demonstrate this explicitly for the $B\bar{B} \to B\bar{B}$ channel, however, the same pattern applies to all the other potentials analogously. For the $B\bar{B} \to B\bar{B}$ potential, as shown in Fig. 4, we have two triangle diagrams denoted as $T_{1.1}$ and $T_{1.2}$. The potential from the first diagram is (The labels on the potentials given below refer to those in the related figures),

$$\begin{aligned} iV_{T_{1.1}} = \sum_\lambda \int \frac{d^4l}{(2\pi)^4}\frac{1}{4f_\pi^2}(2l_0\epsilon_{cdh}(\tau_1)_h)\frac{i}{l^2-m_\pi^2}\frac{i}{(-l_0+i\epsilon)} \\ \times\left(\frac{g}{2f_\pi}(\epsilon_j(\lambda)(-l)_j)(\tau_2^c)_d\right)\left(\frac{g}{2f_\pi}(\epsilon_i^*(\lambda)(l+q)_i)(\tau_2^c)_c\right)\frac{i}{(l+q)^2-m_\pi^2}, \end{aligned} \tag{23}$$

The potential can thus be written as

$$V_{T_{1.1}} = \frac{g^2}{4f_\pi^4}(\boldsymbol{\tau_1}\cdot\boldsymbol{\tau_2})I_{\text{tr}}, \tag{24}$$

where we used $\sum_\lambda \epsilon_i^*(\lambda)\epsilon_j(\lambda) = \delta_{ij}$. The analytic expression for the integral I_{tr} is provided in Eq. (18). The second diagram simplifies to

$$V_{T_{1,2}} = -\frac{g^2}{4f_\pi^4}(\boldsymbol{\tau_1}\cdot\boldsymbol{\tau_2})I_{\rm tr}, \tag{25}$$

where the change in sign resulted from the appearance of the charge conjugate isospin matrix at the lower, $\pi\bar{B}\to\pi\bar{B}$ vertex. The total contribution therefore cancels. If, instead, we calculated the BB potential, $V_{T_{1,2}}$ would appear with a positive sign, and the two triangle contributions would be summed.

The potential for the football diagram reads

$$V_{F_1} = \frac{1}{2f_\pi^4}(\boldsymbol{\tau_1}\cdot\boldsymbol{\tau_2})I_{\rm fb} \tag{26}$$

where $I_{\rm fb}$ is given by,

$$I_{\rm fb} = i\int\frac{d^4l}{(2\pi)^4}\frac{(l^0)^2}{[(l+q)^2-m_\pi^2+i\epsilon][l^2-m_\pi^2+i\epsilon]}. \tag{27}$$

The evaluation of this integral is provided in the Appendix A 2. A closed form expression for this integral at the order χ^2 reads

$$I_{\rm fb} = \frac{\boldsymbol{q}^2}{96\pi^2}\left\{\frac{\mathcal{R}}{2}-\frac{5}{6}+\ln\left(\frac{m_\pi}{\mu}\right)+L(q)\right\}+\mathcal{O}(\chi^4). \tag{28}$$

3. Box diagrams

The box diagrams are made from four pion–heavy-meson vertices contracted with two pion propagators. These form either a planar box or a crossed box. To avoid double counting, only the irreducible two-heavy meson part of the planar box is kept in the potential, as the reducible parts are generated through iterations in the Lippmann-Schwinger equation. Again, for illustration, the $B\bar{B}\to B\bar{B}$ case is discussed explicitly. For the planar box B_1 in Fig. 4 one finds

$$\begin{aligned} iV_{B_1} = \sum_{\lambda_1,\lambda_2}\int\frac{d^4l}{(2\pi)^4}&\left[\frac{g}{2f_\pi}(\epsilon_i(\lambda_1)(-q_2)_i)(\tau_1)_d\right]\frac{i}{-l_0+i\epsilon}\left[\frac{g}{2f_\pi}(\epsilon_j^*(\lambda_1)(q_1)_j)(\tau_1)_c\right]\frac{i}{q_1^2-m_\pi^2}\\ &\times\left[\frac{g}{2f_\pi}(\epsilon_n(\lambda_2)(q_2)_n)(\tau_2^c)_d\right]\frac{i}{q_2^2-m_\pi^2}\left[\frac{g}{2f_\pi}(\epsilon_m^*(\lambda_2)(-q_1)_m)(\tau_2^c)_c\right]\frac{i}{l_0+i\epsilon}. \end{aligned} \tag{29}$$

Here, q_1 and q_2 are the momenta of the two pions and, to the order we are working, one finds $q_1=(l_0,\boldsymbol{p}-\boldsymbol{l})$, $q_2=(l_0,\boldsymbol{p}'-\boldsymbol{l})$, and $q=(0,\boldsymbol{p}'-\boldsymbol{p})=(0,\boldsymbol{q})$, where l is the loop momentum. This can be written as

$$V_{B_1} = \frac{g^4}{16f_\pi^4}(3-2(\boldsymbol{\tau_1}\cdot\boldsymbol{\tau_2}))I_{\rm box}^{(1)} \tag{30}$$

where we used $(\tau_1)_d(\tau_1)_c(\tau_2)_d(\tau_2)_c = (3-2(\boldsymbol{\tau_1}\cdot\boldsymbol{\tau_2}))$ and

$$I_{\rm box}^{(1)} = i\int\frac{d^4l}{(2\pi)^4}\frac{(\boldsymbol{q_2}\cdot\boldsymbol{q_1})^2}{[l^0+i\epsilon][l^0-i\epsilon][q_2^2-m_\pi^2][q_1^2-m_\pi^2]}. \tag{31}$$

For the crossed box (C_1 in Fig. 4) the simplified expression reads

$$V_{C_1} = \frac{g^4}{16f_\pi^4}(-3-2(\boldsymbol{\tau_1}\cdot\boldsymbol{\tau_2}))I_{\rm box}^{(2)} \tag{32}$$

where, we used $(\tau_1)_d(\tau_1)_c(\tau_2)_c(\tau_2)_d = 3+2(\boldsymbol{\tau_1}\cdot\boldsymbol{\tau_2})$, and $I_{\rm box}^{(2)}$ is given by,

$$I_{\rm box}^{(2)} = i\int\frac{d^4l}{(2\pi)^4}\frac{(\boldsymbol{q_2}\cdot\boldsymbol{q_1})^2}{[l_0-i\epsilon]^2[q_2^2-m_\pi^2][q_1^2-m_\pi^2]}. \tag{33}$$

The only difference between $I_{\rm box}^{(1)}$ and $I_{\rm box}^{(2)}$ is the sign in the $i\epsilon$ term in one of the heavy meson propagators. Just because of this sign change the former integral contains a reducible contribution, while the latter does not. In Ref. [74] and Appendix A 4 it is shown that the irreducible contribution of the integral $I_{\rm box}^{(1)}$ is identical to $I_{\rm box}^{(2)}$. Accordingly, the resulting irreducible contribution of the box diagrams to the effective potential for $B\bar{B}\to B\bar{B}$ reads

$$V_{B\bar{B}\to B\bar{B}}^{\rm box} = V_{B_1}+V_{C_1} = -\frac{g^4}{4f_\pi^4}(\boldsymbol{\tau}_1\cdot\boldsymbol{\tau}_2)I_{\rm box}^{(2)}. \tag{34}$$

The derivation of this integral is provided in Appendix A 3 a, the final result at $\mathcal{O}(\chi^2)$ reads

$$I_{\rm box}^{(2)} = \frac{-23\boldsymbol{q}^2}{96\pi^2}\left\{\frac{\mathcal{R}}{2}+\frac{5}{138}+\ln\left(\frac{m_\pi}{\mu}\right)+L(q)\right\}+\mathcal{O}(\chi^4). \tag{35}$$

The effective potentials for the OPE and TPE in the case of all possible transitions for $B^{(*)}\bar{B}^{(*)}\to B^{(*)}\bar{B}^{(*)}$ scatterings are listed in the Appendix C.

C. $B^{(*)}B^{(*)}\to B^{(*)}B^{(*)}$ scattering

The same topologies as discussed above also contribute to $B^{(*)}B^{(*)}$ scattering. However, in contrast to $\bar{B}$, for B mesons there is no charge-conjugated Pauli matrix ($\boldsymbol{\tau}^c=-\boldsymbol{\tau}$). It is evident that this change does not affect

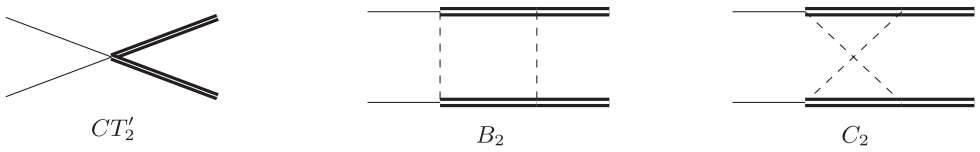

FIG. 5. NLO diagrams for $B\bar{B} \to B^*\bar{B}^*$.

the box diagrams as there is an even number of pion-emission vertices on each heavy meson line. However, this sign change is important for the one-pion exchange, the football diagrams and also some triangle diagrams, with an odd number of vertices in the antimeson line. For example, for elastic BB^* scattering these changes will affect diagrams O_4 and O_5 in Fig. 3 and diagrams F_3, $T_{3.2}$, and $T_{3.3}$ in Fig. 6. As a consequence of this, for B-mesons the triangle diagrams do not cancel. Additionally, we note that the isospin coefficients for scattering of two heavy mesons are generally different from those of one heavy meson one heavy antimeson, because of the differences in their isospin wave functions. In particular, the $\boldsymbol{\tau_1} \cdot \boldsymbol{\tau_2}$ matrix element for a heavy meson-antimeson system is given by Eq. (22), resulting in -3 for $I = 0$ and $+1$ for $I = 1$. The same values are obtained for isospin matrix elements in elastic transitions between two identical bosons, namely $PP \to PP$ and $VV \to VV$, where P and V represent pseudoscalar and vector mesons, respectively. However, for the PV system, the matrix element depends on the topology, namely on

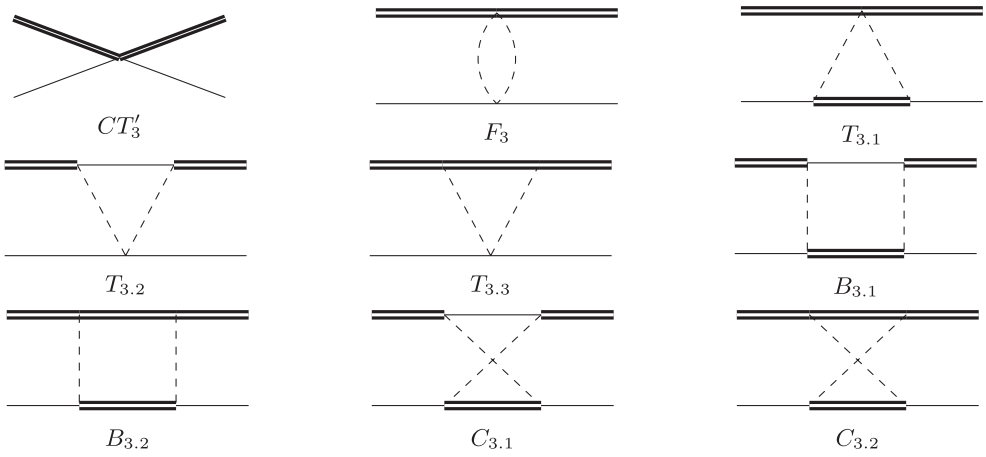

FIG. 6. NLO diagrams for $B^*\bar{B} \to B^*\bar{B}$.

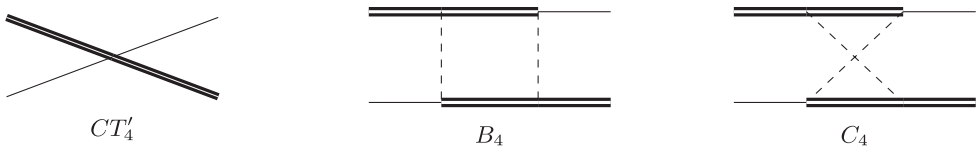

FIG. 7. NLO diagrams for $B^*\bar{B} \to B\bar{B}^*$.

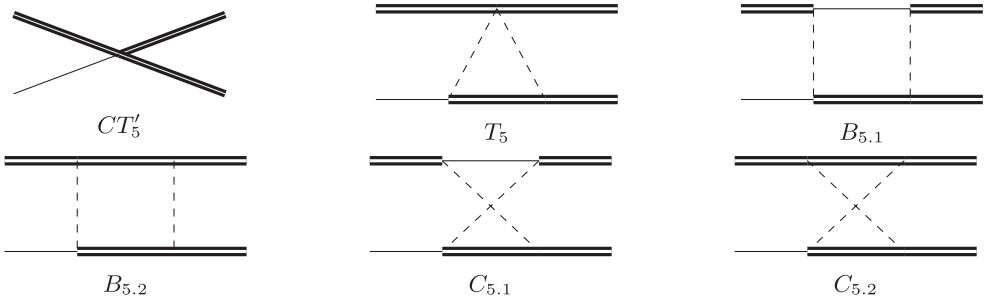

FIG. 8. NLO diagrams for $B^*\bar{B} \to B^*\bar{B}^*$.

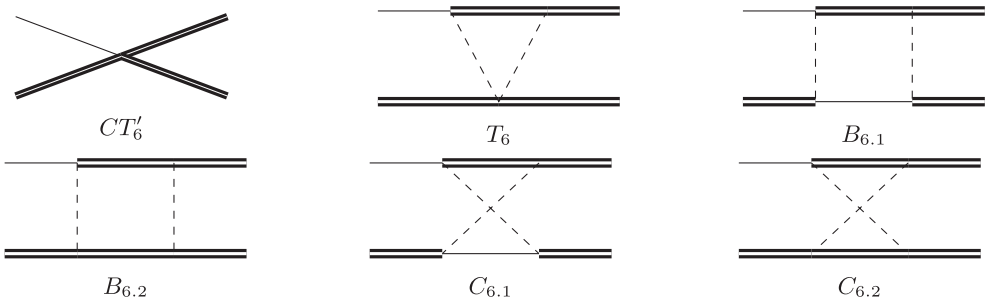

FIG. 9. NLO diagrams for $B\bar{B}^* \to B^*\bar{B}^*$.

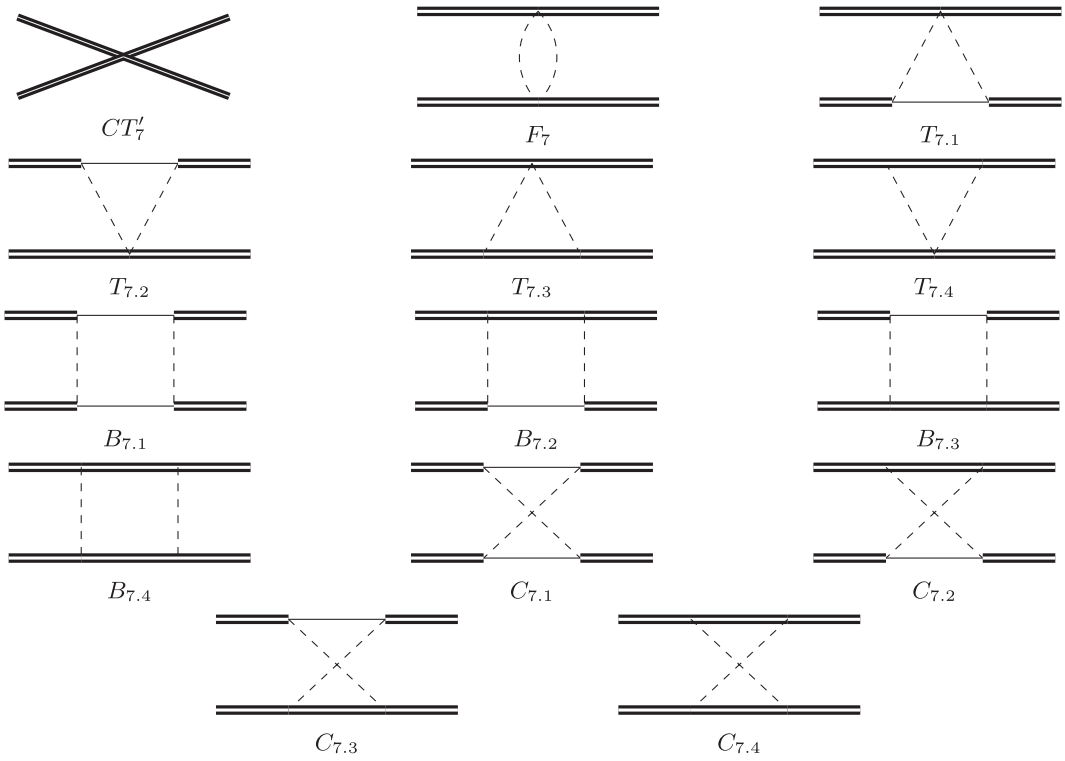

FIG. 10. NLO diagrams for $B^*\bar{B}^* \to B^*\bar{B}^*$.

whether the initial PV transform to the final VP (u-channel) or PV state (t-channel)

$$\langle (PV)_I | \boldsymbol{\tau_1} \cdot \boldsymbol{\tau_2} | (VP)_I \rangle_{\text{u-channel}} = \begin{cases} 3; & I = 0 \\ 1; & I = 1 \end{cases} \tag{36}$$

$$\langle (PV)_I | \boldsymbol{\tau_1} \cdot \boldsymbol{\tau_2} | (PV)_I \rangle_{\text{t-channel}} = \begin{cases} -3; & I = 0 \\ 1; & I = 1, \end{cases} \tag{37}$$

Specifically, the isoscalar transition in the u-channel has a different sign, as compared to all other isoscalar transitions.

The explicit expressions for the $B^{(*)}B^{(*)} \to B^{(*)}B^{(*)}$ potentials are provided in Appendix C.

V. PARTIAL WAVE DECOMPOSITION

In this section, the effective potentials from the earlier section are decomposed into four channels

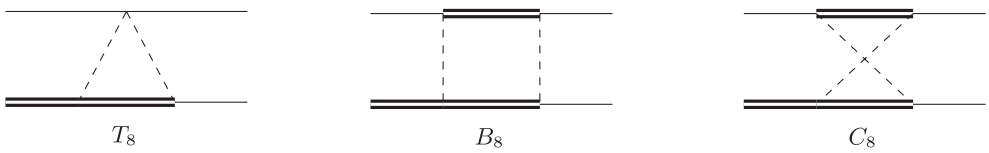

FIG. 11. NLO diagrams for $B\bar{B}^* \to B\bar{B}$.

$J^{PC} = 0^{++}, 1^{++}, 1^{+-}, 2^{++}$. For those we chose the following bases [40]

$$\begin{aligned}
0^{++}&: \alpha,\beta = \{B\bar{B}(^1S_0), B^*\bar{B}^*(^1S_0), B^*\bar{B}^*(^5D_0)\}\\
1^{++}&: \alpha,\beta = \{B\bar{B}^*(^3S_1,+), B\bar{B}^*(^3D_1,+), B^*\bar{B}^*(^5D_1)\}\\
1^{+-}&: \alpha,\beta = \{B\bar{B}^*(^3S_1,-), B\bar{B}^*(^3D_1,-),\\
&\qquad B^*\bar{B}^*(^3S_1), B^*\bar{B}^*(^3D_1)\}\\
2^{++}&: \alpha,\beta = \{B\bar{B}(^1D_2), B\bar{B}^*(^3D_2), B^*\bar{B}^*(^5S_2),\\
&\qquad B^*\bar{B}^*(^1D_2), B^*\bar{B}^*(^5D_2), B^*\bar{B}^*(^5G_2)\}. \qquad (38)
\end{aligned}$$

The individual partial waves are labeled as $^{2S+1}L_J$ with S, L, and J denoting the total spin, the angular momentum and the total momentum, respectively. The sign in parentheses for $B\bar{B}^*$ states corresponds to their C-parity which is given by

$$|B\bar{B}^*,\pm\rangle = \frac{1}{\sqrt{2}}(|B\bar{B}^*\rangle \pm |B^*\bar{B}\rangle). \qquad (39)$$

The partial wave decomposition (PWD) of the potentials is done using the formalism of Ref. [40], which gives

$$V_{\alpha\beta}(J^{\mathrm{PC}}) = \frac{1}{2J+1}\int \frac{d\Omega_n}{4\pi}\frac{d\Omega_{n'}}{4\pi}\mathrm{Tr}[P^\dagger(\alpha,\boldsymbol{n})VP(\beta,\boldsymbol{n}')] \qquad (40)$$

where $\boldsymbol{n} = \boldsymbol{p}/|\boldsymbol{p}|$, $\boldsymbol{n}' = \boldsymbol{p}'/|\boldsymbol{p}'|$, $P^\dagger(\alpha,\boldsymbol{n})$, and $P(\beta,\boldsymbol{n}')$ are outgoing and incoming normalized projectors respectively with α and β being the bases states mentioned in Eq. (38) and finally, V are the potentials calculated earlier. Due to the spacial symmetry of this $2\to 2$ reaction, only the angle θ between the incoming and outgoing momentum needs to be considered and we use the notation $x = \cos(\theta)$. Then the above expression simplifies to

$$V_{\alpha\beta}(J^{\mathrm{PC}}) = \frac{1}{2J+1}\int_{-1}^{+1}\frac{dx}{2}\mathrm{Tr}[P^\dagger(\alpha,\boldsymbol{n}')VP(\beta,\boldsymbol{n})], \qquad (41)$$

with the trace taken over the spin indices. The partial wave projectors used to calculate the potentials are provided in Ref. [40] and repeated in Appendix B to keep the presentation self-contained. Using the effective potentials derived here, the scattering amplitudes can be obtained as a solution of the partial-wave decomposed coupled-channel Lippmann-Schwinger equation

$$\begin{aligned}
T_{\alpha\beta}(E,p,p') &= V_{\alpha\beta}(E,p,p')\\
&- \int_0^\Lambda \frac{\mathrm{d}qq^2}{2\pi^2}V_{\alpha\gamma}(E,p,q)G(E,q)T_{\gamma\beta}(E,q,p'), \qquad (42)
\end{aligned}$$

where the sharp cutoff Λ is introduced to render the integral equation well defined. Alternatively, the potentials in the Lippmann-Schwinger equation can be regularized using the method proposed in the NN sector in Ref. [75], which explicitly preserves long-range interactions (see also Ref. [76] for related work in the double-quarkonium sector). We expect both methods to yield similar results and defer explicit checks to future work.

Further, the two-body propagator in the channel γ from the list given in Eq. (38) is

$$G_\gamma = (q^2/(2\mu_\gamma) + m_{1,\gamma} + m_{2,\gamma} - \sqrt{s} - i\epsilon)^{-1}, \qquad (43)$$

where $\sqrt{s}$ is the total energy and the reduced mass of two heavy mesons with the masses $m_{1,\gamma}$ and $m_{2,\gamma}$ in the channel γ reads

$$\mu_\gamma = \frac{m_{1,\gamma}m_{2,\gamma}}{m_{1,\gamma}+m_{2,\gamma}}. \qquad (44)$$

The partial wave projected potentials for $B^{(*)}\bar{B}^{(*)} \to B^{(*)}\bar{B}^{(*)}$ in the $J^{\mathrm{PC}} = 0^{++}$ channel are presented here and the partial wave projected potentials for the rest of the channels ($J^{\mathrm{PC}} = 1^{++}, 1^{+-}, 2^{++}$) are listed in Appendix D. The pertinent integrals used in PWD are abbreviated as $Q(p',p)$, $R(p',p)$, $S(p',p)$. Their explicit expressions are given in the Appendix E. We denote $|\boldsymbol{p}'| = p'$ and $|\boldsymbol{p}| = p$.

A. $B^{(*)}\bar{B}^{(*)} \to B^{(*)}\bar{B}^{(*)}$

1. $J^{PC} = 0^{++}$

$$V_{\mathrm{CT}}^{0^{++},I} = \begin{pmatrix}
\mathcal{C}_d^I + \frac{1}{2}\mathcal{C}_f^I + (\mathcal{D}_d^I + \frac{1}{2}\mathcal{D}_f^I)(p^2+p'^2) & \frac{1}{2}\sqrt{3}(\mathcal{C}_f^I + \mathcal{D}_f^I(p^2+p'^2)) & -\sqrt{3}\mathcal{D}_{SD}^I p'^2\\
\frac{1}{2}\sqrt{3}(\mathcal{C}_f^I + \mathcal{D}_f^I(p^2+p'^2)) & \mathcal{C}_d^I - \frac{1}{2}\mathcal{C}_f^I + (\mathcal{D}_d^I - \frac{1}{2}\mathcal{D}_f^I)(p^2+p'^2) & -\mathcal{D}_{SD}^I p'^2\\
-\sqrt{3}\mathcal{D}_{SD}^I p^2 & -\mathcal{D}_{SD}^I p^2 & 0
\end{pmatrix}, \qquad (45)$$

where the index I stands for isospin and the parameters are convenient linear combinations of the Lagrangian parameters of Eq. (3).

$$V_{\rm OPE}^{0^{++}} = -\frac{g^2}{4f_\pi^2}(\boldsymbol{\tau_1}\cdot\boldsymbol{\tau_2})\begin{pmatrix} 0 & \frac{1}{\sqrt{3}}Q_2 & \frac{1}{\sqrt{6}}(Q_2-3Q_{n'}) \\ \frac{1}{\sqrt{3}}Q_2 & -\frac{2}{3}Q_2 & \frac{1}{\sqrt{2}}(\frac{Q_2}{3}-Q_{n'}) \\ \frac{1}{\sqrt{6}}(Q_2-3Q_n) & \frac{1}{\sqrt{2}}(\frac{Q_2}{3}-Q_n) & \frac{3}{2}(5Q_2-6Q_n-6Q_{n'}+18Q_x-9Q_{x^2}) \end{pmatrix} \tag{46}$$

$$V_{\rm TPE}^{0^{++}} = \frac{1}{16\pi^2 f_\pi^4}\begin{pmatrix} (V_{\rm TPE}^{0^{++}})_{11} & \frac{\sqrt{3}}{4}g^4(V_{\rm TPE}^{0^{++}})_{12} & \frac{3\sqrt{3}}{8\sqrt{2}}g^4(V_{\rm TPE}^{0^{++}})_{13} \\ \frac{\sqrt{3}}{4}g^4(V_{\rm TPE}^{0^{++}})_{21} & (V_{\rm TPE}^{0^{++}})_{22} & \frac{-1}{16\sqrt{2}}g^4(V_{\rm TPE}^{0^{++}})_{23} \\ \frac{3\sqrt{3}}{8\sqrt{2}}g^4(V_{\rm TPE}^{0^{++}})_{31} & \frac{-1}{16\sqrt{2}}g^4(V_{\rm TPE}^{0^{++}})_{32} & (V_{\rm TPE}^{0^{++}})_{33} \end{pmatrix} \tag{47}$$

where,

$$(V_{\rm TPE}^{0^{++}})_{11} = \bar{S}_0(p',p) \tag{48}$$

$$(V_{\rm TPE}^{0^{++}})_{12} = (V_{\rm TPE}^{0^{++}})_{21} = (p'^2+p^2)\left[-\mathcal{R}+1-2\ln\left(\frac{m_\pi}{\mu}\right)\right] - 2R_2(p',p) \tag{49}$$

$$(V_{\rm TPE}^{0^{++}})_{13} = \frac{2}{3}(p'^2)\left[-\mathcal{R}+1-2\ln\left(\frac{m_\pi}{\mu}\right)\right] - 2R_{n'}(p',p) + \frac{2}{3}R_2(p',p) \tag{50}$$

$$(V_{\rm TPE}^{0^{++}})_{22} = \bar{S}_0 + \frac{g^4}{4}\left\{2\mathcal{R}(p'^2+p^2) - 2(p'^2+p^2) + [4(p'^2+p^2)]\ln\left(\frac{m_\pi}{\mu}\right) + 4R_2(p',p)\right\} \tag{51}$$

$$(V_{\rm TPE}^{0^{++}})_{23} = 2p'^2\left[2\mathcal{R}-2+4\ln\left(\frac{m_\pi}{\mu}\right)\right] + 4\{3R_{n'}(p',p) - R_2(p',p)\} \tag{52}$$

$$(V_{\rm TPE}^{0^{++}})_{31} = \frac{2}{3}(p^2)\left[-\mathcal{R}+1-2\ln\left(\frac{m_\pi}{\mu}\right)\right] - 2R_n(p',p) + \frac{2}{3}R_2(p',p) \tag{53}$$

$$(V_{\rm TPE}^{0^{++}})_{32} = 2p^2\left[2\mathcal{R}-2+4\ln\left(\frac{m_\pi}{\mu}\right)\right] + 4\{3R_n(p',p) - R_2(p',p)\} \tag{54}$$

$$\begin{aligned}(V_{\rm TPE}^{0^{++}})_{33} = \bar{S}_2 + \frac{g^4}{4}\Bigg\{&\frac{-15}{64p'p}\left[\frac{\rho^4}{4}-\rho^4 L(\rho)\right]_{p'-p}^{p'+p} - \frac{45}{8}R_{x^2}(p',p) \\ &- \frac{21}{8}\left(R_n(p',p)+R_{n'}(p',p)-\frac{1}{2}R_2(p',p)-3R_x(p',p)\right)\Bigg\}\end{aligned} \tag{55}$$

and,

$$\begin{aligned}\bar{S}_0(p',p) &= \int_{-1}^{1}\frac{dx}{2}(\boldsymbol{\tau_1}\cdot\boldsymbol{\tau_2})\boldsymbol{q}^2\left\{\mathcal{R}\left[\frac{23}{48}g^4+\frac{1}{24}\right] + \left(\frac{5}{144}g^4-\frac{5}{72}\right) + \ln\left(\frac{m_\pi}{\mu}\right)\left(\frac{23}{24}g^4+\frac{1}{12}\right) + L(q)\left(\frac{23}{24}g^4+\frac{1}{12}\right)\right\} \\ &= (\boldsymbol{\tau_1}\cdot\boldsymbol{\tau_2})\Bigg\{\mathcal{R}(p'^2+p^2)\left(\frac{23}{48}g^4+\frac{1}{24}\right) + (p'^2+p^2)\left(\frac{5}{144}g^4-\frac{5}{72}\right) + (p'^2+p^2)\left(\frac{23}{24}g^4+\frac{1}{12}\right)\ln\left(\frac{m_\pi}{\mu}\right) \\ &\quad + R_2(p',p)\left(\frac{23}{24}g^4+\frac{1}{12}\right)\Bigg\}\end{aligned} \tag{56}$$

$$\begin{aligned}\bar{S}_2(p',p) &= \int_{-1}^{1}\frac{dx}{2}\frac{(3x^2-1)}{2}(\boldsymbol{\tau_1}\cdot\boldsymbol{\tau_2})\boldsymbol{q}^2\left\{\mathcal{R}\left[\frac{23}{48}g^4+\frac{1}{24}\right] + \left(\frac{5}{144}g^4-\frac{5}{72}\right) + \ln\left(\frac{m_\pi}{\mu}\right)\left(\frac{23}{24}g^4+\frac{1}{12}\right) + L(q)\left(\frac{23}{24}g^4+\frac{1}{12}\right)\right\} \\ &= \frac{(\boldsymbol{\tau_1}\cdot\boldsymbol{\tau_2})}{8p'^2p^2}\left\{[3R_6(p',p) - 6(p'^2+p^2)R_4(p',p) + (3(p'^2+p^2)^2 - 4p'^2p^2)R_2(p',p)]\left(\frac{23}{24}g^4+\frac{1}{12}\right)\right\}\end{aligned} \tag{57}$$

B. $B^{(*)}B^{(*)} \to B^{(*)}B^{(*)}$

The PWD potentials can be obtained in exactly the same way as for $B^{(*)}\bar{B}^{(*)} \to B^{(*)}\bar{B}^{(*)}$. However, in this case due to Bose symmetry for identical heavy mesons, certain partial wave transitions are forbidden by quantum number constraints. In particular,

$$V^{I=0}(B^{(*)}B^{(*)} \to B^{(*)}B^{(*)}, 0^+) = V^{I=0}(B^*B^* \to B^*B^*, 2^+) = 0$$

and

$$V^{I=1}(BB^* \to B^*B^*, 1^+) = V^{I=1}(B^*B^* \to B^*B^*, 1^+) = 0.$$

Also, the additional contribution from the triangle diagrams and the signs, as discussed in Sec. IV C, have to be incorporated. The additional triangle contribution can be included in the PWD potentials of $B^{(*)}B^{(*)}$ by changing the $\bar{S}_k(p', p)$ functions [which includes $\bar{S}_0(p', p)$, $\bar{S}_2(p', p)$, and $\bar{S}_4(p', p)$] to $S_k(p', p)$ functions [$S_0(p', p)$, $S_2(p', p)$, and $S_4(p', p)$], where $S_k(p', p)$ is given by,

$$S_k(p', p) = \int_{-1}^{1} \frac{dx}{2} P_k(x)(\boldsymbol{\tau_1}\cdot\boldsymbol{\tau_2})\boldsymbol{q}^2 \left\{ \mathcal{R}\left[\frac{23}{48}g^4 - \frac{5}{24}g^2 - \frac{1}{24}\right] + \left(\frac{5}{144}g^4 + \frac{13}{72}g^2 + \frac{5}{72}\right) + \ln\left(\frac{m_\pi}{\mu}\right)\left(\frac{23}{24}g^4 - \frac{5}{12}g^2 - \frac{1}{12}\right) + L(q)\left(\frac{23}{24}g^4 - \frac{5}{12}g^2 - \frac{1}{12}\right)\right\}, \tag{58}$$

where $P_k(x)$ denotes the kth Legendre polynomial ($k = 0, 2, 4$; in our case).

VI. CHECKS OF THE RESULTS

A nontrivial cross check of our results is provided by the renormalization of the formally divergent loops, which has to work at each order in the power counting separately. Specifically, the divergent terms [$\mathcal{R}$-terms—see Eq. (20)], contained in the loop contributions of $B^{(*)}\bar{B}^{(*)}$ (and similarly $B^{(*)}B^{(*)}$) TPE potentials must consistently match to the LECs of the contact interactions. This matching has to work for each type of diagram separately: the footballs, scaling with g^0, the triangles $\sim g^2$, and the boxes $\sim g^4$.

We take the case of $(V^{0^{++}}_{\rm TPE})_{12}$ from Eq. (49) in Sec. V A 1 and relate it to $(V^{0^{++}}_{\rm CT})_{12}$ in the 0^{++} channel as an example. By equating the divergence of the TPE loop integral with the LECs $(\mathcal{C}^I_f, \mathcal{D}^I_f)$ for the g^4 contribution, one finds for the divergent parts of the counterterms

$$\mathcal{C}^I_f = 0 \tag{59}$$

$$\mathcal{D}^I_f = \frac{-\mathcal{R}g^4}{32\pi^2 f_\pi^4}. \tag{60}$$

Similarly, equating the divergence of $(V^{0^{++}}_{\rm TPE})_{11}$ and $(V^{0^{++}}_{\rm TPE})_{22}$ with $(V^{0^{++}}_{\rm CT})_{11}$ and $(V^{0^{++}}_{\rm CT})_{22}$, respectively for g^4 contribution, results in

$$\mathcal{C}^I_d = 0 \tag{61}$$

$$\mathcal{D}^I_d = \frac{\mathcal{R}g^4}{64\pi^2 f_\pi^4}\left(\frac{23}{12}(\boldsymbol{\tau_1}\cdot\boldsymbol{\tau_2}) + 1\right) \tag{62}$$

Following the same procedure for $(V^{0^{++}}_{\rm CT})_{13}$ and $(V^{0^{++}}_{\rm TPE})_{13}$ with its prefactors, one finds the divergent part of $\mathcal{D}^I_{\rm SD}$ as

$$\mathcal{D}^I_{\rm SD} = \frac{\sqrt{2}\mathcal{R}g^4}{128\pi^2 f_\pi^4}. \tag{63}$$

Similarly, when performing this exercise for all g^0 terms in $B^{(*)}\bar{B}^{(*)}$ case, one finds

$$\mathcal{C}^I_d = \mathcal{C}^I_f = \mathcal{D}^I_f = \mathcal{D}^I_{\rm SD} = 0 \tag{64}$$

$$\mathcal{D}^I_d = \frac{\mathcal{R}}{384\pi^2 f_\pi^4}(\boldsymbol{\tau_1}\cdot\boldsymbol{\tau_2}) \tag{65}$$

and in the g^2 case

$$\mathcal{C}^I_d = \mathcal{C}^I_f = \mathcal{D}^I_f = \mathcal{D}^I_{\rm SD} = 0 \tag{66}$$

$$\mathcal{D}^I_d = \frac{-5\mathcal{R}g^2}{384\pi^2 f_\pi^4}(\boldsymbol{\tau_1}\cdot\boldsymbol{\tau_2}) \tag{67}$$

The renormalization program provides a nontrivial cross check of the calculations. For example, the divergent terms of the PWD potentials $(V^{0^{++}}_{\rm CT})_{13}$ and $(V^{0^{++}}_{\rm CT})_{23}$ corresponding to $B\bar{B}(^1S_0) \to B^*\bar{B}^*(^5D_0)$ and $B^*\bar{B}^*(^1S_0) \to B^*\bar{B}^*(^5D_0)$, respectively, must be related such that their infinities can be absorbed into one single $\mathcal{D}^I_{\rm SD}$ term in Eq. (63). Performing the same exercise for the remaining transitions, we confirm that $\mathcal{C}^I_d$, $\mathcal{C}^I_f$, $\mathcal{D}^I_d$, and $\mathcal{D}^I_f$ absorb all the divergences of $B\bar{B}(^1S_0) \to B\bar{B}(^1S_0)$, $B\bar{B}(^1S_0) \to B^*\bar{B}^*(^1S_0)$, and $B^*\bar{B}^*(^1S_0) \to B^*\bar{B}^*(^1S_0)$ PWD potentials consistently. Moreover, we verified that with the counterterms determined above, all $B^{(*)}\bar{B}^{(*)}$ transitions with the quantum numbers 0^{++}, 1^{++}, 1^{+-}, and 2^{++} are finite.

As a further nontrivial cross check we verified that the triangle contributions add up in the $B^{(*)}B^{(*)}$ case and cancel for $B^{(*)}\bar{B}^{(*)}$, by computing the diagrams in particle basis for both cases.

VII. PLOTS OF POTENTIALS

In this section we present some representative plots for the TPE potentials in momentum space. Please note that, although in what follows we refer to the results for B-mesons, the heavy meson mass does not explicitly enter the TPE contributions at the given order. Therefore, these results are equally applicable to $D^{(*)}D^{(*)}$ and $D^{(*)}\bar{D}^{(*)}$ scattering at the order we are working. The only difference to keep in mind is that for the physical pion mass, the three-body cuts in the TPE diagrams will contribute to the imaginary part of the scattering amplitude. These contributions are not captured by our power counting but may become important if one aims for a high-accuracy calculation of this quantity. This is particularly important in the context of accurately extracting the width of the T_{cc} state from data [77].

In what follows, for the sake of illustration, we present the heavy meson heavy (anti)meson TPE potentials for various partial waves and typical momentum regimes. We also compare the momentum dependence of these potentials with that from the pure LO + NLO contact interactions and demonstrate in this way that, to the accuracy assigned to this chiral order, the full potentials are represented well by the contact terms only. This suggests that the nonanalytic contributions are suppressed. In this section, we also discuss the contributions of the individual TPE diagrams to the full results. To generate the plots, we set $\mu = 1.156$ GeV and neglect the R term, as it contains divergences that are absorbed by the contact terms, as discussed in the previous section.

Figures 12 and 13 show the results for the $I = 1$ $B^{(*)}\bar{B}^{(*)}$ TPE potentials with initial momenta of $p = 500$ MeV and $p = m_\pi$ respectively, plotted as a function of the final momentum.[2] Similarly, Figs. 14 and 15 show the results for the $B^{(*)}B^{(*)}$ system under the same conditions for the initial momenta. In the $B^{(*)}B^{(*)}$ system, however, only those transitions are shown that are allowed by Bose symmetry. In all these plots, the red solid lines represent the full potentials, which include terms additionally suppressed by $(m_\pi^2/p_{\rm typ}^2)$, while the red dashed lines correspond to the potentials expanded to $\mathcal{O}(Q^2)$—see, e.g., Eqs. (18) and (19) for details. As one can see for all cases shown, the deviation between these curves is well below the expectations from the power counting. As expected, the discrepancies for $p = m_\pi$ are slightly larger than those for $p \sim p_{\rm typ}$. Additionally, it is observed that the TPE potentials in the kinematic region where $p \sim p' \sim p_{\rm typ}$ are larger compared to those at lower momenta. Specifically, $V_{\rm TPE}(m_\pi, m_\pi)$ is significantly smaller than $V_{\rm TPE}(p_{\rm typ}, p_{\rm typ})$ in line with the power counting.

As the corresponding black lines we also show the results of fits of the pertinent contact terms from Eq. (45) [see also Eqs. (D1), (D11), and (D26)] to the full potentials. The fits were done for $p = 500$ MeV, with the LO contact terms fixed by the values of the potentials at $p' = 0$, and the NLO contact terms adjusted by fitting the slope. By fitting two different TPE potentials [e.g., $B\bar{B}(^1S_0) \to B\bar{B}(^1S_0)$ and $B\bar{B}(^1S_0) \to B^*\bar{B}^*(^1S_0)$] we were able to individually extract the values of the low-energy constants $\mathcal{C}_d$, $\mathcal{C}_f$, $\mathcal{D}_d$, and $\mathcal{D}_f$, that represent the TPE contributions best. All other coupled-channel transitions with different $J^{\rm PC}$ are therefore predictions, with all LEC's fixed. Remarkably, the curves representing the contact interactions for $p \simeq p_{\rm typ}$ show excellent agreement with the TPE contributions across the entire momentum range of p', including $p' \simeq p_{\rm typ}$. The deviations are more sizeable for $p = m_\pi$, however, not exceeding expectations from the power counting. Moreover, the contact terms fixed from the $^1S_0$ transition also represent well the TPE potentials for the other quantum numbers. For illustration, we show the 1^{+-} potentials, which are shown in the lower panels in Figs. 12 and 13. Similar to $S-S$ transitions, we extracted the value of $\mathcal{D}_{\rm SD}$ for a particular $S-D$ transition, which was chosen to be $B\bar{B}^*(^3S_1) \to B\bar{B}^*(^3D_1)$. With this value fixed, the $S-D$ contact interaction also provides reasonable estimates for all other $S-D$ transitions as illustrated in Fig. 16 for $p = 500$ MeV and Fig. 17 for $p = m_\pi$. In these plots, we present results for various $B^{(*)}\bar{B}^{(*)}$ transitions in the 1^{+-} channel as an example; however, the results for all other transitions with different quantum numbers exhibit a very similar pattern. The results shown in Figs. 12–17 for both $B^{(*)}\bar{B}^{(*)}$ and $B^{(*)}B^{(*)}$ demonstrate that the leading contribution of the TPE interactions is predominantly polynomial in momenta, while the nonanalytic logarithmic contributions are suppressed.

Clearly, the values of the LECs extracted above are not their physical values, which can only be determined from a fit to the data. What we aimed at here was more the demonstration that the TPE contributions can be largely represented by contact terms, suggesting, in particular, that the results of Refs. [39,40] for a coupled-channel analysis of the Belle data in the context of $Z_b(10610)$ and $Z_b(10650)$ and their possible spin partners, can be interpreted as a reasonable representation of an NLO calculation. However, to obtain accurate results, e.g., for the pole locations of the Z_b states with fully controlled uncertainty estimates, a data analysis that includes the TPE contributions is needed.

In Fig. 18, we show contributions from individual diagram types—football, triangle, and box—to the TPE scattering potential for three representative partial waves.

[2]Note that the characteristic momentum $p_{\rm typ} \approx 500$ MeV for both BB- and DD-meson systems.

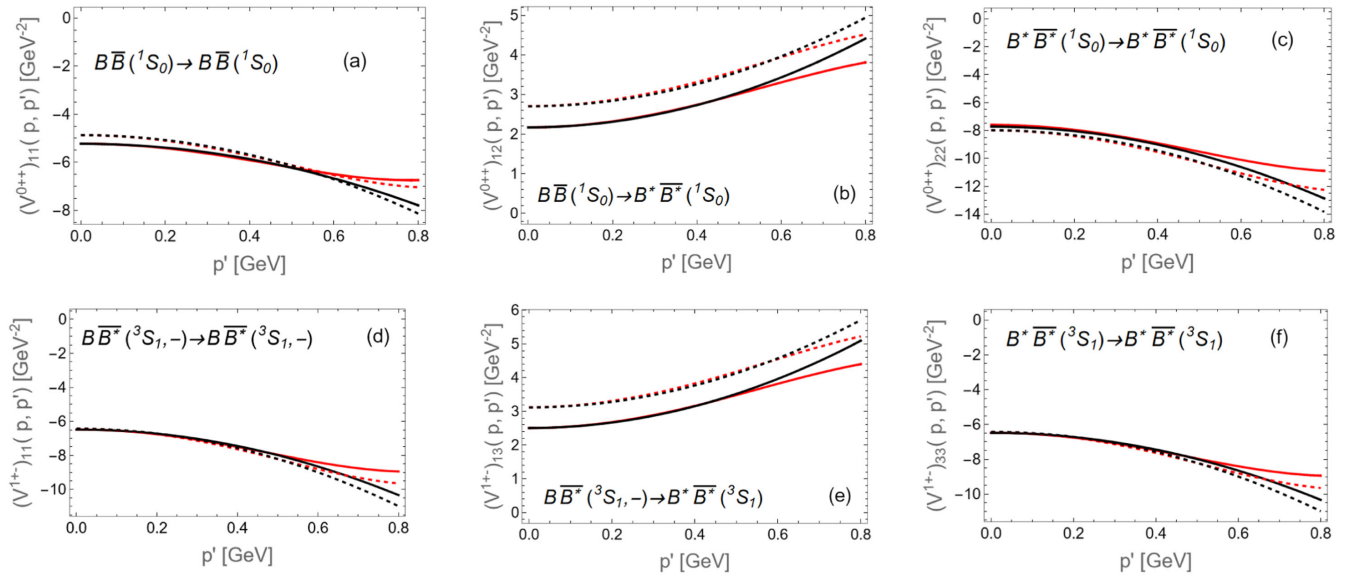

FIG. 12. The TPE and contact potentials of the $B^{(*)}\bar{B}^{(*)}$ system in the momentum space as a function of the final momentum p' for the initial momentum $p = 500$ MeV. The solid (dotted) red lines represent the full [expanded to $\mathcal{O}(Q^2)$] TPE potential, while the solid (dotted) black lines illustrate the results of the fit of the contact potential at $p = 500$ MeV to the full (expanded) TPE potential, as described in the main text. Figures (a)–(c) depict transitions in the 0^{++} channels, namely $(V^{0^{++}}_{\rm TPE})_{11}$, $(V^{0^{++}}_{\rm TPE})_{12}$, and $(V^{0^{++}}_{\rm TPE})_{22}$, respectively. Figures (d)–(f) show transitions in the 1^{+-} channels, namely $(V^{1^{+-}}_{\rm TPE})_{11}$, $(V^{1^{+-}}_{\rm TPE})_{13}$, and $(V^{1^{+-}}_{\rm TPE})_{33}$, respectively. All figures correspond to $I = 1$.

All contributions for $B\bar{B}^{(*)}$ are evaluated for $I = 1$. For $BB^{(*)}$, we display only the transitions allowed by Bose statistics: the elastic $BB(^1S_0)$ transition for $I = 1$ (d), and the $BB^*(^3S_1)$ transitions for $I = 0$ (e) and $I = 1$ (f). Additionally, the elastic $B^*\bar{B}^*(^3S_1)$ contributions are identical to those for $B\bar{B}^*(^3S_1)$, as are $B^*B^*(^3S_1)(I = 0)$ and $BB^*(^3S_1)(I = 0)$, so these are not shown.

It can be seen that the box contributions, proportional to g^4 (indicated by orange dashed lines), are generally the smallest among the different types. For a given isospin, these contributions are identical for both meson-meson and meson-antimeson scattering [see panels (a) and (d) in Fig. 18 for $(^1S_0)$, and (c) and (f) in Fig. 18 for $(^3S_1)$ partial waves, all with $I = 1$]. The triangle contributions (terms

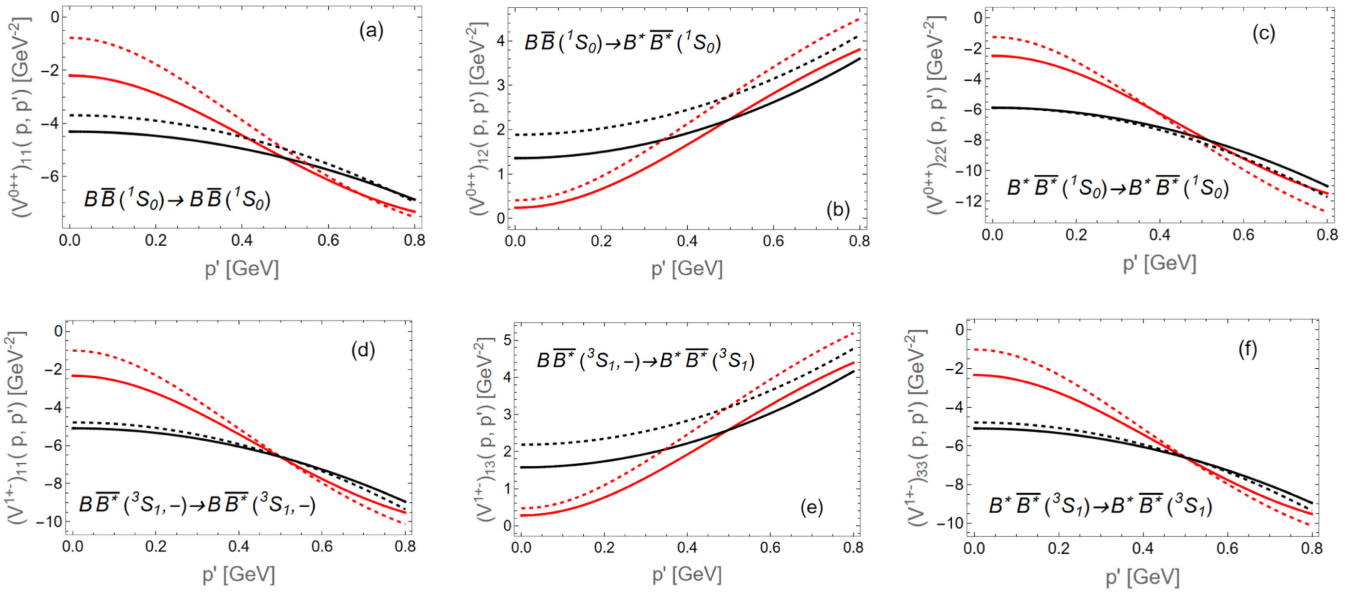

FIG. 13. Same as in Fig. 12 but for the initial momentum $p = m_\pi$.

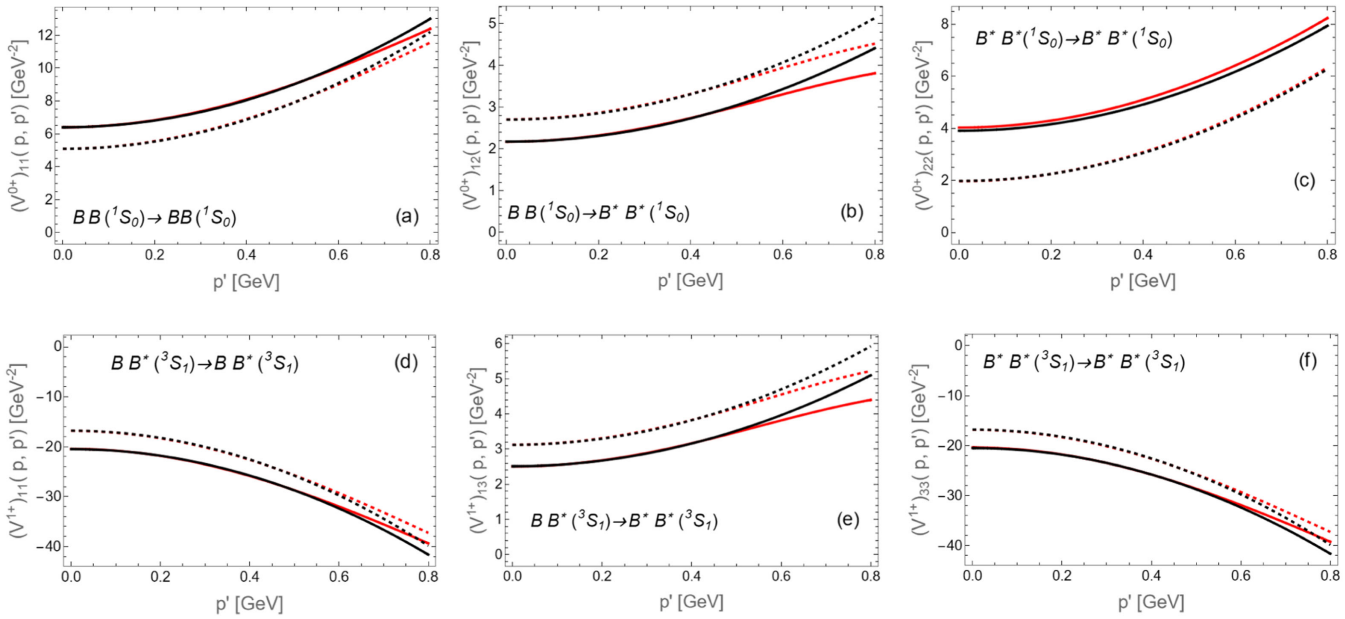

FIG. 14. The TPE and the contact potentials of the $B^{(*)}B^{(*)}$ system in the momentum space, allowed by Bose symmetry, as a function of the final momentum p' for the initial momentum $p = 500$ MeV. The solid (dotted) red lines represent the full [expanded to $\mathcal{O}(Q^2)$] TPE potential, while the solid (dotted) black lines show the results of the fit of the contact potential at $p = 500$ MeV to the full (expanded) TPE potential, as described in the main text. Figures (a)–(c) depict transitions in the 0^+ channels for $I = 1$, namely $(V^{0^+}_{\rm TPE})_{11}$, $(V^{0^+}_{\rm TPE})_{12}$, and $(V^{0^+}_{\rm TPE})_{22}$, respectively. Figures (d)–(f) show transitions in the 1^+ channels for $I = 0$, namely $(V^{1^+}_{\rm TPE})_{11}$, $(V^{1^+}_{\rm TPE})_{13}$, and $(V^{1^+}_{\rm TPE})_{33}$ respectively.

$\sim g^2$, shown by green dashed lines), cancel out for $B^{(*)}\bar{B}^{(*)}$ scattering, but do not vanish in the $B^{(*)}B^{(*)}$ sector. They are positive for $BB(^1S_0)$ and $BB^*(^3S_1)(I = 1)$ and negative for $BB^*(^3S_1)(I = 0)$, with these differences arising from the different isospin coefficients in Eq. (37). Finally, the football diagrams, which change sign when switching from $B^{(*)}\bar{B}^{(*)}$ to $B^{(*)}B^{(*)}$, show a behavior very similar to that of the triangles in the $B^{(*)}B^{(*)}$ sector.

All in all, the resulting $B\bar{B}^{(*)}$ TPE contributions are always negative. In contrast, the TPE contributions for

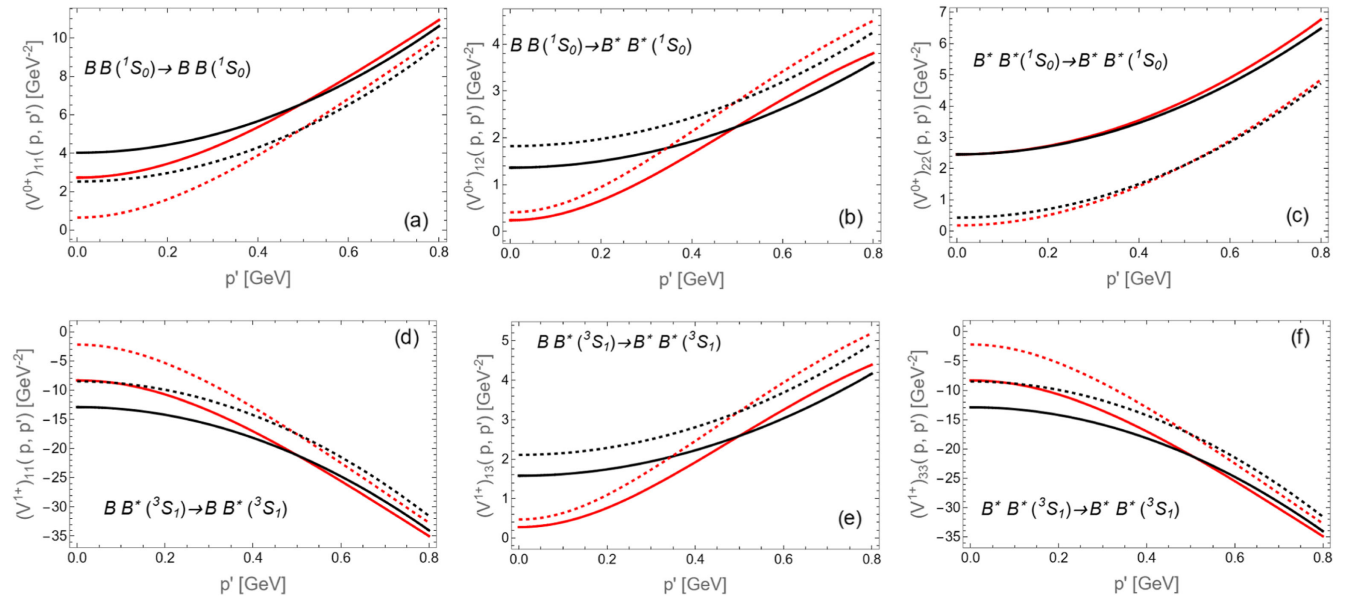

FIG. 15. Same as in Fig. 14 but for the initial momentum $p = m_\pi$.

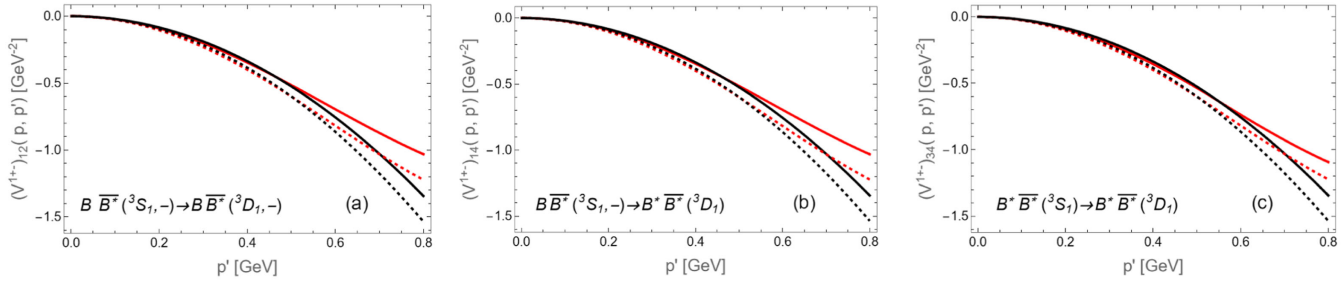

FIG. 16. The TPE and contact S to D wave transitions of the $B^{(*)}\bar{B}^{(*)}$ system in the momentum space are presented as a function of the final momentum for the initial momentum $p = 500$ MeV. Since the S to D transitions arise solely from the box diagrams, which are the same for $B^{(*)}\bar{B}^{(*)}$ and $B^{(*)}B^{(*)}$ before the partial wave decomposition, only the $B^{(*)}\bar{B}^{(*)}$ contributions are shown. The solid (dotted) red lines represent the full [expanded to $\mathcal{O}(Q^2)$] TPE potential, while the solid (dotted) black lines show the results of the fit of the contact potential at $p = 500$ MeV to the full (expanded) potential, as described in the main text. Figures (a)–(c) depict $(V^{1^+-}_{\rm TPE})_{12}$, $(V^{1^+-}_{\rm TPE})_{14}$, and $(V^{1^+-}_{\rm TPE})_{34}$ respectively.

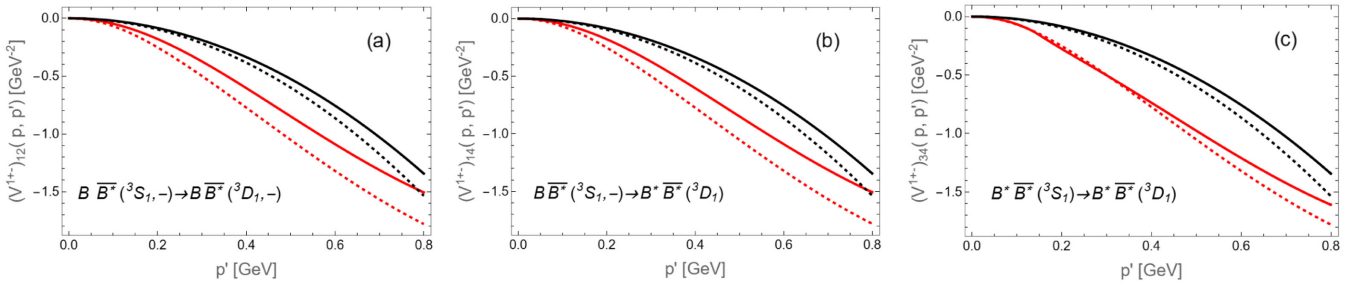

FIG. 17. Same as in Fig. 16 but for the initial momentum $p = m_\pi$.

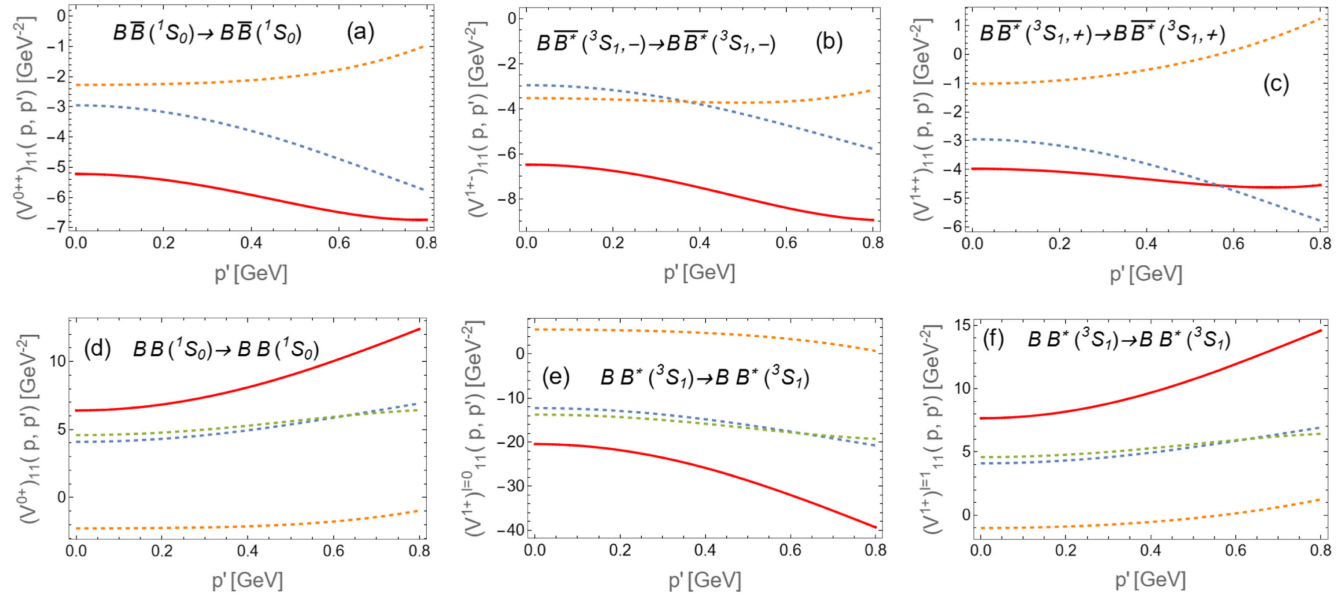

FIG. 18. The individual contributions to the TPE potentials for the $B^{(*)}\bar{B}^{(*)}$ (first line) and the $B^{(*)}B^{(*)}$ (second line) system in momentum space for $p = 500$ MeV. Here, the red solid line represents the full TPE potential and the blue dashed, green dashed, and orange dashed lines represent the contributions proportional to g^0 (footballs), g^2 (triangles), g^4 (boxes), respectively. Figures (a)–(c) depict $(V^{0^{++}}_{\rm TPE})_{11}$, $(V^{1^{+-}}_{\rm TPE})_{11}$, and $(V^{1^{++}}_{\rm TPE})_{11}$ for $I = 1$ in the $B^{(*)}\bar{B}^{(*)}$ system, respectively. Figures (d)–(f) depict $(V^{0^+}_{\rm TPE})_{11}$ for $I = 1$, $(V^{1^+}_{\rm TPE})_{11}$ for $I = 0$ and $(V^{1^+}_{\rm TPE})_{11}$ for $I = 1$ in the $B^{(*)}B^{(*)}$ system, respectively.

$BB^{(*)}$ depend on isospin: they are notably large and negative for $I = 0$, indicating strong attraction, while they are positive for $I = 1$, corresponding to repulsion. It is important to note that while the results presented here are for B-mesons, the derived TPE contributions up to order $\mathcal{O}(Q^2)$ are independent of the heavy-meson mass. Thus, they also apply to other heavy-meson heavy-(anti)meson systems, such as $D^{(*)}D^* - D^{(*)}D^*$ scattering, particularly in the context of the T_{cc} ($I = 0$) and its possible partner states. Recently, $DD^* \to DD^*$ scattering with $J^P = 1(^3S_1)$ was investigated on the lattice at $m_\pi = 280$ MeV for both $I = 0$ [54,56] and $I = 1$ [78], see also Refs. [79,80] for related lattice investigations. An analysis of the individual correlators contributing to both isospins revealed that the difference between the two isospin channels is associated with isovector-vector exchanges, such as the TPE contributions in the ρ-meson channel, yielding attraction for $I = 0$ and repulsion for $I = 1$ [78]. We note also that Ref. [81] pointed out the role of the TPE in the $I = 0$ DD^* potential at separations $r \simeq 1$–2 fm and nearly physical m_π, though the isospin and total spin of the $\pi\pi$ system were not specified—see also Ref. [67] for a related discussion. The pattern discussed above is in line with our calculations at the physical pion mass [see panels (e) and (f) in Fig. 18]. Additionally, repeating the calculations at $m_\pi = 280$ MeV shows qualitatively similar results also at this pion mass, with a significant attraction for $I = 0$ and a milder repulsion for $I = 1$.

VIII. COMPARISON TO EARLIER WORKS

When comparing our OPE results with the ones calculated by Wang *et al.* [39] [given in Eqs. (22)–(28)], one finds that their results calculated for the isovector case agree with ours. Also the PWD contact interactions in [40] [see Eqs. (12)–(15) in this reference] agree with ours.

For the TPE contribution in $B^{(*)}\bar{B}^{(*)} \to B^{(*)}\bar{B}^{(*)}$ scattering, however, our results disagree with those of Wang *et al.* [66] [given in Eq. (10)]. In this work, there is a net triangle contribution (terms proportional to g^2) in the total TPE potential, which in our case is absent. At the same time, their total TPE potential does not have any box contributions (terms proportional to g^4), which are present in our case. Only in case of the football diagrams (terms proportional to g^0) we agree to the results of Ref. [66].

Furthermore, we compared our results to the TPE potentials of Wang *et al.* [65] for $\bar{B}^{(*)}\bar{B}^{(*)}$ scattering. Contrary to the meson-antimeson scattering amplitudes of Ref. [66] referred to above, the TPE potentials for antimeson-antimeson scattering in [65] contain all types, namely football, triangle, and box contributions. However, a direct comparison with our potentials is difficult, since the results are given in quite different form compared to ours.

IX. SUMMARY AND OUTLOOK

Chiral effective field theory has recently become a precision tool for analyzing low-energy few-nucleon reactions, nuclear structure, and form factors. Combined with heavy-quark spin symmetry, this model-independent approach also allows one to probe the properties and internal structure of exotic states in the quarkonium sector, provided they are located near certain hadronic thresholds. This work is part of a series dedicated to a systematic understanding of the nature and properties of the $Z_b(10610)$ and $Z_b(10650)$ states in the bottomonium spectrum within chiral EFT.

In Refs. [39,40,50], analyses of the experimental data for the Z_b states in the elastic and inelastic channels were conducted, from which the pole positions of these states were extracted. Given that the spin-partner states $Z_b(10610)$ and $Z_b(10650)$ are located near the $B\bar{B}^*$ and $B^*\bar{B}^*$ thresholds, respectively, and that these hadronic channels can couple to each other, a hierarchy of operators was developed using a power counting, where the typical momenta Q are associated with the coupled-channel momentum scale between $B\bar{B}^{(*)}$ and $B^*\bar{B}^{(*)}$, $Q \sim p_{\rm typ} = \sqrt{m_B\delta}$, with $\delta = m_{B^*} - m_B$ representing the $B^* - B$ mass difference. A very similar counting was employed in pion production in nucleon-nucleon collisions, specifically the reaction $NN \to NN\pi$, leading to significant progress in understanding the data [58,59].

In the analyses of Refs. [39,40], all diagrams up to and including $\mathcal{O}(Q^2)$ were incorporated in the effective potential except for two-pion exchanges. These one-loop contributions contain information about intermediate-range forces, and need to be considered for systematic uncertainty estimates of the theoretical results and reliable extraction of the pole positions of the $Z_b(10610)$ and $Z_b(10650)$ states from data. In this work, we complete the calculation of diagrams at order $\mathcal{O}(Q^2)$ by deriving the missing two-pion exchange operators.

The TPE operators at order $\mathcal{O}(Q^2)$ consist of four topologies: triangle, football, box, and crossed box (see Figs. 4–11 for details). We provide closed-form expressions for all of them, as detailed in Appendix C. We also present the results for the effective potentials up to $\mathcal{O}(Q^2)$ for $B^{(*)}B^{(*)}$ scattering, a doubly bottom analog of the doubly charm case investigated by the LHCb collaboration. Notably, we find that the sum of all triangle diagrams vanishes for all $B^{(*)}\bar{B}^{(*)}$ transitions, while it yields a finite result for $B^{(*)}B^{(*)}$ case. An important self-consistency check of the results is provided by renormalization: The loop integrals are divergent and were regularized using dimensional regularization. These divergent parts must be absorbed by the counterterms in the course of renormalization. However, because of heavy-quark spin symmetry, at order $\mathcal{O}(Q^2)$ there are only three contact terms, while the number of allowed transitions is

significantly larger. Therefore, after absorbing three divergent contributions into the redefined contact terms, no additional divergences should occur. We verified that this is indeed the case. To ease the implementation of the results for calculating observables, we present the effective potential in the form of partial wave decomposition.

Moreover, we show that the TPE potentials can be largely represented by the contact term contributions, suggesting that the incomplete NLO calculations presented in Refs. [39,40] already provided a fair representation of the physics to this order, although a calculation including the full NLO potential would be desirable to find results for the pole parameters of the Z_b states and their spin partners with controlled uncertainties.

Finally, it is important to note that, although the results discussed here are presented for B-mesons, the heavy meson mass does not explicitly enter the TPE operators at the order we are working. As a result, these findings are equally valid for coupled-channel $D^{(*)}D^{(*)}$ and $D^{(*)}\bar{D}^{(*)}$ scattering at the same order. The main difference to consider is that, with a physical pion mass, the three-body cuts in the TPE diagrams will contribute to the imaginary part of the D-meson scattering amplitudes. While these contributions are beyond the order we are working here, they may become significant for high-precision calculations, particularly in the context of accurately extracting the width of the T_{cc} state from data [77]. Apart from that, we emphasize that the differences between isovector and isoscalar $J^P = 1^+ DD^*$ potentials, attributed to isovector-vector exchanges in Ref. [78], can be naturally explained by the TPE contributions. We stress that the TPE contributions for $D^{(*)}D^{(*)}$ scattering can be largely absorbed into the $O(Q^2)$ contact interactions, with minor residual nonanalytic contributions. This conclusion should also hold for unphysically large pion masses, at least as long as the corrections scaling as $m_\pi^2/p_{\rm typ}^2$ remain suppressed.

ACKNOWLEDGMENTS

We would like to thank Evgeny Epelbaum, Arseniy Filin and Jambul Gegelia for valuable discussions. This work is supported in part by the NSFC and the Deutsche Forschungsgemeinschaft (DFG) through the funds provided to the Sino-German Collaborative Research Center "Symmetries and the Emergence of Structure in QCD" (NSFC Grant No. 11621131001, DFG Grant No. CRC110).

DATA AVAILABILITY

The data supporting this study's findings are available within the article.

APPENDIX A: CALCULATION OF PERTINENT INTEGRALS

1. Calculation of triangle integral

$$I_{\rm tr} = i\int \frac{d^4l}{(2\pi)^4}\frac{l_0}{(l_0-i\epsilon)}\frac{(\boldsymbol{l}+\boldsymbol{q})\cdot\boldsymbol{l}}{[(l+q)^2-m_\pi^2+i\epsilon][l^2-m_\pi^2+i\epsilon]} \tag{A1}$$

Introducing Feynman parameters, shifting $l \to l - qx$, dropping all odd powers of l due to symmetry and using $q^0 = 0$, one finds

$$I_{\rm tr} = i\int_0^1 dx \int \frac{d^3\boldsymbol{l}}{(2\pi)^3}\int \frac{dl_0}{2\pi}\frac{l_0}{(l_0-i\epsilon)} \times \frac{\boldsymbol{l}^2-\boldsymbol{q}^2x(1-x)}{[(l_0)^2-\boldsymbol{l}^2-\boldsymbol{q}^2x(1-x)-m_\pi^2+i\epsilon]^2}. \tag{A2}$$

Executing the l^0-integration with the residue theorem and setting $\epsilon \to 0$,

$$I_{\rm tr} = \frac{i^2}{4}\int_0^1 dx \int \frac{d^3\boldsymbol{l}}{(2\pi)^3}\frac{\boldsymbol{l}^2-\boldsymbol{q}^2x(1-x)}{[\boldsymbol{l}^2+\boldsymbol{q}^2x(1-x)+m_\pi^2]^{3/2}}. \tag{A3}$$

Going to $(D-1)$ -dimensional spherical coordinates and inserting μ,

$$I_{\rm tr} = \frac{-\sqrt{\pi}}{(4\pi)^{D/2}}\frac{\mu^{4-D}}{\Gamma(\frac{D-1}{2})}\int_0^1 dx \times \int_0^\infty dl \frac{l^D - l^{D-2}\boldsymbol{q}^2x(1-x)}{[\boldsymbol{l}^2+\boldsymbol{q}^2x(1-x)+m_\pi^2]^{3/2}}. \tag{A4}$$

Executing the l-integration and inserting $D = 4-\xi$,

$$I_{\rm tr} = \frac{-1}{16\pi^2}\int_0^1 dx\Bigg\{\left(\frac{5}{2}\boldsymbol{q}^2x(1-x)+\frac{3}{2}m_\pi^2\right) \times\left(-\frac{2}{\epsilon}+\gamma_E-1-\ln(4\pi)+\ln\left(\frac{\boldsymbol{q}^2x(1-x)+m_\pi^2}{\mu^2}\right)\right) + 2\boldsymbol{q}^2x(1-x)+m_\pi^2\Bigg\} \tag{A5}$$

Doing the x-integration, one finally obtains

$$\begin{aligned} I_{\rm tr} &= \frac{-1}{16\pi^2}\left\{\left(\frac{5}{12}\boldsymbol{q}^2+\frac{3}{2}m_\pi^2\right)\mathcal{R}-\frac{13}{36}\boldsymbol{q}^2-\frac{m_\pi^2}{3} + \left(\frac{5}{6}\boldsymbol{q}^2+3m_\pi^2\right)\ln\left(\frac{m_\pi}{\mu}\right)+\left(\frac{5}{6}\boldsymbol{q}^2+\frac{4}{3}m_\pi^2\right)L(q)\right\} \\ &= \frac{-\boldsymbol{q}^2}{16\pi^2}\left\{\frac{5}{12}\mathcal{R}-\frac{13}{36}+\frac{5}{6}\ln\left(\frac{m_\pi}{\mu}\right)+\frac{5}{6}L(q)\right\}+\mathcal{O}(\chi^4), \end{aligned} \tag{A6}$$

where $\mathcal{R}$ and $L(q)$ are given by

$$\mathcal{R} = -\frac{2}{\xi} + \gamma_E - 1 - \ln(4\pi). \tag{A7}$$

$$L(q) = \frac{\sqrt{4m_\pi^2 + q^2}}{q} \ln\left(\frac{\sqrt{4m_\pi^2 + q^2} + q}{2m_\pi}\right). \tag{A8}$$

and γ_E is the Euler-Mascheroni constant.

2. Calculation of football integral

$$I_{\rm fb} = i \int \frac{d^4 l}{(2\pi)^4} \frac{(l^0)^2}{[(l+q)^2 - m_\pi^2 + i\epsilon][l^2 - m_\pi^2 + i\epsilon]} \tag{A9}$$

Introducing Feynman parameters, shifting $l \to l - qx$, dropping all odd powers of l due to symmetry and executing the l^0-integration,

$$I_{fb} = \frac{1}{4}\int_0^1 dx \int \frac{d^3\boldsymbol{l}}{(2\pi)^3} \frac{1}{[\boldsymbol{l}^2 + \boldsymbol{q}^2 x(1-x) + m_\pi^2]^{1/2}}. \tag{A10}$$

Going to $(D-1)$-dimensional spherical coordinates and inserting μ,

$$I_{fb} = \frac{\sqrt{\pi}}{(4\pi)^{D/2}} \frac{\mu^{4-D}}{\Gamma(\frac{D-1}{2})} \int_0^1 dx \times \int_0^\infty dl \frac{l^{D-2}}{[\boldsymbol{l}^2 + \boldsymbol{q}^2 x(1-x) + m_\pi^2 + i\epsilon]^{1/2}}. \tag{A11}$$

Executing the l-integration and inserting $D = 4 - \xi$

$$I_{fb} = \frac{1}{32\pi^2}\int_0^1 dx (\boldsymbol{q}^2 x(1-x) + m_\pi^2) \times \left(-\frac{2}{\xi} + \gamma_E - 1 - \ln(4\pi) + \ln\left(\frac{\boldsymbol{q}^2 x(1-x) + m_\pi^2}{\mu^2}\right)\right) \tag{A12}$$

Doing the x-integration, we obtain

$$I_{fb} = \frac{-1}{16\pi^2}\left\{-\left(\frac{\boldsymbol{q}^2}{12} + \frac{m_\pi^2}{2}\right)\mathcal{R} + \frac{5}{36}\boldsymbol{q}^2 + \frac{2m_\pi^2}{3} - \left(\frac{\boldsymbol{q}^2}{6} + m_\pi^2\right)\ln\left(\frac{m_\pi}{\mu}\right) - \left(\frac{\boldsymbol{q}^2}{6} + \frac{4}{6}m_\pi^2\right)L(q)\right\} = \frac{\boldsymbol{q}^2}{96\pi^2}\left\{\frac{\mathcal{R}}{2} - \frac{5}{6} + \ln\left(\frac{m_\pi}{\mu}\right) + L(q)\right\} + \mathcal{O}(\chi^4). \tag{A13}$$

3. Calculation of crossed box integrals

a. $I^{(2)}_{\rm box}$

We encounter the $I^{(2)}_{\rm box}$ integral in the crossed box diagrams contributing to $B\bar{B} \to B\bar{B}$, $B^*\bar{B} \to B^*\bar{B}$, and $B^*\bar{B}^* \to B^*\bar{B}^*$ and accordingly to the $B^{(*)}B^{(*)}$ counterparts. The $I^{(2)}_{\rm box}$ integral is given by

$$I^{(2)}_{\rm box} = i \int \frac{d^4 l}{(2\pi)^4} \frac{(\boldsymbol{q_1}\cdot\boldsymbol{q_2})^2}{(l^0 - i\epsilon)^2[q_2^2 - m_\pi^2 + i\epsilon][q_1^2 - m_\pi^2 + i\epsilon]} \tag{A14}$$

Expanding $q_1^2 = (l^0)^2 - \boldsymbol{q_1}^2$ and $q_2^2 = (l^0)^2 - \boldsymbol{q_2}^2$ and introducing the Feynman parameter x, one finds

$$I^{(2)}_{\rm box} = i\int_0^1 dx \int \frac{d^3\boldsymbol{l}}{(2\pi)^3}(\boldsymbol{q}_1\cdot\boldsymbol{q}_2)^2 \times \int \frac{dl^0}{2\pi}\frac{1}{[l^0 - i\epsilon]^2}\frac{1}{[(l_0)^2 - a^2 + i\epsilon]^2}, \tag{A15}$$

where $a^2 = (\boldsymbol{q_2}^2 - \boldsymbol{q_1}^2)x + \boldsymbol{q_1}^2 + m_\pi^2$. Executing l^0 integration gives

$$I^{(2)}_{\rm box} = \frac{-3}{4}\int_0^1 dx \int \frac{d^3\boldsymbol{l}}{(2\pi)^3}\frac{(\boldsymbol{q_1}\cdot\boldsymbol{q_2})^2}{[(\boldsymbol{q_2}^2 - \boldsymbol{q_1}^2)x + \boldsymbol{q_1}^2 + m_\pi^2]^{5/2}}. \tag{A16}$$

Shifting $\boldsymbol{l} \to \boldsymbol{l} + \boldsymbol{p}$ such that $\boldsymbol{q_1} = \boldsymbol{p} - \boldsymbol{l} \to -\boldsymbol{l}$ and $\boldsymbol{q_2} = \boldsymbol{p}' - \boldsymbol{l} \to -\boldsymbol{l} + \boldsymbol{q}$ with $\boldsymbol{q} = \boldsymbol{p}' - \boldsymbol{p}$,

$$I^{(2)}_{\rm box} = \frac{-3}{4}\int_0^1 dx \int \frac{d^3\boldsymbol{l}}{(2\pi)^3}\frac{(\boldsymbol{l}\cdot(\boldsymbol{l}-\boldsymbol{q}))^2}{[\boldsymbol{l}^2 + (-2\boldsymbol{l}\cdot\boldsymbol{q} + \boldsymbol{q}^2)x + m_\pi^2]^{5/2}}. \tag{A17}$$

Following the same steps as for the above integrals,

$$I^{(2)}_{\rm box} = \frac{-1}{16\pi^2}\int_0^1 dx\Bigg\{\left(\left[-\frac{35}{2}x^2 + \frac{35}{2}x - 1\right]\boldsymbol{q}^2 + \frac{15}{2}m_\pi^2\right)\mathcal{R} + (-22x^2 + 22x - 1)\boldsymbol{q}^2 + 8m_\pi^2 + \frac{2\boldsymbol{q}^4 x^2(1-x)^2}{m_\pi^2 + \boldsymbol{q}^2 x(1-x)} + \left(\left[-\frac{35}{2}x^2 + \frac{35}{2}x - 1\right]\boldsymbol{q}^2 + \frac{15}{2}m_\pi^2\right) \times \ln\left(\frac{\boldsymbol{q}^2 x(1-x) + m_\pi^2}{\mu^2}\right)\Bigg\} \tag{A18}$$

Performing the x-integration, one finally obtains

$$I^{(2)}_{\rm box} = \frac{-1}{16\pi^2}\left\{\left(\frac{23}{12}\boldsymbol{q}^2+\frac{15}{2}m_\pi^2\right)\mathcal{R}+\frac{5}{36}\boldsymbol{q}^2+\frac{8}{3}m_\pi^2 + \left(\frac{23}{6}\boldsymbol{q}^2+15m_\pi^2\right)\ln\left(\frac{m_\pi}{\mu}\right) + \left(\frac{23}{6}\boldsymbol{q}^2+\frac{10}{3}m_\pi^2+\frac{8m_\pi^4}{4m_\pi^2+\boldsymbol{q}^2}\right)L(q)\right\} = \frac{-23\boldsymbol{q}^2}{96\pi^2}\left\{\frac{\mathcal{R}}{2}+\frac{5}{138}+\ln\left(\frac{m_\pi}{\mu}\right)+L(q)\right\}+\mathcal{O}(\chi^4). \tag{A19}$$

4. Calculation of planar box integral

As mentioned earlier, the $I^{(1)}_{\rm box}$ integral splits into a reducible and an irreducible TPE contribution. Because the iterations of the OPE within the Lippmann-Schwinger equation take care of the reducible part, it is omitted here and one gets $I^{(1)}_{\rm box} \to I^{(2)}_{\rm box}$ [74], with the box integrals defined in Eqs. (31) and (33). For the sake of completeness, below we provide a derivation of this result.

The starting point is the planar box integral

$$I^{(1)}_{\rm box} = i\int\frac{d^4l}{(2\pi)^4}\frac{1}{[l^0+i\epsilon][l^0-i\epsilon]} \times\frac{(\boldsymbol{q_2}\cdot\boldsymbol{q_1})^2}{[q_2^2-m_\pi^2+i\epsilon][q_1^2-m_\pi^2+i\epsilon]}. \tag{A20}$$

Expanding $q_1^2=(l^0)^2-\boldsymbol{q_1^2}$ and $q_2^2=(l^0)^2-\boldsymbol{q_2^2}$ and introducing the Feynman parameter x,

$$I^{(1)}_{\rm box} = i\int_0^1 dx\int\frac{d^3\boldsymbol{l}}{(2\pi)^3}(\boldsymbol{q_1}\cdot\boldsymbol{q_2})^2 \times\int\frac{dl^0}{2\pi}\frac{1}{[l^0+i\epsilon][l^0-i\epsilon]}\frac{1}{[(l_0)^2-a^2+i\epsilon]^2}, \tag{A21}$$

where $a^2=(\boldsymbol{q_2^2}-\boldsymbol{q_1^2})x+\boldsymbol{q_1^2}+m_\pi^2$. In contrast to the crossed box integral $I^{(2)}_{\rm box}$, the l^0-integration diverges as $\epsilon\to 0$, and our LO approximation of the heavy-meson propagator produces nonphysical poles. We can avoid this pinch singularity (the singularity is squeezed between $+i\epsilon$ and $-i\epsilon$), by including higher-order corrections to the heavy meson propagator [82]. Specifically, including $\mathcal{O}(Q^2)$ terms, namely the kinetic energies of the heavy mesons, shifts the poles in the heavy mesons propagators, making them distinct and, consequently, avoiding the singularity. This can be achieved by replacing $i\epsilon\to i\zeta$, with

$$i\zeta=\frac{\boldsymbol{k}^2}{2m_B}-\frac{\boldsymbol{l}^2}{2m_B}+i\epsilon, \tag{A22}$$

where k is the on shell momentum of the heavy mesons, $k^2=m_BE$. One finds

$$I^{(1)}_{\rm box} = i\int_0^1 dx\int\frac{d^3\boldsymbol{l}}{(2\pi)^3}(\boldsymbol{q_1}\cdot\boldsymbol{q_2})^2\int\frac{dl^0}{2\pi}\frac{1}{[l^0+i\zeta][l^0-i\zeta]} \times\frac{1}{[(l_0)^2-a^2+i\epsilon]^2}. \tag{A23}$$

Executing l^0-integration,

$$I^{(1)}_{\rm box} = i\int_0^1 dx\int\frac{d^3\boldsymbol{l}}{(2\pi)^3}(\boldsymbol{q_1}\cdot\boldsymbol{q_2})^2\frac{i}{4}\frac{2a-i\zeta}{[i\zeta a^3(a-i\zeta)^2]}. \tag{A24}$$

Expanding the fraction for $a\gg i\zeta$ and dropping terms of order $\mathcal{O}(\zeta)$,

$$I^{(1)}_{\rm box} = i\int_0^1 dx\int\frac{d^3\boldsymbol{l}}{(2\pi)^3}(\boldsymbol{q_1}\cdot\boldsymbol{q_2})^2\frac{i}{4}\left(\frac{3}{a^5}+\frac{2}{i\zeta a^4}+\mathcal{O}(\zeta)\right). \tag{A25}$$

The first term of the expansion is the integral $I^{(2)}_{\rm box}$ evaluated in the previous section. The second term is the iterated OPE, and the dropped term scales as $(i\zeta)/a^6$. Since $i\zeta\sim p^2_{\rm typ}/m_B$ and $a^2\sim p^2_{\rm typ}$, the neglected term is suppressed as $\mathcal{O}(p_{\rm typ}/m_B)\sim\mathcal{O}(\chi^2)$ relative to the leading one.

Inserting $i\zeta=(\boldsymbol{k}^2-\boldsymbol{l}^2+i\epsilon)/2m_B$, one finds

$$I^{(1)}_{\rm box} = I^{(2)}_{\rm box}+\Delta I, \tag{A26}$$

where

$$\Delta I = i^2m_B\int_0^1 dx \times\int\frac{d^3\boldsymbol{l}}{(2\pi)^3}\frac{(\boldsymbol{q_2}\cdot\boldsymbol{q_1})^2}{[\boldsymbol{k}^2-\boldsymbol{l}^2+i\epsilon][(\boldsymbol{q_2^2}-\boldsymbol{q_1^2})x+\boldsymbol{q_1^2}+m_\pi^2]^2} = i^2m_B\int\frac{d^3\boldsymbol{l}}{(2\pi)^3}\frac{(\boldsymbol{q_2}\cdot\boldsymbol{q_1})^2}{[\boldsymbol{k}^2-\boldsymbol{l}^2+i\epsilon][\boldsymbol{q_2^2}+m_\pi^2][\boldsymbol{q_1^2}+m_\pi^2]}, \tag{A27}$$

which is the nonrelativistic version of the twice iterated OPE. Indeed, the iterated potential can be written as [83,84],

$$V^{\rm eff}_{\rm TPE,it}(\boldsymbol{p}',\boldsymbol{p}) = -m_B\int\frac{d^3\boldsymbol{l}}{(2\pi)^3}\frac{V^{\rm eff}_{\rm OPE}(\boldsymbol{p}',\boldsymbol{l})V^{\rm eff}_{\rm OPE}(\boldsymbol{l},\boldsymbol{p})}{[\boldsymbol{k}^2-\boldsymbol{l}^2+i\epsilon]}, \tag{A28}$$

which is in agreement with (A27).

Since, we only consider irreducible contributions, we drop this reducible term and keep track of the irreducible integral $I^2_{\rm box}$ instead. In summary, the treatment of the planar box comes down to sign flip $+i\epsilon\to-i\epsilon$ for one of the heavy meson propagators.

a. Calculation of $B^*\bar{B}^* \to B^*\bar{B}^*$ and $B^*B^* \to B^*B^*$ pertinent loop integrals

The box contributions are identical for the $B^*\bar{B}^* \to B^*\bar{B}^*$ and $B^*B^* \to B^*B^*$ scattering processes. In total, one has eight box diagrams and the resulting contribution is,

$$\begin{aligned} V^{\rm box}_{B^*\bar{B}^*\to B^*\bar{B}^*} &= V_{B_{7.1}} + V_{B_{7.2}} + V_{B_{7.3}} + V_{B_{7.4}} + V_{C_{7.1}} + V_{C_{7.2}} + V_{C_{7.3}} + V_{C_{7.4}} \\ &= \frac{g^4}{16 f_\pi^4}(\epsilon_{1,i}\epsilon^*_{1',k}\epsilon_{2,l}\epsilon^*_{2',n}) i \int \frac{d^4 l}{(2\pi)^4} \frac{[3A - 2(\boldsymbol{\tau}_1\cdot\boldsymbol{\tau}_2)B]}{[l_0 - i\epsilon]^2[q_2^2 - m_\pi^2][q_1^2 - m_\pi^2]} \end{aligned} \tag{A29}$$

where,

$$\begin{aligned} A = {} & 2[(q_2)_k(q_1)_i(q_2)_n(q_1)_l - (q_2)_i(q_1)_k(q_2)_n(q_1)_l - (q_2)_k(q_1)_i(q_2)_l(q_1)_n + (q_2)_i(q_1)_k(q_2)_l(q_1)_n] \\ & + 2\delta_{ik}(\boldsymbol{q_2}\cdot\boldsymbol{q_1})[(q_2)_n(q_1)_l - (q_2)_l(q_1)_n)] \end{aligned} \tag{A30}$$

and

$$B = 2\delta_{ik}\delta_{ln}(\boldsymbol{q_2}\cdot\boldsymbol{q_1})^2 + 2\delta_{ln}(\boldsymbol{q_2}\cdot\boldsymbol{q_1})^2[(q_2)_k(q_1)_i - (q_2)_i(q_1)_k] \tag{A31}$$

The last term in A and the second term in B will vanish, due to tensor decomposition being symmetric. Solving the remaining terms using tensor decomposition,

$$\begin{aligned} V^{\rm box}_{B^*\bar{B}^*\to B^*\bar{B}^*} = {} & \frac{g^4}{4 f_\pi^4}(\epsilon_{1,i}\epsilon^*_{1',k}\epsilon_{2,l}\epsilon^*_{2',n})\Big\{-(\boldsymbol{\tau_1}\cdot\boldsymbol{\tau_2})\delta_{ik}\delta_{ln} I^{(2)}_{\rm box} + \frac{1}{2}[\delta_{il}\delta_{kn} - \delta_{\rm in}\delta_{kl}][I^{(3)}_{\rm box} - I^{(2)}_{\rm box} + \frac{1}{\boldsymbol{q}^2}(I^{(4)}_{\rm box} - I^{(5)}_{\rm box})] \\ & + \frac{3}{4\boldsymbol{q}^4}[q_k q_n \delta_{il} - q_k q_l \delta_{\rm in} + q_i q_l \delta_{kn} - q_i q_n \delta_{kl}][I^{(5)}_{\rm box} - I^{(4)}_{\rm box}]\Big\} \end{aligned} \tag{A32}$$

where,

$$\begin{aligned} I^{(3)}_{\rm box} &= i\int \frac{d^4 l}{(2\pi)^4} \frac{\boldsymbol{q_1}^2\boldsymbol{q_2}^2}{(l^0 - i\epsilon)^2[q_2^2 - m_\pi^2 + i\epsilon][q_1^2 - m_\pi^2 + i\epsilon]}, \qquad I^{(4)}_{\rm box} = i\int \frac{d^4 l}{(2\pi)^4} \frac{\boldsymbol{q_1}^2(\boldsymbol{q_2}\cdot\boldsymbol{q})^2}{(l^0 - i\epsilon)^2[q_2^2 - m_\pi^2 + i\epsilon][q_1^2 - m_\pi^2 + i\epsilon]} \\ I^{(5)}_{\rm box} &= i\int \frac{d^4 l}{(2\pi)^4} \frac{\boldsymbol{q_2}^2(\boldsymbol{q_1}\cdot\boldsymbol{q})^2}{(l^0 - i\epsilon)^2[q_2^2 - m_\pi^2 + i\epsilon][q_1^2 - m_\pi^2 + i\epsilon]} \end{aligned} \tag{A33}$$

We will solve each of the three integral, starting with the $I^{(3)}_{\rm box}$ integral. Expanding $q_1^2 = (l^0)^2 - \boldsymbol{q_1}^2$ and $q_2^2 = (l^0)^2 - \boldsymbol{q_2}^2$, using Feynman parameters and executing the l^0-integration (and setting $\epsilon \to 0$).

$$I^{(3)}_{\rm box} = \frac{-3}{4}\int_0^1 dx \int \frac{d^3\boldsymbol{l}}{(2\pi)^3} \frac{\boldsymbol{q_1}^2\boldsymbol{q_2}^2}{[(\boldsymbol{q_2}^2 - \boldsymbol{q_1}^2)x + \boldsymbol{q_1}^2 + m_\pi^2]^{5/2}} \tag{A34}$$

Shifting $\boldsymbol{l} \to \boldsymbol{l} + \boldsymbol{p}$ such that $\boldsymbol{q_1} = \boldsymbol{p} - \boldsymbol{l} \to -\boldsymbol{l}$ and $\boldsymbol{q_2} = \boldsymbol{p}' - \boldsymbol{l} \to -\boldsymbol{l} + \boldsymbol{q}$ with $\boldsymbol{q} = \boldsymbol{p}' - \boldsymbol{p}$,

$$I^{(3)}_{\rm box} = \frac{-3}{4}\int_0^1 dx \int \frac{d^3\boldsymbol{l}}{(2\pi)^3} \frac{\boldsymbol{l}^2(\boldsymbol{l} - \boldsymbol{q})^2}{[\boldsymbol{l}^2 + (-2\boldsymbol{l}\cdot\boldsymbol{q} + \boldsymbol{q}^2)x + m_\pi^2]^{5/2}}. \tag{A35}$$

Following the same steps as for the earlier integrals, one finds

$$\begin{aligned} I^{(3)}_{\rm box} &= \frac{-1}{16\pi^2}\left\{\left(\frac{15}{2}m_\pi^2 - \frac{1}{12}\boldsymbol{q}^2\right)\mathcal{R} + \frac{1}{4}\boldsymbol{q}^2 + \frac{8}{3}m_\pi^2 + \left(15m_\pi^2 - \frac{1}{6}\boldsymbol{q}^2\right)\ln\left(\frac{m_\pi}{\mu}\right) + \left(\frac{10}{3}m_\pi^2 - \frac{1}{6}\boldsymbol{q}^2 + \frac{8m_\pi^4}{4m_\pi^2 + \boldsymbol{q}^2}\right)L(q)\right\} \\ &= \frac{-\boldsymbol{q}^2}{16\pi^2}\left\{\frac{-1}{12}\mathcal{R} + \frac{1}{4} - \frac{1}{6}\ln\left(\frac{m_\pi}{\mu}\right) - \frac{1}{6}L(q)\right\} + \mathcal{O}(\chi^4) \end{aligned} \tag{A36}$$

One proceeds in a similar manner for the integral $I^4_{\rm box}$

$$I^4_{\rm box} = i\int \frac{d^4l}{(2\pi)^4} \times \int_0^1 dx \frac{\boldsymbol{q_1}^2(\boldsymbol{q}_2\cdot\boldsymbol{q})^2}{(l^0-i\epsilon)^2[(l^0)^2-(\boldsymbol{q_2}^2-\boldsymbol{q_1}^2)x-\boldsymbol{q_1}^2-m_\pi^2+i\epsilon]^2}. \tag{A37}$$

Executing the l^0-integration, setting $\epsilon\to 0$ and shifting $\boldsymbol{l}\to \boldsymbol{l}+\boldsymbol{p}$ such that $\boldsymbol{q_1}=\boldsymbol{p}-\boldsymbol{l}\to -\boldsymbol{l}$ and $\boldsymbol{q_2}=\boldsymbol{p}'-\boldsymbol{l}\to -\boldsymbol{l}+\boldsymbol{q}$,

$$I^4_{\rm box} = i^2\frac{3}{4}\int_0^1 dx\int \frac{d^3\boldsymbol{l}}{(2\pi)^3}\frac{\boldsymbol{l}^2[(\boldsymbol{l}-\boldsymbol{q})\cdot\boldsymbol{q}]^2}{[\boldsymbol{l}^2+(-2\boldsymbol{l}\cdot\boldsymbol{q}+\boldsymbol{q}^2)x+m_\pi^2]^{5/2}} \tag{A38}$$

Solving the l-integration, inserting $D=4-\epsilon$ and doing the x-integration, one finds

$$\begin{aligned} I^{(4)}_{\rm box} &= \frac{-1}{16\pi^2}\boldsymbol{q}^2\left\{\left(\frac{5}{2}m_\pi^2-\frac{7}{12}\boldsymbol{q}^2\right)\mathcal{R}-\frac{7}{36}\boldsymbol{q}^2-\frac{7}{3}m_\pi^2 \right. \\ &\quad +\left(5m_\pi^2-\frac{7}{6}\boldsymbol{q}^2\right)\ln\left(\frac{m_\pi}{\mu}\right) \\ &\quad \left.+\left(\frac{10}{3}m_\pi^2-\frac{7}{6}\boldsymbol{q}^2+\frac{8m_\pi^4}{4m_\pi^2+\boldsymbol{q}^2}\right)L(q)\right\} \\ &= \frac{-\boldsymbol{q}^4}{16\pi^2}\left\{\frac{-7}{12}\mathcal{R}-\frac{7}{36}-\frac{7}{6}\ln\left(\frac{m_\pi}{\mu}\right)-\frac{7}{6}L(q)\right\}+\mathcal{O}(\chi^4) \end{aligned} \tag{A39}$$

Finally, performing the calculations along the lines given above, one finds that the $I^{(5)}_{\rm box}$ integral is given by

$$\begin{aligned} I^{(5)}_{\rm box} &= \frac{-1}{16\pi^2}\boldsymbol{q}^2\left\{\left(\frac{5}{2}m_\pi^2-\frac{1}{4}\boldsymbol{q}^2\right)\mathcal{R}-\frac{1}{12}\boldsymbol{q}^2+3m_\pi^2 \right. \\ &\quad +\left(2m_\pi^2-\frac{1}{6}\boldsymbol{q}^2\right)\ln\left(\frac{m_\pi}{\mu}\right) \\ &\quad \left.+\left(\frac{7}{3}\boldsymbol{q}^2-\frac{8}{3}m_\pi^2+\frac{8m_\pi^4}{4m_\pi^2+\boldsymbol{q}^2}\right)L(q)\right\} \\ &= \frac{-\boldsymbol{q}^4}{16\pi^2}\left\{\frac{-1}{4}\mathcal{R}-\frac{1}{12}-\frac{1}{6}\ln\left(\frac{m_\pi}{\mu}\right)+\frac{7}{3}L(q)\right\}+\mathcal{O}(\chi^4) \end{aligned} \tag{A40}$$

b. $(I^{(6)}_{\rm box})_{\rm in}$

We encounter this integral in $B^*\bar{B}\to B\bar{B}^*$, $B\bar{B}\to B^*\bar{B}^*$ and in the subsequent $B^{(*)}B^{(*)}$ counterparts. The $(I^{(6)}_{\rm box})_{\rm in}$ integral is given by,

$$(I^{(6)}_{\rm box})_{\rm in} = i\int\frac{d^4l}{(2\pi)^4}\frac{\epsilon_{ijs}\epsilon_{nrm}(q_2)_j(q_1)_s(q_2)_r(q_1)_m}{[l_0-i\epsilon]^2[q_2^2-m_\pi^2+i\epsilon][q_1^2-m_\pi^2+i\epsilon]}. \tag{A41}$$

Repeating the same steps as in the earlier cases gives

$$\begin{aligned} &(I^{(6)}_{\rm box})_{\rm in} \\ &= \frac{-3}{4}\mu^{4-D}\int_0^1 dx\int\frac{d^{D-1}\boldsymbol{l}}{(2\pi)^{D-1}}\epsilon_{ijs}\epsilon_{nrm} \\ &\quad\times\frac{[l_j+q_j(x-1)](l_s+q_s s)[l_r+q_r(x-1)](l_m+q_m x)}{[\boldsymbol{l}^2+\boldsymbol{q}^2x(1-x)+m_\pi^2]^{5/2}}. \end{aligned} \tag{A42}$$

Due to antisymmetry of the Levi-Civita tensor, most of the numerator vanishes,

$$\begin{aligned} (I^{(6)}_{\rm box})_{\rm in} &= \frac{-3}{4}\mu^{4-D}\int_0^1 dx \\ &\quad\times\int\frac{d^{D-1}\boldsymbol{l}}{(2\pi)^{D-1}}\frac{\epsilon_{ijs}\epsilon_{nrm}(-l_s q_j)(-l_m q_r)}{[\boldsymbol{l}^2+\boldsymbol{q}^2x(1-x)+m_\pi^2]^{5/2}}. \end{aligned} \tag{A43}$$

Going to $(D-1)$-dimensional spherical coordinates and using $l_i l_j\to\frac{l^2\delta_{ij}}{D-1}$, we get

$$\begin{aligned} (I^{(6)}_{\rm box})_{\rm in} &= \frac{-3\sqrt{\pi}}{(4\pi)^{D/2}}\frac{\mu^{4-D}}{\Gamma(\frac{D-1}{2})}\int_0^1 dx(\delta_{\rm in}\boldsymbol{q}^2-q_i q_n) \\ &\quad\times\int_0^\infty dl\frac{\frac{l^D}{D-1}}{[\boldsymbol{l}^2+\boldsymbol{q}^2x(1-x)+m_\pi^2]^{5/2}}. \end{aligned} \tag{A44}$$

Doing the l- and x- integration and inserting $D=4-\xi$, one finally finds

$$\begin{aligned} (I^{(6)}_{\rm box})_{\rm in} &= \frac{-1}{16\pi^2}(\delta_{\rm in}\boldsymbol{q}^2-q_i q_n) \\ &\quad\times\left\{-\mathcal{R}+1-2L(q)-2\ln\left(\frac{m_\pi}{\mu}\right)\right\}. \end{aligned} \tag{A45}$$

c. $(I^{(7)}_{\rm box})_{ikn}$

We encounter this integral in $B^*\bar{B}\to B^*\bar{B}^*$, $B\bar{B}^*\to B^*\bar{B}^*$ and in the subsequent $B^{(*)}B^{(*)}$ counterparts. The $(I^{(7)}_{\rm box})_{ikn}$ integral is given by,

$$\begin{aligned} (I^{(7)}_{\rm box})_{ikn} &= i\int\frac{d^4l}{(2\pi)^4} \\ &\quad\times\frac{((q_2)_k(q_1)_i-(q_2)_i(q_1)_k)\epsilon_{\rm num}(q_2)_u(q_1)_m}{[l_0-i\epsilon]^2[q_2^2-m_\pi^2][q_1^2-m_\pi^2]} \end{aligned} \tag{A46}$$

Introducing Feynman parameters, executing the l^0-integration, and shifting $\boldsymbol{l} \to \boldsymbol{l} + \boldsymbol{p}$ such that $\boldsymbol{q_1} = \boldsymbol{p} - \boldsymbol{l} \to -\boldsymbol{l}$ and $\boldsymbol{q_2} = \boldsymbol{p}' - \boldsymbol{l} \to -\boldsymbol{l} + \boldsymbol{q}$ with $\boldsymbol{q} = \boldsymbol{p}' - \boldsymbol{p}$:

$$(I^{(7)}_{\text{box}})_{ikn} = \frac{-3}{4}\int_0^1 dx \int \frac{d^3\boldsymbol{l}}{(2\pi)^3} \times \frac{((l-q)_k(l)_i - (l-q)_i(l)_k)\epsilon_{\text{num}}(l-q)_u(l)_m}{[\boldsymbol{l}^2 + (-2\boldsymbol{l}\cdot\boldsymbol{q} + \boldsymbol{q}^2)x + m_\pi^2]^{5/2}}. \tag{A47}$$

All terms proportional to $\epsilon_{\text{num}} l_u l_m$ or $\epsilon_{\text{num}} q_u q_m$ and every term of odd power in l vanishes due to symmetry resulting in

$$(I^{(7)}_{\text{box}})_{ikn} = \frac{-3}{4}\mu^{4-D}\int_0^1 dx \times \int \frac{d^{D-1}\boldsymbol{l}}{(2\pi)^{D-1}} \frac{(l_k q_i - l_i q_k)\epsilon_{\text{num}}(-l_m q_u)}{[\boldsymbol{l}^2 + (-2\boldsymbol{l}\cdot\boldsymbol{q} + \boldsymbol{q}^2)x + m_\pi^2]^{5/2}}. \tag{A48}$$

Solving the remaining integral like in the earlier integral yields

$$(I^{(7)}_{\text{box}})_{ikn} = \frac{-1}{16\pi^2}(\epsilon_{nku} q_u q_i - \epsilon_{niu} q_u q_k) \times \left\{-\mathcal{R} + 1 - 2L(q) - 2\ln\left(\frac{m_\pi}{\mu}\right)\right\}. \tag{A49}$$

APPENDIX B: PARTIAL WAVE PROJECTORS

In this section, we have presented the complete set of partial wave projectors used for calculating the potentials [40]. In what follows, ϵ refers to the polarization vector of the heavy vector meson and $\boldsymbol{n} = \boldsymbol{p}/p$.

$$P(B\bar{B}(^1S_0)) = 1 \tag{B1}$$

$$P(B^*\bar{B}^*(^1S_0)) = \frac{1}{\sqrt{3}}(\boldsymbol{\epsilon_1}\cdot\boldsymbol{\epsilon_2}) \tag{B2}$$

$$P(B^*\bar{B}^*(^5D_0)) = -\sqrt{\frac{3}{8}} S_{xy} v_{xy} \tag{B3}$$

$$P(B\bar{B}^*(^3S_1))_x = \epsilon_{2,x} \tag{B4}$$

$$P(B^*\bar{B}(^3S_1))_h = \epsilon_{1,h} \tag{B5}$$

$$P(B\bar{B}^*(^3D_1))_x = -\frac{3}{\sqrt{2}}\epsilon_{2,y} v_{xy} \tag{B6}$$

$$P(B^*\bar{B}(^3D_1))_x = -\frac{3}{\sqrt{2}}\epsilon_{1,y} v_{xy} \tag{B7}$$

$$P(B^*\bar{B}^*(^5D_1))_h = -\frac{\sqrt{3}}{2} i\epsilon_{hxj} S_{xy} v_{jy} \tag{B8}$$

$$P(B^*\bar{B}^*(^3S_1))_x = A_x \tag{B9}$$

$$P(B^*\bar{B}^*(^3D_1))_h = -\frac{3}{\sqrt{2}} A_x v_{hx} \tag{B10}$$

$$P(B\bar{B}(^1D_2))_{xy} = -\sqrt{\frac{15}{2}} v_{xy} \tag{B11}$$

$$P(B\bar{B}^*(^3D_2))_{zy} = -\frac{\sqrt{5}}{2} i\epsilon_{2,h}(\epsilon_{zhx} v_{xy} + \epsilon_{yhx} v_{xz}) \tag{B12}$$

$$P(B^*\bar{B}^*(^5S_2))_{xy} = \frac{1}{2} S_{xy} \tag{B13}$$

$$P(B^*\bar{B}^*(^1D_2))_{xy} = -\sqrt{\frac{5}{2}}(\boldsymbol{\epsilon_1}\cdot\boldsymbol{\epsilon_2}) v_{xy} \tag{B14}$$

$$P(B^*\bar{B}^*(^5D_2))_{zy} = -\sqrt{\frac{45}{56}}\left(S_{zx} v_{xy} + S_{yx} v_{xz} - \frac{2}{3}\delta_{xy} S_{lx} v_{lx}\right) \tag{B15}$$

$$P(B^*\bar{B}^*(^5G_2))_{zw} = \sqrt{\frac{175}{32}} S_{xy} v_{xyzw} \tag{B16}$$

where,

$$v_{xy} = n_x n_y - \frac{1}{3}\delta_{xy} \tag{B17}$$

$$S_{xy} = \epsilon_{1,x}\epsilon_{2,y} + \epsilon_{1,y}\epsilon_{2,x} - \frac{2}{3}\delta_{xy}(\boldsymbol{\epsilon_1}\cdot\boldsymbol{\epsilon_2}) \tag{B18}$$

$$A_x = \frac{i}{\sqrt{2}}\epsilon_{xyz}\epsilon_{1,y}\epsilon_{2,z} \tag{B19}$$

$$v_{xyzw} = n_x n_y n_z n_w - \frac{1}{7}(n_x n_y \delta_{zw} + n_x n_z \delta_{yw} + n_x n_w \delta_{yz} + n_y n_z \delta_{xw} + n_y n_w \delta_{xz} + n_z n_w \delta_{xy}) + \frac{1}{35}(\delta_{xy}\delta_{zw} + \delta_{xz}\delta_{yw} + \delta_{xw}\delta_{yz}) \tag{B20}$$

The projectors are normalized as

$$\int \frac{d\Omega_n}{4\pi} P^\dagger(\alpha, \boldsymbol{n}) P(\alpha, \boldsymbol{n}) = 2J + 1 \tag{B21}$$

APPENDIX C: THE EFFECTIVE POTENTIALS

In this section, all the OPE and TPE potentials to $B^{(*)}\bar{B}^{(*)} \to B^{(*)}\bar{B}^{(*)}$ and $B^{(*)}B^{(*)} \to B^{(*)}B^{(*)}$ scattering are presented.

1. $B\bar{B} \to B\bar{B}$

$$V_{\mathrm{OPE}}(B\bar{B} \to B\bar{B}) = 0 \tag{C1}$$

$$\begin{aligned} V_{\mathrm{TPE}}(B\bar{B} \to B\bar{B}) &= \frac{1}{2f_\pi^4}(\boldsymbol{\tau_1}\cdot\boldsymbol{\tau_2})\left(I_{fb} - \frac{g^4}{2}I^{(2)}_{\mathrm{box}}\right) \\ &= \frac{\boldsymbol{q}^2}{16\pi^2 f_\pi^4}(\boldsymbol{\tau_1}\cdot\boldsymbol{\tau_2})\left\{\mathcal{R}\left[\frac{23}{48}g^4 + \frac{1}{24}\right] + \left(\frac{5}{144}g^4 - \frac{5}{72}\right) + \left(\frac{23}{24}g^4 + \frac{1}{12}\right)\ln\left(\frac{m_\pi}{\mu}\right) + L(q)\left(\frac{23}{24}g^4 + \frac{1}{12}\right)\right\} \end{aligned} \tag{C2}$$

2. $B\bar{B} \to B^*\bar{B}^*$

$$V_{\mathrm{OPE}}(B\bar{B} \to B^*\bar{B}^*) = -\frac{g^2}{4f_\pi^2}(\boldsymbol{\tau_1}\cdot\boldsymbol{\tau_2})(\epsilon^*_{1',k}\epsilon^*_{2',n})\frac{q_k q_n}{\boldsymbol{q}^2 + m_\pi^2} \tag{C3}$$

$$V_{\mathrm{TPE}}(B\bar{B} \to B^*\bar{B}^*) = \frac{3}{128\pi^2 f_\pi^4}g^4(\epsilon^*_{1',k}\epsilon^*_{2',n})(\delta_{kn}\boldsymbol{q}^2 - q_k q_n)\left\{-\mathcal{R} + 1 - 2L(q) - 2\ln\left(\frac{m_\pi}{\mu}\right)\right\} \tag{C4}$$

3. $B^*\bar{B} \to B^*\bar{B}$

$$V_{\mathrm{OPE}}(B^*\bar{B} \to B^*\bar{B}) = 0 \tag{C5}$$

$$V_{\mathrm{TPE}}(B^*\bar{B} \to B^*\bar{B}) = (\epsilon^*_{1'}\cdot\epsilon_1)V_{\mathrm{TPE}}(B\bar{B} \to B\bar{B}) \tag{C6}$$

4. $B^*\bar{B} \to B\bar{B}^*$

$$V_{\mathrm{OPE}}(B^*\bar{B} \to B\bar{B}^*) = -\frac{g^2}{4f_\pi^2}(\boldsymbol{\tau_1}\cdot\boldsymbol{\tau_2})(\epsilon^*_{2',n}\epsilon_{1,i})\frac{q_i q_n}{\boldsymbol{q}^2 + m_\pi^2} \tag{C7}$$

$$V_{\mathrm{TPE}}(B^*\bar{B} \to B\bar{B}^*) = \frac{3}{128\pi^2 f_\pi^4}g^4(\epsilon^*_{2',n}\epsilon_{1,i})(\delta_{\mathrm{in}}\boldsymbol{q}^2 - q_i q_n)\left\{-\mathcal{R} + 1 - 2L(q) - 2\ln\left(\frac{m_\pi}{\mu}\right)\right\} \tag{C8}$$

5. $B^*\bar{B} \to B^*\bar{B}^*$

$$V_{\mathrm{OPE}}(B^*\bar{B} \to B^*\bar{B}^*) = i\frac{g^2}{4f_\pi^2}(\boldsymbol{\tau_1}\cdot\boldsymbol{\tau_2})\epsilon_{ikr}(\epsilon_{1,i}\epsilon^*_{1',k}\epsilon^*_{2',n})\frac{q_r q_n}{\boldsymbol{q}^2 + m_\pi^2} \tag{C9}$$

$$V_{\mathrm{TPE}}(B^*\bar{B} \to B^*\bar{B}^*) = i\frac{3}{128\pi^2 f_\pi^4}g^4(\epsilon_{1,i}\epsilon^*_{1',k}\epsilon^*_{2',n})(\epsilon_{nku}q_u q_i - \epsilon_{niu}q_u q_k)\left\{-\mathcal{R} + 1 - 2L(q) - 2\ln\left(\frac{m_\pi}{\mu}\right)\right\} \tag{C10}$$

6. $B\bar{B}^* \to B^*\bar{B}^*$

$$V_{\mathrm{OPE}}(B\bar{B}^* \to B^*\bar{B}^*) = i\frac{g^2}{4f_\pi^2}(\boldsymbol{\tau_1}\cdot\boldsymbol{\tau_2})\epsilon_{lns}(\epsilon_{2,l}\epsilon^*_{1',k}\epsilon^*_{2',n})\frac{q_k q_s}{\boldsymbol{q}^2 + m_\pi^2} \tag{C11}$$

$$V_{\mathrm{TPE}}(B\bar{B}^* \to B^*\bar{B}^*) = i\frac{3}{128\pi^2 f_\pi^4}g^4(\epsilon_{2,l}\epsilon^*_{1',k}\epsilon^*_{2',n})(\epsilon_{knu}q_u q_l - \epsilon_{klu}q_u q_n)\left\{-\mathcal{R} + 1 - 2L(q) - 2\ln\left(\frac{m_\pi}{\mu}\right)\right\} \tag{C12}$$

7. $B^*\bar{B}^* \to B^*\bar{B}^*$

$$V_{\rm OPE}(B^*\bar{B}^* \to B^*\bar{B}^*) = \frac{g^2}{4f_\pi^2}(\boldsymbol{\tau_1}\cdot\boldsymbol{\tau_2})\epsilon_{ikr}\epsilon_{lns}(\epsilon_{1,i}\epsilon^*_{1',k}\epsilon_{2,l}\epsilon^*_{2',n})\frac{q_r q_s}{\boldsymbol{q}^2+m_\pi^2} \tag{C13}$$

$$\begin{aligned} V_{\rm TPE}(B^*\bar{B}^* \to B^*\bar{B}^*) = {} & \frac{\boldsymbol{q}^2}{16\pi^2 f_\pi^4}(\boldsymbol{\tau_1}\cdot\boldsymbol{\tau_2})(\epsilon_1\cdot\epsilon^*_{1'})(\epsilon_2\cdot\epsilon^*_{2'})\left\{\mathcal{R}\left[\frac{23}{48}g^4+\frac{1}{24}\right]+\left(\frac{5}{144}g^4-\frac{5}{72}\right)\right. \\ & \left.+\ln\left(\frac{m_\pi}{\mu}\right)\left(\frac{23}{24}g^4+\frac{1}{12}\right)+L(q)\left(\frac{23}{24}g^4+\frac{1}{12}\right)\right\} \\ & +\frac{\boldsymbol{q}^2 g^4}{128\pi^2 f_\pi^4}(\epsilon_{1,i}\epsilon^*_{1',k}\epsilon_{2,l}\epsilon^*_{2',n})(\delta_{\rm in}\delta_{kl}-\delta_{il}\delta_{kn})\left\{\frac{-7}{3}\mathcal{R}-5\ln\left(\frac{m_\pi}{\mu}\right)-\frac{15}{2}L(q)\right\} \\ & +\frac{g^4}{16\pi^2 f_\pi^4}(\epsilon_{1,i}\epsilon^*_{1',k}\epsilon_{2,l}\epsilon^*_{2',n})[q_k q_n\delta_{il}-q_k q_l\delta_{\rm in}+q_i q_l\delta_{kn}-q_i q_n\delta_{kl}] \\ & \times\frac{3}{16}\left\{2\mathcal{R}-2+4\ln\left(\frac{m_\pi}{\mu}\right)+4L(q)\right\} \end{aligned} \tag{C14}$$

8. $B\bar{B}^* \to B\bar{B}$

$$V_{\rm OPE}(B\bar{B}^* \to B\bar{B}) = V_{\rm TPE}(B\bar{B}^* \to B\bar{B}) = 0 \tag{C15}$$

9. $BB \to BB$

$$V_{\rm OPE}(BB \to BB) = 0 \tag{C16}$$

$$\begin{aligned} V_{\rm TPE}(BB \to BB) &= \frac{1}{2f_\pi^4}(\boldsymbol{\tau_1}\cdot\boldsymbol{\tau_2})\left(-I_{fb}+g^2 I_{\rm tr}-\frac{g^4}{2}I^{(2)}_{\rm box}\right) \\ &= \frac{\boldsymbol{q}^2}{16\pi^2 f_\pi^4}(\boldsymbol{\tau_1}\cdot\boldsymbol{\tau_2})\left\{\mathcal{R}\left[\frac{23}{48}g^4-\frac{5}{24}g^2-\frac{1}{24}\right]+\left(\frac{5}{144}g^4+\frac{13}{72}g^2+\frac{5}{72}\right)+\ln\left(\frac{m_\pi}{\mu}\right)\left(\frac{23}{24}g^4-\frac{5}{12}g^2-\frac{1}{12}\right)\right. \\ &\quad \left.+L(q)\left(\frac{23}{24}g^4-\frac{5}{12}g^2-\frac{1}{12}\right)\right\} \end{aligned} \tag{C17}$$

10. $BB \to B^*B^*$

$$V_{\rm OPE}(BB \to B^*B^*) = \frac{g^2}{4f_\pi^2}(\boldsymbol{\tau_1}\cdot\boldsymbol{\tau_2})(\epsilon^*_{1',k}\epsilon^*_{2',n})\frac{q_k q_n}{\boldsymbol{q}^2+m_\pi^2} \tag{C18}$$

$$V_{\rm TPE}(BB \to B^*B^*) = \frac{3}{128\pi^2 f_\pi^4}g^4(\epsilon^*_{1',k}\epsilon^*_{2',n})(\delta_{kn}\boldsymbol{q}^2-q_k q_n)\left\{-\mathcal{R}+1-2L(q)-2\ln\left(\frac{m_\pi}{\mu}\right)\right\} \tag{C19}$$

11. $B^*B \to B^*B$

$$V_{\rm OPE}(B^*B \to B^*B) = 0 \tag{C20}$$

$$V_{\rm TPE}(B^*B \to B^*B) = (\epsilon^*_{1'}\cdot\epsilon_1)V_{\rm TPE}(BB \to BB) \tag{C21}$$

12. $B^*B \to BB^*$

$$V_{\rm OPE}(B^*B \to BB^*) = \frac{g^2}{4f_\pi^2}(\boldsymbol{\tau_1}\cdot\boldsymbol{\tau_2})(\epsilon^*_{2',n}\epsilon_{1,i})\frac{q_iq_n}{\boldsymbol{q}^2+m_\pi^2} \tag{C22}$$

$$V_{\rm TPE}(B^*B \to BB^*) = \frac{3}{128\pi^2 f_\pi^4}g^4(\epsilon^*_{2',n}\epsilon_{1,i})(\delta_{\rm in}\boldsymbol{q}^2 - q_iq_n)\left\{-\mathcal{R}+1-2L(q)-2\ln\left(\frac{m_\pi}{\mu}\right)\right\} \tag{C23}$$

13. $B^*B \to B^*B^*$

$$V_{\rm OPE}(B^*B \to B^*B^*) = -i\frac{g^2}{4f_\pi^2}(\boldsymbol{\tau_1}\cdot\boldsymbol{\tau_2})\epsilon_{ikr}(\epsilon_{1,i}\epsilon^*_{1',k}\epsilon^*_{2',n})\frac{q_rq_n}{\boldsymbol{q}^2+m_\pi^2} \tag{C24}$$

$$V_{\rm TPE}(B^*B \to B^*B^*) = i\frac{3}{128\pi^2 f_\pi^4}g^4(\epsilon_{1,i}\epsilon^*_{1',k}\epsilon^*_{2',n})(\epsilon_{nku}q_uq_i - \epsilon_{niu}q_uq_k)\left\{-\mathcal{R}+1-2L(q)-2\ln\left(\frac{m_\pi}{\mu}\right)\right\} \tag{C25}$$

14. $BB^* \to B^*B^*$

$$V_{\rm OPE}(BB^* \to B^*B^*) = -i\frac{g^2}{4f_\pi^2}(\boldsymbol{\tau_1}\cdot\boldsymbol{\tau_2})\epsilon_{lns}(\epsilon_{2,l}\epsilon^*_{1',k}\epsilon^*_{2',n})\frac{q_kq_s}{\boldsymbol{q}^2+m_\pi^2} \tag{C26}$$

$$V_{\rm TPE}(BB^* \to B^*B^*) = i\frac{3}{128\pi^2 f_\pi^4}g^4(\epsilon_{2,l}\epsilon^*_{1',k}\epsilon^*_{2',n})(\epsilon_{knu}q_uq_l - \epsilon_{klu}q_uq_n)\left\{-\mathcal{R}+1-2L(q)-2\ln\left(\frac{m_\pi}{\mu}\right)\right\} \tag{C27}$$

15. $B^*B^* \to B^*B^*$

$$V_{\rm OPE}(B^*B^* \to B^*B^*) = -\frac{g^2}{4f_\pi^2}(\boldsymbol{\tau_1}\cdot\boldsymbol{\tau_2})\epsilon_{ikr}\epsilon_{lns}(\epsilon_{1,i}\epsilon^*_{1',k}\epsilon_{2,l}\epsilon^*_{2',n})\frac{q_rq_s}{\boldsymbol{q}^2+m_\pi^2} \tag{C28}$$

$$\begin{aligned}V_{\rm TPE}(B^*B^* \to B^*B^*) = {}& \frac{\boldsymbol{q}^2}{16\pi^2 f_\pi^4}(\boldsymbol{\tau_1}\cdot\boldsymbol{\tau_2})(\epsilon_1\cdot\epsilon^*_{1'})(\epsilon_2\cdot\epsilon^*_{2'})\left\{\mathcal{R}\left[\frac{23}{48}g^4-\frac{5}{24}g^2-\frac{1}{24}\right]+\left(\frac{5}{144}g^4+\frac{13}{72}g^2+\frac{5}{72}\right)\right.\\ &\left.+\ln\left(\frac{m_\pi}{\mu}\right)\left(\frac{23}{24}g^4-\frac{5}{12}g^2-\frac{1}{12}\right)+L(q)\left(\frac{23}{24}g^4-\frac{5}{12}g^2-\frac{1}{12}\right)\right\}\\ &+\frac{\boldsymbol{q}^2g^4}{128\pi^2 f_\pi^4}(\epsilon_{1,i}\epsilon^*_{1',k}\epsilon_{2,l}\epsilon^*_{2',n})(\delta_{\rm in}\delta_{kl}-\delta_{il}\delta_{kn})\left\{\frac{-7}{3}\mathcal{R}-5\ln\left(\frac{m_\pi}{\mu}\right)-\frac{15}{2}L(q)\right\}\\ &+\frac{g^4}{16\pi^2 f_\pi^4}(\epsilon_{1,i}\epsilon^*_{1',k}\epsilon_{2,l}\epsilon^*_{2',n})[q_kq_n\delta_{il}-q_kq_l\delta_{\rm in}+q_iq_l\delta_{kn}-q_iq_n\delta_{kl}]\\ &\times\frac{3}{16}\left\{2\mathcal{R}-2+4\ln\left(\frac{m_\pi}{\mu}\right)+4L(q)\right\}\end{aligned} \tag{C29}$$

16. $BB^* \to BB$

$$V_{\rm OPE}(BB^* \to BB) = V_{\rm TPE}(BB^* \to BB) = 0 \tag{C30}$$

APPENDIX D: PARTIAL WAVE DECOMPOSITION

Here, we present the partial wave projected potentials for the rest of the channels, apart from with $J^{PC} = 0^{++}$, which is given in the main text.

1. $J^{PC} = 1^{++}$

$$V_{\rm CT}^{1^{++},I} = \begin{pmatrix} \mathcal{C}_d^I + \mathcal{C}_f^I + (\mathcal{D}_d^I + \mathcal{D}_f^I)(p^2 + p'^2) & -\mathcal{D}_{SD}^I p'^2 & -\sqrt{3}\mathcal{D}_{SD}^I p'^2 \\ -\mathcal{D}_{SD}^I p'^2 & 0 & 0 \\ -\sqrt{3}\mathcal{D}_{SD}^I p^2 & 0 & 0 \end{pmatrix} \tag{D1}$$

$$V_{\rm OPE}^{1^{++}} = -\frac{g^2}{4f_\pi^2}(\boldsymbol{\tau_1}\cdot\boldsymbol{\tau_2}) \begin{pmatrix} \frac{1}{3}Q_2 & \frac{1}{\sqrt{18}}(3Q_{n'} - Q_2) & \frac{7}{18\sqrt{6}}(3Q_{n'} - Q_2) \\ \frac{1}{\sqrt{18}}(3Q_n - Q_2) & -\frac{1}{6}(V_{\rm OPE}^{1^{++}})_{22} & 0 \\ \frac{7}{18\sqrt{6}}(3Q_n - Q_2) & 0 & \frac{5}{162}(Q_{x^2} + Q_x) \end{pmatrix} \tag{D2}$$

$$(V_{\rm OPE}^{1^{++}})_{22} = 3Q_{n'} + 3Q_n - 9Q_x - Q_2 \tag{D3}$$

$$V_{\rm TPE}^{1^{++}} = \frac{1}{16\pi^2 f_\pi^4} \begin{pmatrix} (V_{\rm TPE}^{1^{++}})_{11} & \frac{3}{8\sqrt{2}}g^4(V_{\rm TPE}^{1^{++}})_{12} & \frac{9}{4\sqrt{24}}g^4(V_{\rm TPE}^{1^{++}})_{13} \\ \frac{3}{8\sqrt{2}}g^4(V_{\rm TPE}^{1^{++}})_{21} & (V_{\rm TPE}^{1^{++}})_{22} & \frac{3\sqrt{3}}{8}g^4(V_{\rm TPE}^{1^{++}})_{23} \\ \frac{9}{4\sqrt{24}}g^4(V_{\rm TPE}^{1^{++}})_{31} & \frac{3\sqrt{3}}{8}g^4(V_{\rm TPE}^{1^{++}})_{32} & (V_{\rm TPE}^{1^{++}})_{33} \end{pmatrix} \tag{D4}$$

where,

$$(V_{\rm TPE}^{1^{++}})_{11} = \bar{S}_0 + \frac{g^4}{4}\left\{(p'^2 + p^2)\left[-\mathcal{R} + 1 - 2\ln\left(\frac{m_\pi}{\mu}\right)\right] - 2R_2(p', p)\right\} \tag{D5}$$

$$(V_{\rm TPE}^{1^{++}})_{12} = (V_{\rm TPE}^{1^{++}})_{13} = \frac{2}{3}(p'^2)\left[-\mathcal{R} + 1 - 2\ln\left(\frac{m_\pi}{\mu}\right)\right] + \frac{2}{3}R_2(p', p) - 2R_{n'}(p', p) \tag{D6}$$

$$(V_{\rm TPE}^{1^{++}})_{21} = (V_{\rm TPE}^{1^{++}})_{31} = \frac{2}{3}(p^2)\left[-\mathcal{R} + 1 - 2\ln\left(\frac{m_\pi}{\mu}\right)\right] + \frac{2}{3}R_2(p', p) - 2R_n(p', p) \tag{D7}$$

$$(V_{\rm TPE}^{1^{++}})_{22} = \bar{S}_2 + g^4\frac{3}{8}\left\{R_0(p', p) - 3R_{2x}(p', p) + 3R_x(p', p) - R_{n'}(p', p) - R_n(p', p) + \frac{1}{3}R_2(p', p)\right\} \tag{D8}$$

$$(V_{\rm TPE}^{1^{++}})_{23} = (V_{\rm TPE}^{1^{++}})_{32} = \frac{2}{3}R_2(p', p) + 3R_x(p', p) - R_{n'}(p', p) - R_n(p', p) - R_{x^2}(p', p) \tag{D9}$$

$$(V_{\rm TPE}^{1^{++}})_{33} = 7\bar{S}_2 + \frac{g^4}{4}\left\{\frac{45}{2}R_2(p', p) - \frac{135}{2}R_{x^2}(p', p) - \frac{7}{12}(15R_n(p', p) + 15R_{n'}(p', p) + 8R_2(p', p) - 45R_x(p', p) - 39R_{x^2}(p', p))\right\} \tag{D10}$$

2. $J^{PC} = 1^{+-}$

$$V_{\mathrm{CT}}^{1^{+-},I} = \begin{pmatrix} \mathcal{C}_d^I + \mathcal{D}_d^I(p^2+p'^2) & \mathcal{D}_{SD}^I p'^2 & \mathcal{C}_f^I + \mathcal{D}_f^I(p^2+p'^2) & \mathcal{D}_{SD}^I p'^2 \\ \mathcal{D}_{SD}^I p^2 & 0 & \mathcal{D}_{SD}^I p^2 & 0 \\ \mathcal{C}_f^I + \mathcal{D}_f^I(p^2+p'^2) & \mathcal{D}_{SD}^I p'^2 & \mathcal{C}_d^I + \mathcal{D}_d^I(p^2+p'^2) & \mathcal{D}_{SD}^I p'^2 \\ \mathcal{D}_{SD}^I p^2 & 0 & \mathcal{D}_{SD}^I p^2 & 0 \end{pmatrix} \tag{D11}$$

$$V_{\mathrm{OPE}}^{1^{+-}} = -\frac{g^2}{4f_\pi^2}(\tau_1\cdot\tau_2)\begin{pmatrix} -\frac{1}{3}Q_2 & \frac{1}{\sqrt{18}}(3Q_{n'}-Q_2) & \frac{2}{3}Q_2 & \frac{1}{\sqrt{18}}(3Q_{n'}-Q_2) \\ \frac{1}{\sqrt{18}}(3Q_n-Q_2) & -\frac{1}{6}(V_{\mathrm{OPE}}^{1^{+-}})_{22} & \frac{1}{\sqrt{18}}(3Q_n-Q_2) & (V_{\mathrm{OPE}}^{1^{+-}})_{24} \\ \frac{2}{3}Q_2 & \frac{1}{\sqrt{18}}(3Q_{n'}-Q_2) & -\frac{1}{3}Q_2 & \frac{1}{\sqrt{18}}(3Q_{n'}-Q_2) \\ \frac{1}{\sqrt{18}}(3Q_n-Q_2) & (V_{\mathrm{OPE}}^{1^{+-}})_{24} & \frac{1}{\sqrt{18}}(3Q_n-Q_2) & -\frac{1}{6}(V_{\mathrm{OPE}}^{1^{+-}})_{22} \end{pmatrix} \tag{D12}$$

where,

$$(V_{\mathrm{OPE}}^{1^{+-}})_{22} = 3Q_n(p',p) + 3Q_{n'}(p',p) - 9Q_x(p',p) - Q_{x^2}(p',p) \tag{D13}$$

$$(V_{\mathrm{OPE}}^{1^{+-}})_{24} = \frac{1}{2}Q_n(p',p) + \frac{1}{2}Q_{n'}(p',p) - \frac{3}{2}Q_x(p',p) + \frac{3}{2}Q_{x^2}(p',p) - \frac{2}{3}Q_2(p',p) \tag{D14}$$

$$V_{\mathrm{TPE}}^{1^{+-}} = \frac{1}{16\pi^2 f_\pi^4}\begin{pmatrix} (V_{\mathrm{TPE}}^{1^{+-}})_{11} & \frac{-3}{8\sqrt{2}}g^4(V_{\mathrm{TPE}}^{1^{+-}})_{12} & (2g^4)(V_{\mathrm{TPE}}^{1^{+-}})_{13} & \frac{-3}{8\sqrt{2}}g^4(V_{\mathrm{TPE}}^{1^{+-}})_{14} \\ \frac{-3}{8\sqrt{2}}g^4(V_{\mathrm{TPE}}^{1^{+-}})_{21} & (V_{\mathrm{TPE}}^{1^{+-}})_{22} & \frac{-3}{8\sqrt{2}}g^4(V_{\mathrm{TPE}}^{1^{+-}})_{23} & \frac{1}{4}g^4(V_{\mathrm{TPE}}^{1^{+-}})_{24} \\ (2g^4)(V_{\mathrm{TPE}}^{1^{+-}})_{31} & \frac{-3}{8\sqrt{2}}g^4(V_{\mathrm{TPE}}^{1^{+-}})_{32} & (V_{\mathrm{TPE}}^{1^{+-}})_{33} & \frac{1}{16\sqrt{2}}g^4(V_{\mathrm{TPE}}^{1^{+-}})_{34} \\ \frac{-3}{8\sqrt{2}}g^4(V_{\mathrm{TPE}}^{1^{+-}})_{41} & \frac{1}{4}g^4(V_{\mathrm{TPE}}^{1^{+-}})_{42} & \frac{1}{16\sqrt{2}}g^4(V_{\mathrm{TPE}}^{1^{+-}})_{43} & (V_{\mathrm{TPE}}^{1^{+-}})_{44} \end{pmatrix} \tag{D15}$$

where,

$$(V_{\mathrm{TPE}}^{1^{+-}})_{11} = \bar{S}_0 - \frac{g^4}{4}\left\{(p'^2+p^2)\left[-\mathcal{R}+1-2\ln\left(\frac{m_\pi}{\mu}\right)\right] - 2R_2(p',p)\right\} \tag{D16}$$

$$(V_{\mathrm{TPE}}^{1^{+-}})_{12} = (V_{\mathrm{TPE}}^{1^{+-}})_{14} = (V_{\mathrm{TPE}}^{1^{+-}})_{32} = \frac{2}{3}(p'^2)\left[-\mathcal{R}+1-2\ln\left(\frac{m_\pi}{\mu}\right)\right] + \frac{2}{3}R_2(p',p) - 2R_{n'}(p',p) \tag{D17}$$

$$(V_{\mathrm{TPE}}^{1^{+-}})_{13} = (V_{\mathrm{TPE}}^{1^{+-}})_{31} = \frac{1}{4}(p'^2+p^2)\left[-\mathcal{R}+1-2\ln\left(\frac{m_\pi}{\mu}\right)\right] - 2R_2(p',p) \tag{D18}$$

$$(V_{\mathrm{TPE}}^{1^{+-}})_{21} = (V_{\mathrm{TPE}}^{1^{+-}})_{23} = (V_{\mathrm{TPE}}^{1^{+-}})_{41} = \frac{2}{3}(p^2)\left[-\mathcal{R}+1-2\ln\left(\frac{m_\pi}{\mu}\right)\right] + \frac{2}{3}R_2(p',p) - 2R_n(p',p) \tag{D19}$$

$$(V_{\mathrm{TPE}}^{1^{+-}})_{22} = \bar{S}_2 - g^4\frac{3}{8}\left\{R_0(p',p) - 3R_{2x}(p',p) + 3R_x(p',p) - R_{n'}(p',p) - R_n(p',p) + \frac{1}{3}R_2(p',p)\right\} \tag{D20}$$

$$(V_{\mathrm{TPE}}^{1^{+-}})_{24} = (V_{\mathrm{TPE}}^{1^{+-}})_{42} = \frac{9}{4}R_{x^2}(p',p) - \frac{27}{4}R_x(p',p) + \frac{9}{4}R_{n'}(p',p) + \frac{9}{4}R_n(p',p) - \frac{3}{2}R_2(p',p) \tag{D21}$$

$$(V_{\mathrm{TPE}}^{1^{+-}})_{33} = \bar{S}_0 - \frac{g^4}{8}\left\{-2(p^2+p'^2)\mathcal{R} + 2(p^2+p'^2) - 4(p^2+p'^2)\ln\left(\frac{m_\pi}{\mu}\right) - 4R_2(p',p)\right\} \tag{D22}$$

$$(V^{1^+-}_{\rm TPE})_{34} = 2p'^2\left[2\mathcal{R} - 2 + 4\ln\left(\frac{m_\pi}{\mu}\right)\right] + 4[3R_{n'}(p',p) - R_2(p',p)] \tag{D23}$$

$$(V^{1^+-}_{\rm TPE})_{43} = 2p^2\left[2\mathcal{R} - 2 + 4\ln\left(\frac{m_\pi}{\mu}\right)\right] + 4[3R_{n}(p',p) - R_2(p',p)] \tag{D24}$$

$$(V^{1^+-}_{\rm TPE})_{44} = -\bar{S}_2 + \frac{g^4}{16}\left\{\frac{15}{2}R_2(p',p) - \frac{45}{2}R_{x^2}(p',p) + \frac{21}{2}\left(2R_n(p',p) + 2R_{n'}(p',p) - \frac{8}{3}R_2(p',p) - 6R_x(p',p) + 6R_{x^2}(p',p)\right)\right\} \tag{D25}$$

3. $\mathbf{J^{PC} = 2^{++}}$

$$V^{2^{++},I}_{\rm CT} = \begin{pmatrix} 0 & 0 & -\sqrt{\frac{3}{5}}\mathcal{D}^I_{SD}p^2 & 0 & 0 & 0 \\ 0 & 0 & -\frac{3}{\sqrt{5}}\mathcal{D}^I_{SD}p^2 & 0 & 0 & 0 \\ -\sqrt{\frac{3}{5}}\mathcal{D}^I_{SD}p'^2 & -\frac{3}{\sqrt{5}}\mathcal{D}^I_{SD}p'^2 & \mathcal{C}^I_d + \mathcal{C}^I_f + (\mathcal{D}^I_d + \mathcal{D}^I_f)(p^2 + p'^2) & -\frac{1}{\sqrt{5}}\mathcal{D}^I_{SD}p'^2 & \sqrt{\frac{7}{5}}\mathcal{D}^I_{SD}p'^2 & 0 \\ 0 & 0 & -\frac{1}{\sqrt{5}}\mathcal{D}^I_{SD}p^2 & 0 & 0 & 0 \\ 0 & 0 & \sqrt{\frac{7}{5}}\mathcal{D}^I_{SD}p^2 & 0 & 0 & 0 \\ 0 & 0 & 0 & 0 & 0 & 0 \end{pmatrix} \tag{D26}$$

$$V^{2^{++}}_{\rm OPE} = -\frac{g^2}{4f_\pi^2}(\tau_1\cdot\tau_2) \times \begin{pmatrix} 0 & 0 & -\frac{1}{\sqrt{30}}(3Q_{n'} - Q_2) & \frac{1}{\sqrt{12}}(3Q_{x^2} - Q_2) & -\frac{1}{\sqrt{21}}K_{15} & -\frac{3}{\sqrt{560}}K_{16} \\ 0 & 0 & \frac{1}{\sqrt{20}}(3Q_{n'} - Q_2) & 0 & \frac{1}{\sqrt{504}}K_{25} & -\frac{1}{\sqrt{1400}}K_{26} \\ -\frac{1}{\sqrt{30}}(3Q_n - Q_2) & \frac{1}{\sqrt{20}}(3Q_n - Q_2) & -\frac{1}{12}Q_2 & \frac{1}{\sqrt{90}}(3Q_n - Q_2) & -\sqrt{\frac{7}{90}}(3Q_n - Q_2) & 0 \\ \frac{1}{\sqrt{12}}(3Q_{x^2} - Q_2) & 0 & \frac{1}{\sqrt{90}}(3Q_{n'} - Q_2) & \frac{1}{6}(3Q_{x^2} - Q_2) & \frac{1}{\sqrt{63}}K_{45} & \frac{1}{8\sqrt{35}}K_{46} \\ -\frac{1}{\sqrt{21}}K_{51} & \frac{1}{\sqrt{504}}K_{52} & -\sqrt{\frac{7}{90}}(3Q_{n'} - Q_2) & \frac{1}{\sqrt{63}}K_{54} & \frac{3}{14}K_{55} & -\frac{1}{56\sqrt{5}}K_{56} \\ -\frac{3}{\sqrt{560}}K_{61} & -\frac{1}{\sqrt{1400}}K_{62} & 0 & \frac{1}{8\sqrt{35}}K_{64} & -\frac{1}{56\sqrt{5}}K_{65} & \frac{1}{28}K_{66} \end{pmatrix} \tag{D27}$$

where,

$$K_{51} = K_{15} = 3Q_{x^2} - 9Q_x + 3Q_x + 3Q_{n'} - 2Q_2 \tag{D28}$$

$$K_{61} = 35Q_{n'x^2} - Q_{x^2} + 20Q_x - 5Q_{n'} + 2Q_n + Q_2 \tag{D29}$$

$$K_{16} = 35Q_{nx^2} - Q_{x^2} + 20Q_x - 5Q_n + 2Q_{n'} + Q_2 \tag{D30}$$

$$K_{52} = K_{25} = 18Q_{x^2} - 18Q_x + 6Q_{n'} + 6Q_n + 8Q_2 \tag{D31}$$

$$K_{62} = 35Q_{n'x^2} - 5Q_{x^2} - 20Q_x - 5Q_{n'} + 2Q_n + Q_2 \tag{D32}$$

$$K_{26} = 35Q_{nx^2} - 5Q_{x^2} - 20Q_x - 5Q_n + 2Q_{n'} + Q_2 \tag{D33}$$

$$K_{54} = K_{45} = 3Q_{x^2} - Q_x + 3Q_{n'} + 3Q_n - 2Q_2 \tag{D34}$$

$$K_{64} = 35Q_{n'x^2} - 35Q_{x^2} - 140Q_x - 5Q_{n'} + 2Q_n + Q_2 \tag{D35}$$

$$K_{46} = 35Q_{nx^2} - 35Q_{x^2} - 140Q_x - 5Q_n + 2Q_{n'} + Q_2 \tag{D36}$$

$$K_{55} = -8Q_{x^2} + 11Q_x - 6(Q_{n'} + Q_n) + 7Q_2 \tag{D37}$$

$$K_{65} = 35Q_{n'x^2} - 5Q_{x^2} + 20Q_x - 5Q_{n'} + 2Q_n + Q_2 \tag{D38}$$

$$K_{56} = 35Q_{nx^2} - 5Q_{x^2} + 20Q_x - 5Q_n + 2Q_{n'} + Q_2 \tag{D39}$$

$$K_{66} = 245Q_{x^3} - 105(Q_{n'x^2} + Q_{nx^2}) + 15Q_{x^2} + 15(Q_{n'} + Q_n) + 5Q_x - 3Q_2 \tag{D40}$$

$$V^{2^{++}}_{\mathrm{TPE}} = \frac{1}{16\pi^2 f_\pi^4} \times \begin{pmatrix} (V^{2^{++}}_{\mathrm{TPE}})_{11} & 0 & \frac{3\sqrt{3}}{8\sqrt{10}} g^4 (V^{2^{++}}_{\mathrm{TPE}})_{13} & \frac{\sqrt{3}}{8} g^4 (V^{2^{++}}_{\mathrm{TPE}})_{14} & \frac{3\sqrt{3}}{4\sqrt{7}} g^4 (V^{2^{++}}_{\mathrm{TPE}})_{15} & \frac{1}{32\sqrt{105}} g^4 (V^{2^{++}}_{\mathrm{TPE}})_{16} \\ 0 & 0 & \frac{9}{8\sqrt{10}} g^4 (V^{2^{++}}_{\mathrm{TPE}})_{23} & 0 & \frac{-9}{8\sqrt{14}} g^4 (V^{2^{++}}_{\mathrm{TPE}})_{25} & \frac{-3}{8\sqrt{70}} g^4 (V^{2^{++}}_{\mathrm{TPE}})_{26} \\ \frac{3\sqrt{3}}{8\sqrt{10}} g^4 (V^{2^{++}}_{\mathrm{TPE}})_{31} & \frac{9}{8\sqrt{10}} g^4 (V^{2^{++}}_{\mathrm{TPE}})_{32} & (V^{2^{++}}_{\mathrm{TPE}})_{33} & \frac{-1}{16\sqrt{10}} g^4 (V^{2^{++}}_{\mathrm{TPE}})_{34} & \frac{\sqrt{7}}{16\sqrt{10}} g^4 (V^{2^{++}}_{\mathrm{TPE}})_{35} & 0 \\ \frac{\sqrt{3}}{8} g^4 (V^{2^{++}}_{\mathrm{TPE}})_{41} & 0 & \frac{-1}{16\sqrt{10}} g^4 (V^{2^{++}}_{\mathrm{TPE}})_{43} & (V^{2^{++}}_{\mathrm{TPE}})_{44} & \frac{1}{16\sqrt{7}} g^4 (V^{2^{++}}_{\mathrm{TPE}})_{45} & \frac{-3}{16\sqrt{35}} g^4 (V^{2^{++}}_{\mathrm{TPE}})_{46} \\ \frac{3\sqrt{3}}{4\sqrt{7}} g^4 (V^{2^{++}}_{\mathrm{TPE}})_{51} & \frac{-9}{8\sqrt{14}} g^4 (V^{2^{++}}_{\mathrm{TPE}})_{52} & \frac{\sqrt{7}}{16\sqrt{10}} g^4 (V^{2^{++}}_{\mathrm{TPE}})_{53} & \frac{1}{16\sqrt{7}} g^4 (V^{2^{++}}_{\mathrm{TPE}})_{54} & (V^{2^{++}}_{\mathrm{TPE}})_{55} & \frac{3}{224\sqrt{5}} g^4 (V^{2^{++}}_{\mathrm{TPE}})_{56} \\ \frac{1}{32\sqrt{105}} g^4 (V^{2^{++}}_{\mathrm{TPE}})_{61} & \frac{-3}{8\sqrt{70}} g^4 (V^{2^{++}}_{\mathrm{TPE}})_{62} & 0 & \frac{-3}{16\sqrt{35}} g^4 (V^{2^{++}}_{\mathrm{TPE}})_{64} & \frac{3}{224\sqrt{5}} g^4 (V^{2^{++}}_{\mathrm{TPE}})_{65} & (V^{2^{++}}_{\mathrm{TPE}})_{66} \end{pmatrix} \tag{D41}$$

where,

$$(V^{2^{++}}_{\mathrm{TPE}})_{11} = \bar{S}_2(p', p) \tag{D42}$$

$$(V^{2^{++}}_{\mathrm{TPE}})_{13} = (V^{2^{++}}_{\mathrm{TPE}})_{23} = \frac{2}{3} p^2 \left[-\mathcal{R} + 1 - 2\ln\left(\frac{m_\pi}{\mu}\right) \right] + \frac{2}{3} R_2(p', p) - 2R_n(p', p) \tag{D43}$$

$$(V^{2^{++}}_{\mathrm{TPE}})_{14} = (V^{2^{++}}_{\mathrm{TPE}})_{41} = 3R_{x^2}(p', p) - 9R_{2x}(p', p) + 3R_0(p', p) - R_2(p', p) \tag{D44}$$

$$(V^{2^{++}}_{\mathrm{TPE}})_{15} = (V^{2^{++}}_{\mathrm{TPE}})_{25} = (V^{2^{++}}_{\mathrm{TPE}})_{51} = (V^{2^{++}}_{\mathrm{TPE}})_{52} = \frac{2}{3} R_2(p', p) + 3R_x(p', p) - R_n(p', p) - R_{n'}(p', p) - R_{x^2}(p', p) \tag{D45}$$

$$(V^{2^{++}}_{\mathrm{TPE}})_{16} = 63R_{n'x^2}(p', p) - 90R_{x^2}(p', p) - 360R_x(p', p) - 90R_{n'}(p', p) + 36R_n(p', p) + 18R_2(p', p) \tag{D46}$$

$$(V^{2^{++}}_{\mathrm{TPE}})_{26} = 35R_{n'x^2}(p', p) - 5R_{x^2}(p', p) - 2R_x(p', p) - 5R_{n'}(p', p) + 2R_n(p', p) + R_2(p', p) \tag{D47}$$

$$(V^{2^{++}}_{\mathrm{TPE}})_{31} = (V^{2^{++}}_{\mathrm{TPE}})_{32} = \frac{2}{3} p'^2 \left[-\mathcal{R} + 1 - 2\ln\left(\frac{m_\pi}{\mu}\right) \right] + \frac{2}{3} R_2(p', p) - 2R_{n'}(p', p) \tag{D48}$$

$$(V^{2^{++}}_{\mathrm{TPE}})_{33} = \bar{S}_0 + \frac{g^4}{8} \left\{ -2(p^2 + p'^2)\mathcal{R} + 2(p^2 + p'^2) - 4(p^2 + p'^2)\ln\left(\frac{m_\pi}{\mu}\right) - 4R_2(p', p) \right\} \tag{D49}$$

$$(V^{2^{++}}_{\mathrm{TPE}})_{34} = (V^{2^{++}}_{\mathrm{TPE}})_{35} = 2p'^2 \left[2\mathcal{R} - 2 + 4\ln\left(\frac{m_\pi}{\mu}\right) \right] + 4[3R_{n'}(p', p) - R_2(p', p)] \tag{D50}$$

$$(V^{2^{++}}_{\mathrm{TPE}})_{43} = (V^{2^{++}}_{\mathrm{TPE}})_{53} = 2p^2 \left[2\mathcal{R} - 2 + 4\ln\left(\frac{m_\pi}{\mu}\right) \right] + 4[3R_n(p', p) - R_2(p', p)] \tag{D51}$$

$$(V^{2^{++}}_{\mathrm{TPE}})_{44} = \bar{S}_2 + \frac{g^4}{8} \left\{ \frac{45}{2} R_{x^2}(p', p) - \frac{15}{2} R_2(p', p) + \frac{7}{2} R_0(p', p) - \frac{21}{2} R_{2x}(p', p) \right\} \tag{D52}$$

$$(V_{\mathrm{TPE}}^{2^{++}})_{45} = (V_{\mathrm{TPE}}^{2^{++}})_{54} = -\frac{7}{2}[3R_n(p',p) + 3R_{n'}(p',p) - 9R_x(p',p) + 3R_{x^2}(p',p) - 2R_2(p',p)] \tag{D53}$$

$$(V_{\mathrm{TPE}}^{2^{++}})_{46} = (V_{\mathrm{TPE}}^{2^{++}})_{56} = -\frac{7}{2}[35R_{n'x^2}(p',p) - 5R_{n'}(p',p) - 20R_x(p',p) + R_2(p',p) + 2R_n(p',p) - 5R_{x^2}(p',p)] \tag{D54}$$

$$(V_{\mathrm{TPE}}^{2^{++}})_{55} = \bar{S}_2 + \frac{g^4}{16}\left\{\frac{15}{2}R_2(p',p) - \frac{45}{2}R_{x^2}(p',p) - \frac{1}{4}(-9R_n(p',p) - 9R_{n'}(p',p) - 51R_{x^2}(p',p) + 27R_x(p',p) + 20R_2(p',p))\right\} \tag{D55}$$

$$(V_{\mathrm{TPE}}^{2^{++}})_{61} = 63R_{nx^2}(p',p) - 90R_{x^2}(p',p) - 360R_x(p',p) - 90R_n(p',p) + 36R_{n'}(p',p) + 18R_2(p',p) \tag{D56}$$

$$(V_{\mathrm{TPE}}^{2^{++}})_{62} = 35R_{nx^2}(p',p) - 5R_{x^2}(p',p) - 2R_x(p',p) - 5R_n(p',p) + 2R_{n'}(p',p) + R_2(p',p) \tag{D57}$$

$$(V_{\mathrm{TPE}}^{2^{++}})_{64} = (V_{\mathrm{TPE}}^{2^{++}})_{65} = -\frac{7}{2}[35R_{nx^2}(p',p) - 5R_n(p',p) - 20R_x(p',p) + R_2(p',p) + 2R_{n'}(p',p) - 5R_{x^2}(p',p)] \tag{D58}$$

$$(V_{\mathrm{TPE}}^{2^{++}})_{66} = \bar{S}_4 - \frac{15g^4}{32}[35R_{x^4}(p',p) - 30R_{x^2}(p',p) + 3R_2(p',p)] + \frac{3g^4}{112}\left\{-\frac{7}{2}(105R_{n'x^2}(p',p) + 105R_{nx^2}(p',p) - 15R_{n'}(p',p) - 15R_n(p',p) + 45R_x(p',p) + 3R_2(p',p) - 15R_{x^2}(p',p) - 245R_{nn'x^3}(p',p))\right\} \tag{D59}$$

and

$$\bar{S}_4 = \int_{-1}^{1}\frac{dx}{2}\frac{(35x^4 - 30x^2 + 3)}{8}(\boldsymbol{\tau_1}\cdot\boldsymbol{\tau_2})\boldsymbol{q}^2\left\{\mathcal{R}\left[\frac{23}{48}g^4 + \frac{1}{24}\right] + \left(\frac{5}{144}g^4 - \frac{5}{72}\right) + \ln\left(\frac{m_\pi}{\mu}\right)\left(\frac{23}{24}g^4 + \frac{1}{12}\right) + L(q)\left(\frac{23}{24}g^4 + \frac{1}{12}\right)\right\} \tag{D60}$$

All the Q and R functions mentioned above are functions of p and p' [as in $Q(p',p)$], but for simplicity reasons the (p',p) was avoided.

APPENDIX E: CALCULATION OF INTEGRALS OF PARTIAL WAVE DECOMPOSITION

The calculations of integrals from partial wave decomposition are shown here. Specifically, we present the integration of Q, R, S, and T terms encountered in the partial wave decomposition here. The following notation is used below: $|\boldsymbol{p}'| = p'$, $|\boldsymbol{p}| = p$,$|\boldsymbol{q}| = q$, $\mathbf{n} = \boldsymbol{p}/p$, $\mathbf{n}' = \boldsymbol{p}'/p'$. In addition, $\boldsymbol{q}^2 = p'^2 + p^2 - 2p'px$ and $\boldsymbol{n}'\cdot\boldsymbol{n}$ and

$$\boldsymbol{n}\cdot\boldsymbol{q} = p'x - p = \frac{p'^2 - p^2 - q^2}{2p} \tag{E1}$$

$$\boldsymbol{n}'\cdot\boldsymbol{q} = p' - px = \frac{p'^2 - p^2 + q^2}{2p'} \tag{E2}$$

1. Q-integrals

$$Q_2(p',p) = \int_{-1}^{1}\frac{dx}{2}\frac{\boldsymbol{q}^2}{\boldsymbol{q}^2 + m_\pi^2} = 1 + \mathcal{O}(\chi^4) \tag{E3}$$

$$Q_n(p',p) = \int_{-1}^{1}\frac{dx}{2}\frac{(\boldsymbol{n}\cdot\boldsymbol{q})^2}{\boldsymbol{q}^2 + m_\pi^2} = 1 - \frac{p'^2 + p^2}{4p^2} + \frac{(p'^2 - p^2)^2}{8p'p^3}\operatorname{arctanh}\left(\frac{2p'p}{p'^2 + p^2 + m_\pi^2}\right) + \mathcal{O}(\chi^4) \tag{E4}$$

$$Q_{n'}(p',p)=\int_{-1}^{1}\frac{dx}{2}\frac{(\boldsymbol{n}'\cdot\boldsymbol{q})^2}{\boldsymbol{q}^2+m_\pi^2}=1-\frac{p'^2+p^2}{4p'^2}+\frac{(-p'^2+p^2)^2}{8p'^3p}\operatorname{arctanh}\left(\frac{2p'p}{p'^2+p^2+m_\pi^2}\right)+\mathcal{O}(\chi^4) \tag{E5}$$

$$Q_x(p',p)=\int_{-1}^{1}\frac{dx}{2}\frac{(\boldsymbol{n}'\cdot\boldsymbol{q})(\boldsymbol{n}\cdot\boldsymbol{q})x}{\boldsymbol{q}^2+m_\pi^2}=\frac{5}{12}-\frac{p'^4+p^4}{8p'^2p^2}+\frac{((p'^2-p^2)^2)(p'^2+p^2)}{16p'^3p^3}\operatorname{arctanh}\left(\frac{2p'p}{p'^2+p^2+m_\pi^2}\right)+\mathcal{O}(\chi^4) \tag{E6}$$

$$Q_{x^2}(p',p)=\int_{-1}^{1}\frac{dx}{2}\frac{(\boldsymbol{q}^2x^2)}{\boldsymbol{q}^2+m_\pi^2}=\frac{1}{3}+\mathcal{O}(\chi^4) \tag{E7}$$

$$Q_{nx^2}(p',p)=\int_{-1}^{1}\frac{dx}{2}\frac{(\boldsymbol{n}\cdot\boldsymbol{q})^2x^2}{\boldsymbol{q}^2+m_\pi^2}=\frac{p^4(5p'^2)-p^6-p'^6}{16p'^2p^4}+\frac{-p'^4}{48p^2p'^2}+\frac{(p^4-p'^4)^2}{32p'^3p^5}\operatorname{arctanh}\left(\frac{2p'p}{p'^2+p^2+m_\pi^2}\right)+\mathcal{O}(\chi^4) \tag{E8}$$

$$Q_{n'x^2}(p',p)=\int_{-1}^{1}\frac{dx}{2}\frac{(\boldsymbol{n}'\cdot\boldsymbol{q})^2x^2}{\boldsymbol{q}^2+m_\pi^2}=\frac{p'^4(5p^2)-p'^6-p^6}{16p^2p'^4}+\frac{-p^4}{48p'^2p^2}+\frac{(p'^4-p^4)^2}{32p'^5p^3}\operatorname{arctanh}\left(\frac{2p'p}{p'^2+p^2+m_\pi^2}\right)+\mathcal{O}(\chi^4) \tag{E9}$$

$$\begin{aligned}Q_{x^3}(p',p)=\int_{-1}^{1}\frac{dx}{2}\frac{(\boldsymbol{n}'\cdot\boldsymbol{q})(\boldsymbol{n}\cdot\boldsymbol{q})x^3}{\boldsymbol{q}^2+m_\pi^2}&=\frac{-2p'^6-p^4(2p'^2)}{48p'^4p^2}+\frac{59p'^2}{240p'^2}+\frac{-p^8-p'^8}{32p'^4p^4}\\&+\frac{((p'^2-p^2))(p'^2+p^2)^3}{64p'^5p^5}\operatorname{arctanh}\left(\frac{2p'p}{p'^2+p^2+m_\pi^2}\right)+\mathcal{O}(\chi^4)\end{aligned} \tag{E10}$$

2. *R*-integrals

Since $\boldsymbol{q}^2=p'^2+p^2-2p'px$, we can substitute x inside the R-integrals

$$\frac{dx}{2}=-\frac{q}{2p'p}dq \tag{E11}$$

In the following, q is relabeled as ρ to avoid ambiguity between the transferred momentum and the integration variable. The limits of integration are

$$x_b=1\rightarrow\rho_b=p'-p \tag{E12}$$

$$x_a=-1\rightarrow\rho_a=p'+p \tag{E13}$$

The R-integrals are now written as,

$$R_0(p',p)=\int_{-1}^{1}\frac{dx}{2}L(q)=\frac{1}{2p'p}\int_{p'-p}^{p'+p}d\rho\,\rho L(\rho)=-\frac{1}{2}+\frac{1}{4p'p}[\rho^2L(\rho)]_{p'-p}^{p'+p}+\mathcal{O}(\chi^4) \tag{E14}$$

$$R_2(p',p)=\int_{-1}^{1}\frac{dx}{2}\boldsymbol{q}^2L(q)=\frac{1}{2p'p}\int_{p'-p}^{p'+p}d\rho\,\rho^3L(\rho)=\frac{-1}{8p'p}\left[\frac{\rho^4}{4}-\rho^4L(\rho)\right]_{p'-p}^{p'+p}+\mathcal{O}(\chi^4) \tag{E15}$$

$$R_4(p',p)=\int_{-1}^{1}\frac{dx}{2}\boldsymbol{q}^4L(q)=\frac{1}{12p'p}\left[-\frac{\rho^6}{6}+\rho^6L(\rho)\right]_{p'-p}^{p'+p}+\mathcal{O}(\chi^4) \tag{E16}$$

$$R_6(p',p)=\int_{-1}^{1}\frac{dx}{2}\boldsymbol{q}^6L(q)=-\frac{1}{16p'p}\left[\frac{\rho^8}{8}-\rho^8L(\rho)\right]_{p'-p}^{p'+p}+\mathcal{O}(\chi^4) \tag{E17}$$

$$R_8(p',p)=\int_{-1}^{1}\frac{dx}{2}\boldsymbol{q}^8L(q)=\frac{1}{8p'p}\left[\frac{-\rho^{10}}{25}+\frac{2\rho^{10}}{5}L(\rho)\right]_{p'-p}^{p'+p}+\mathcal{O}(\chi^4) \tag{E18}$$

$$R_{10}(p',p)=\int_{-1}^{1}\frac{dx}{2}\boldsymbol{q}^{10}L(q)=\frac{1}{2p'p}\left[\frac{-\rho^{12}}{144}+\frac{\rho^{12}}{12}L(\rho)\right]_{p'-p}^{p'+p}+\mathcal{O}(\chi^4) \tag{E19}$$

$$\begin{aligned}R_{n}(p',p)&=\int_{-1}^{1}\frac{dx}{2}(\boldsymbol{n}\cdot\boldsymbol{q})^2L(q)=\frac{1}{8p'p^3}\int_{p'-p}^{p'+p}d\rho(\rho^4-2\rho^2(p'^2-p^2)+(p'^2-p^2)^2)\rho\cdot L(\rho)\\&=\frac{1}{4p^2}(R_4(p',p)-2(p'^2-p^2)R_2(p',p)+(p'^2-p^2)^2R_0(p',p))+\mathcal{O}(\chi^4)\end{aligned} \tag{E20}$$

$$R_{n'}(p',p)=\int_{-1}^{1}\frac{dx}{2}(\boldsymbol{n}'\cdot\boldsymbol{q})^2L(q)=\frac{1}{4p'^2}(R_4(p',p)+2(p'^2-p^2)R_2(p',p)+(p'^2-p^2)^2R_0(p',p))+\mathcal{O}(\chi^4) \tag{E21}$$

$$\begin{aligned}R_{x}(p',p)=\int_{-1}^{1}\frac{dx}{2}(\boldsymbol{n}'\cdot\boldsymbol{q})(\boldsymbol{n}\cdot\boldsymbol{q})xL(q)&=\frac{1}{8p'^2p^2}(R_6(p',p)-(p'^2+p^2)R_4(p',p)-(p'^2-p^2)^2R_2(p',p)\\&+(p'^2-p^2)^2(p'^2+p^2)R_0(p',p))+\mathcal{O}(\chi^4)\end{aligned} \tag{E22}$$

$$R_{x^2}(p',p)=\int_{-1}^{1}\frac{dx}{2}\boldsymbol{q}^2x^2L(q)=\frac{1}{4p'^2p^2}(R_6(p',p)-2(p'^2+p^2)R_4(p',p)+(p'^2+p^2)^2R_2(p',p))+\mathcal{O}(\chi^4) \tag{E23}$$

$$R_{2x}(p',p)=\int_{-1}^{1}\frac{dx}{2}x^2L(q)=\frac{1}{4p'^2p^2}(R_4(p',p)-2(p'^2+p^2)R_2(p',p)+(p'^2+p^2)^2R_0(p',p))+\mathcal{O}(\chi^4) \tag{E24}$$

$$\begin{aligned}R_{x^4}(p',p)=\int_{-1}^{1}\frac{dx}{2}x^4\boldsymbol{q}^2L(q)&=\frac{1}{16p'^4p^4}(R_{10}(p',p)-4(p'^2+p^2)R_8(p',p)+6(p'^2+p^2)R_6(p',p)\\&-4(p'^2+p^2)^3R_4(p',p)+(p'^2+p^2)^4R_2(p',p))+\mathcal{O}(\chi^4)\end{aligned} \tag{E25}$$

$$\begin{aligned}R_{nx^2}(p',p)=\int_{-1}^{1}\frac{dx}{2}(\boldsymbol{n}\cdot\boldsymbol{q})x^2L(q)&=\frac{1}{16p'^2p^4}(R_8(p',p)-4p'^2R_6(p',p)+(6p'^4-2p^4)R_4(p',p)\\&+4p'^2(p'^4-p^4)R_2(p',p)+(p'^4-p^4)^2R_0(p',p))+\mathcal{O}(\chi^4)\end{aligned} \tag{E26}$$

$$\begin{aligned}R_{n'x^2}(p',p)=\int_{-1}^{1}\frac{dx}{2}(\boldsymbol{n}'\cdot\boldsymbol{q})x^2L(q)&=\frac{1}{16p'^2p^4}(R_8(p',p)-4p^2R_6(p',p)+(6p^4-2p'^4)R_4(p',p)\\&+4p^2(p^4-p'^4)R_2(p',p)+(p^4-p'^4)^2R_0(p',p))+\mathcal{O}(\chi^4)\end{aligned} \tag{E27}$$

$$\begin{aligned}R_{nn'x^3}(p',p)=\int_{-1}^{1}\frac{dx}{2}(\boldsymbol{n}'\cdot\boldsymbol{q})(\boldsymbol{n}\cdot\boldsymbol{q})x^3L(q)&=\frac{1}{16p'^2p^4}(R_{10}(p',p)-3(p'^2+p^2)R_8(p',p)\\&+2(p^4+4p'^2p^2+p'^4)R_6(p',p)+2(p^6-3p'^2p^4-3p'^4p^2+p'^6)R_4(p',p)-3(p^4-p'^4)^2R_2(p',p)\\&+(p^2-p'^2)^2(p^2+p'^2)^4R_0(p',p))+\mathcal{O}(\chi^4)\end{aligned} \tag{E28}$$

$L(\rho)$ is given by,

$$L(\rho)=\frac{\sqrt{4m_\pi^2+\rho^2}}{\rho}\ln\left(\frac{\sqrt{4m_\pi^2+\rho^2}+\rho}{2m_\pi}\right) \tag{E29}$$

3. $\bar{S}$-integrals and S-integrals

The $\bar{S}$-integrals can be written in general as,

$$\bar{S}_k(p',p)=\int_{-1}^{1}\frac{dx}{2}P_k(x)(\boldsymbol{\tau_1}\cdot\boldsymbol{\tau_2})\boldsymbol{q}^2\left\{\mathcal{R}\left[\frac{23}{48}g^4+\frac{1}{24}\right]+\left(\frac{5}{144}g^4-\frac{5}{72}\right)+\ln\left(\frac{m_\pi}{\mu}\right)\left(\frac{23}{24}g^4+\frac{1}{12}\right)+L(q)\left(\frac{23}{24}g^4+\frac{1}{12}\right)\right\} \tag{E30}$$

where $P_k(x)$ denotes the kth Legendre polynomial.

$$\bar{S}_0(p',p) = (\boldsymbol{\tau_1}\cdot\boldsymbol{\tau_2})\Big\{\mathcal{R}(p'^2+p^2)\left(\frac{23}{24}g^4+\frac{1}{24}\right)+(p'^2+p^2)\left(\frac{5}{144}g^4-\frac{5}{72}\right)+(p'^2+p^2)\left(\frac{23}{24}g^4+\frac{1}{12}\right)\ln\left(\frac{m_\pi}{\mu}\right)$$
$$+R_2(p',p)\left(\frac{23}{24}g^4+\frac{1}{12}\right)\Big\}. \tag{E31}$$

In the case of $\bar{S}_2(p',p)$ and $\bar{S}_4(p',p)$, with the exception of $L(q)$ terms, every other term vanishes after the x-integration.

$$\bar{S}_2(p',p) = (\boldsymbol{\tau_1}\cdot\boldsymbol{\tau_2})\int_{-1}^{1}\frac{dx}{2}\left(\frac{3x^2-1}{2}\right)L(q)\boldsymbol{q}^2\left(\frac{23}{24}g^4+\frac{1}{12}\right)$$
$$=\frac{(\boldsymbol{\tau_1}\cdot\boldsymbol{\tau_2})}{8p'^2p^2}\left\{(3R_6-6(p'^2+p^2)R_4+(3(p'^2+p^2)^2-4p'^2p^2)R_2)\left(\frac{23}{24}g^4+\frac{1}{12}\right)\right\} \tag{E32}$$

$$\bar{S}_4(p',p) = (\boldsymbol{\tau_1}\cdot\boldsymbol{\tau_2})\int_{-1}^{1}\frac{dx}{2}\left(\frac{35x^4-30x^2+3}{8}\right)L(q)\boldsymbol{q}^2\left(\frac{23}{24}g^4+\frac{1}{12}\right)$$
$$=\frac{(\boldsymbol{\tau_1}\cdot\boldsymbol{\tau_2})}{128p'^4p^4}\left\{\Big[(35p^8+35p'^8+20p^6p'^2+18p^4p'^4+20p^2p'^6)R_2+(210p^4+300p^2p'^2+210p'^4)R_6\right.$$
$$\left.-(140p^2+140p'^2)R_8-(140p^6+180p^4p'^2+180p^2p'^4+140p'^6)R_4+35R_{10}\Big]\left(\frac{23}{24}g^4+\frac{1}{12}\right)\right\}. \tag{E33}$$

The S-integrals are given by,

$$S_k(p',p) = \int_{-1}^{1}\frac{dx}{2}P_k(x)(\boldsymbol{\tau_1}\cdot\boldsymbol{\tau_2})\boldsymbol{q}^2\left\{\mathcal{R}\left[\frac{23}{48}g^4-\frac{5}{24}g^2-\frac{1}{24}\right]+\left(\frac{5}{144}g^4+\frac{13}{72}g^2+\frac{5}{72}\right)\right.$$
$$\left.+\ln\left(\frac{m_\pi}{\mu}\right)\left(\frac{23}{24}g^4-\frac{5}{12}g^2-\frac{1}{12}\right)+L(q)\left(\frac{23}{24}g^4-\frac{5}{12}g^2-\frac{1}{12}\right)\right\}. \tag{E34}$$

Starting with $S_0(p',p)$,

$$S_0(p',p) = (\boldsymbol{\tau_1}\cdot\boldsymbol{\tau_2})\Big\{\mathcal{R}(p'^2+p^2)\left(\frac{23}{24}g^4-\frac{5}{24}g^2-\frac{1}{24}\right)+(p'^2+p^2)\left(\frac{5}{144}g^4+\frac{13}{72}g^2+\frac{5}{72}\right)$$
$$+(p'^2+p^2)\left(\frac{23}{24}g^4-\frac{5}{12}g^2-\frac{1}{12}\right)\ln\left(\frac{m_\pi}{\mu}\right)+R_2\left(\frac{23}{24}g^4-\frac{5}{12}g^2-\frac{1}{12}\right)\Big\} \tag{E35}$$

Similar to the earlier case [$\bar{S}_2(p',p)$, $\bar{S}_4(p',p)$], only the $L(q)$ terms contribute in $S_2(p',p)$ and $S_4(p',p)$.

$$S_2(p',p) = (\tau_1\cdot\tau_2)\int_{-1}^{1}\frac{dx}{2}\left(\frac{3x^2-1}{2}\right)L(q)\boldsymbol{q}^2\left(\frac{23}{24}g^4-\frac{5}{12}g^2-\frac{1}{12}\right)$$
$$=\frac{(\boldsymbol{\tau_1}\cdot\boldsymbol{\tau_2})}{8p'^2p^2}\left\{(3R_6-6(p'^2+p^2)R_4+(3(p'^2+p^2)^2-4p'^2p^2)R_2)\left(\frac{23}{24}g^4-\frac{5}{12}g^2-\frac{1}{12}\right)\right\} \tag{E36}$$

$$S_4(p',p) = (\boldsymbol{\tau_1}\cdot\boldsymbol{\tau_2})\int_{-1}^{1}\frac{dx}{2}\left(\frac{35x^4-30x^2+3}{8}\right)L\Big(q)\boldsymbol{q}^2\left(\frac{23}{24}g^4-\frac{5}{12}g^2-\frac{1}{12}\right)$$
$$=\frac{(\boldsymbol{\tau_1}\cdot\boldsymbol{\tau_2})}{128p'^4p^4}\left\{\Big[(35p^8+35p'^8+20p^6p'^2+18p^4p'^4+20p^2p'^6)R_2+(210p^4+300p^2p'^2+210p'^4)R_6\right.$$
$$\left.-(140p^2+140p'^2)R_8-(140p^6+180p^4p'^2+180p^2p'^4+140p'^6)R_4+35R_{10}\Big]\left(\frac{23}{24}g^4-\frac{5}{12}g^2-\frac{1}{12}\right)\right\}. \tag{E37}$$

[1] R. F. Lebed, R. E. Mitchell, and E. S. Swanson, Heavy-quark QCD exotica, Prog. Part. Nucl. Phys. **93**, 143 (2017).

[2] A. Esposito, A. Pilloni, and A. D. Polosa, Multiquark resonances, Phys. Rep. **668**, 1 (2017).

[3] A. Ali, J. S. Lange, and S. Stone, Exotics: Heavy pentaquarks and tetraquarks, Prog. Part. Nucl. Phys. **97**, 123 (2017).

[4] F.-K. Guo, C. Hanhart, U.-G. Meißner, Q. Wang, Q. Zhao, and B.-S. Zou, Hadronic molecules, Rev. Mod. Phys. **90**, 015004 (2018).

[5] S. L. Olsen, T. Skwarnicki, and D. Zieminska, Nonstandard heavy mesons and baryons: Experimental evidence, Rev. Mod. Phys. **90**, 015003 (2018).

[6] Y.-R. Liu, H.-X. Chen, W. Chen, X. Liu, and S.-L. Zhu, Pentaquark and tetraquark states, Prog. Part. Nucl. Phys. **107**, 237 (2019).

[7] N. Brambilla, S. Eidelman, C. Hanhart, A. Nefediev, C.-P. Shen, C. E. Thomas, A. Vairo, and C.-Z. Yuan, The XYZ states: Experimental and theoretical status and perspectives, Phys. Rep. **873**, 1 (2020).

[8] F.-K. Guo, X.-H. Liu, and S. Sakai, Threshold cusps and triangle singularities in hadronic reactions, Prog. Part. Nucl. Phys. **112**, 103757 (2020).

[9] H.-X. Chen, W. Chen, X. Liu, Y.-R. Liu, and S.-L. Zhu, An updated review of the new hadron states, Rep. Prog. Phys. **86**, 026201 (2023).

[10] L. Meng, B. Wang, G.-J. Wang, and S.-L. Zhu, Chiral perturbation theory for heavy hadrons and chiral effective field theory for heavy hadronic molecules, Phys. Rep. **1019**, 1 (2023).

[11] A. Bondar *et al.* (Belle Collaboration), Observation of two charged bottomonium-like resonances in Y(5S) decays, Phys. Rev. Lett. **108**, 122001 (2012).

[12] M. Ablikim *et al.* (BESIII Collaboration), Observation of a charged charmoniumlike structure in $e^+e^- \to \pi^+\pi^- J/\psi$ at $\sqrt{s} = 4.26$ GeV, Phys. Rev. Lett. **110**, 252001 (2013).

[13] Z. Q. Liu *et al.* (Belle Collaboration), Study of $e^+e^- \to \pi^+\pi^- J/\psi$ and observation of a charged charmoniumlike state at Belle, Phys. Rev. Lett. **110**, 252002 (2013); **111**, 019901(E) (2013).

[14] M. Ablikim *et al.* (BESIII Collaboration), Observation of a charged charmoniumlike structure $Z_c(4020)$ and search for the $Z_c(3900)$ in $e^+e^- \to \pi^+\pi^- h_c$, Phys. Rev. Lett. **111**, 242001 (2013).

[15] S. K. Choi *et al.* (Belle Collaboration), Observation of a resonance-like structure in the $pi^{\pm}\psi'$ mass distribution in exclusive $B \to K\pi^{\pm}\psi'$ decays, Phys. Rev. Lett. **100**, 142001 (2008).

[16] R. Mizuk *et al.* (Belle Collaboration), Dalitz analysis of $B \to K\pi^{\pm}\psi'$ decays and the $Z(4430)^+$, Phys. Rev. D **80**, 031104 (2009).

[17] K. Chilikin *et al.* (Belle Collaboration), Experimental constraints on the spin and parity of the $Z(4430)^+$, Phys. Rev. D **88**, 074026 (2013).

[18] R. Aaij *et al.* (LHCb Collaboration), Observation of the resonant character of the $Z(4430)^-$ state, Phys. Rev. Lett. **112**, 222002 (2014).

[19] I. Adachi (Belle Collaboration), Observation of two charged bottomonium-like resonances, in *9th Conference on Flavor Physics and CP Violation* (2011), arXiv:1105.4583.

[20] I. Adachi *et al.* (Belle Collaboration), Study of three-body Y (10860) decays, arXiv:1209.6450.

[21] A. Garmash *et al.* (Belle Collaboration), Observation of $Z_b(10610)$ and $Z_b(10650)$ decaying to B mesons, Phys. Rev. Lett. **116**, 212001 (2016).

[22] A. E. Bondar, A. Garmash, A. I. Milstein, R. Mizuk, and M. B. Voloshin, Heavy quark spin structure in Z_b resonances, Phys. Rev. D **84**, 054010 (2011).

[23] R. M. Albuquerque, J. M. Dias, K. P. Khemchandani, A. Martínez Torres, F. S. Navarra, M. Nielsen, and C. M. Zanetti, QCD sum rules approach to the X, Y and Z states, J. Phys. G **46**, 093002 (2019).

[24] S. Weinberg, Evidence that the deuteron is not an elementary particle, Phys. Rev. **137**, B672 (1965).

[25] D. Morgan, Pole counting and resonance classification, Nucl. Phys. **A543**, 632 (1992).

[26] V. Baru, J. Haidenbauer, C. Hanhart, Y. Kalashnikova, and A. E. Kudryavtsev, Evidence that the $a_0(980)$ and $f_0(980)$ are not elementary particles, Phys. Lett. B **586**, 53 (2004).

[27] I. Matuschek, V. Baru, F.-K. Guo, and C. Hanhart, On the nature of near-threshold bound and virtual states, Eur. Phys. J. A **57**, 101 (2021).

[28] P. C. Bruns, Spatial interpretation of "compositeness" for finite-range potentials, arXiv:1905.09196.

[29] J. A. Oller, New results from a number operator interpretation of the compositeness of bound and resonant states, Ann. Phys. (Amsterdam) **396**, 429 (2018).

[30] X.-W. Kang and J. A. Oller, Different pole structures in line shapes of the $X(3872)$, Eur. Phys. J. C **77**, 399 (2017).

[31] T. Sekihara, Two-body wave functions and compositeness from scattering amplitudes. I. General properties with schematic models, Phys. Rev. C **95**, 025206 (2017).

[32] Y. Kamiya and T. Hyodo, Generalized weak-binding relations of compositeness in effective field theory, Prog. Theor. Exp. Phys. **2017**, 023D02 (2017).

[33] Z.-H. Guo and J. A. Oller, Probabilistic interpretation of compositeness relation for resonances, Phys. Rev. D **93**, 096001 (2016).

[34] T. Sekihara, T. Hyodo, and D. Jido, Comprehensive analysis of the wave function of a hadronic resonance and its compositeness, Prog. Theor. Exp. Phys. **2015**, 063D04 (2015).

[35] F. Aceti and E. Oset, Wave functions of composite hadron states and relationship to couplings of scattering amplitudes for general partial waves, Phys. Rev. D **86**, 014012 (2012).

[36] D. Gamermann, J. Nieves, E. Oset, and E. Ruiz Arriola, Couplings in coupled channels versus wave functions: Application to the X(3872) resonance, Phys. Rev. D **81**, 014029 (2010).

[37] T. Kinugawa and T. Hyodo, Compositeness of near-threshold s-wave resonances, arXiv:2403.12635.

[38] A. A. Filin, A. Romanov, V. Baru, C. Hanhart, Y. S. Kalashnikova, A. E. Kudryavtsev, U.-G. Meißner, and A. V. Nefediev, Comment on "Possibility of deeply bound hadronic molecules from single pion exchange", Phys. Rev. Lett. **105**, 019101 (2010).

[39] Q. Wang, V. Baru, A. A. Filin, C. Hanhart, A. V. Nefediev, and J.-L. Wynen, Line shapes of the $Z_b(10610)$ and

$Z_b(10650)$ in the elastic and inelastic channels revisited, Phys. Rev. D **98**, 074023 (2018).
[40] V. Baru, E. Epelbaum, A. A. Filin, C. Hanhart, A. V. Nefediev, and Q. Wang, Spin partners W_{bJ} from the line shapes of the $Z_b(10610)$ and $Z_b(10650)$, Phys. Rev. D **99**, 094013 (2019).
[41] S. Weinberg, Nuclear forces from chiral Lagrangians, Phys. Lett. B **251**, 288 (1990).
[42] S. R. Beane, P. F. Bedaque, M. J. Savage, and U. van Kolck, Towards a perturbative theory of nuclear forces, Nucl. Phys. **A700**, 377 (2002).
[43] E. Epelbaum, H.-W. Hammer, and U.-G. Meissner, Modern theory of nuclear forces, Rev. Mod. Phys. **81**, 1773 (2009).
[44] V. Baru, E. Epelbaum, A. A. Filin, F.-K. Guo, H.-W. Hammer, C. Hanhart, U.-G. Meißner, and A. V. Nefediev, Remarks on study of X(3872) from effective field theory with pion-exchange interaction, Phys. Rev. D **91**, 034002 (2015).
[45] C. Hanhart, Y. S. Kalashnikova, P. Matuschek, R. V. Mizuk, A. V. Nefediev, and Q. Wang, Practical parametrization for line shapes of near-threshold states, Phys. Rev. Lett. **115**, 202001 (2015).
[46] X.-K. Dong, F.-K. Guo, and B.-S. Zou, Explaining the many threshold structures in the heavy-quark hadron spectrum, Phys. Rev. Lett. **126**, 152001 (2021).
[47] V. Baru, F.-K. Guo, C. Hanhart, and A. Nefediev, How does the X(3872) show up in e^+e^- collisions: Dip versus peak, Phys. Rev. D **109**, L111501 (2024).
[48] V. Baru, X.-K. Dong, M.-L. Du, A. Filin, F.-K. Guo, C. Hanhart, A. Nefediev, J. Nieves, and Q. Wang, Effective range expansion for narrow near-threshold resonances, Phys. Lett. B **833**, 137290 (2022).
[49] V. Baru, C. Hanhart, Y. S. Kalashnikova, A. E. Kudryavtsev, and A. V. Nefediev, Interplay of quark and meson degrees of freedom in a near-threshold resonance, Eur. Phys. J. A **44**, 93 (2010).
[50] V. Baru, E. Epelbaum, A. A. Filin, C. Hanhart, R. V. Mizuk, A. V. Nefediev, and S. Ropertz, Insights into $Z_b(10610)$ and $Z_b(10650)$ from dipion transitions from $\Upsilon(10860)$, Phys. Rev. D **103**, 034016 (2021).
[51] V. Baru, E. Epelbaum, A. A. Filin, C. Hanhart, and A. V. Nefediev, Emergence of heavy quark spin symmetry breaking in heavy quarkonium decays, Phys. Rev. D **107**, 014027 (2023).
[52] V. Baru, E. Epelbaum, A. A. Filin, C. Hanhart, and A. V. Nefediev, Spin partners of the $Z_b(10610)$ and $Z_b(10650)$ revisited, J. High Energy Phys. 06 (2017) 158.
[53] L. Meng, V. Baru, E. Epelbaum, A. A. Filin, and A. M. Gasparyan, Solving the left-hand cut problem in lattice QCD: $T_{cc}(3875)^+$ from finite volume energy levels, Phys. Rev. D **109**, L071506 (2024).
[54] M. Padmanath and S. Prelovsek, Signature of a doubly charm tetraquark pole in DD^* scattering on the lattice, Phys. Rev. Lett. **129**, 032002 (2022).
[55] M.-L. Du, A. Filin, V. Baru, X.-K. Dong, E. Epelbaum, F.-K. Guo, C. Hanhart, A. Nefediev, J. Nieves, and Q. Wang, Role of left-hand cut contributions on pole extractions from lattice data: Case study for Tcc(3875)+, Phys. Rev. Lett. **131**, 131903 (2023).
[56] S. Collins, A. Nefediev, M. Padmanath, and S. Prelovsek, Towards the quark mass dependence of T_{cc}^+ from lattice QCD, Phys. Rev. D **109**, 094509 (2024).
[57] M. Abolnikov, V. Baru, E. Epelbaum, A. A. Filin, C. Hanhart, and L. Meng, Internal structure of the $T_{cc}(3875)^+$ from its light-quark mass dependence, Phys. Lett. B **860**, 139188 (2025).
[58] C. Hanhart, Meson production in nucleon-nucleon collisions close to the threshold, Phys. Rep. **397**, 155 (2004).
[59] V. Baru, C. Hanhart, and F. Myhrer, Effective field theory calculations of $NN \to NN\pi$, Int. J. Mod. Phys. E **23**, 1430004 (2014).
[60] A. A. Filin, V. Baru, E. Epelbaum, H. Krebs, C. Hanhart, and F. Myhrer, Pion production in nucleon-nucleon collisions in chiral effective field theory with $\Delta(1232)$ degrees of freedom, Phys. Rev. C **88**, 064003 (2013).
[61] A. A. Filin, V. Baru, E. Epelbaum, H. Krebs, C. Hanhart, A. E. Kudryavtsev, and F. Myhrer, Pion production in nucleon-nucleon collisions in chiral effective field theory: Next-to-next-to-leading order contributions, Phys. Rev. C **85**, 054001 (2012).
[62] V. Baru, E. Epelbaum, A. A. Filin, C. Hanhart, H. Krebs, and F. Myhrer, Threshold pion production in proton-proton collisions at NNLO in chiral EFT, Eur. Phys. J. A **52**, 146 (2016).
[63] J. M. Dias, F. Aceti, and E. Oset, Study of $B\bar{B}^*$ and $B^*\bar{B}^*$ interactions in $I = 1$ and relationship to the $Z_b(10610)$, $Z_b(10650)$ states, Phys. Rev. D **91**, 076001 (2015).
[64] F. Aceti, M. Bayar, E. Oset, A. Martinez Torres, K. P. Khemchandani, J. M. Dias, F. S. Navarra, and M. Nielsen, Prediction of an $I = 1$ $D\bar{D}^*$ state and relationship to the claimed $Z_c(3900)$, $Z_c(3885)$, Phys. Rev. D **90**, 016003 (2014).
[65] B. Wang, Z.-W. Liu, and X. Liu, $\bar{B}^{(*)}\bar{B}^{(*)}$ interactions in chiral effective field theory, Phys. Rev. D **99**, 036007 (2019).
[66] B. Wang, L. Meng, and S.-L. Zhu, Deciphering the charged heavy quarkoniumlike states in chiral effective field theory, Phys. Rev. D **102**, 114019 (2020).
[67] B. Wang and L. Meng, Revisiting the DD* chiral interactions with the local momentum-space regularization up to the third order and the nature of T_{cc}^+, Phys. Rev. D **107**, 094002 (2023).
[68] H. Xu, B. Wang, Z.-W. Liu, and X. Liu, DD^* potentials in chiral perturbation theory and possible molecular states, Phys. Rev. D **99**, 014027 (2019); **104**, 119903(E) (2021).
[69] T. Mehen and J. W. Powell, Heavy quark symmetry predictions for weakly bound B-meson molecules, Phys. Rev. D **84**, 114013 (2011).
[70] T. Mehen and J. Powell, Line shapes in $\Upsilon(5S) \to B^{(*)}B^{-(*)}\pi$ with Z(10610) and Z(10650) using effective field theory, Phys. Rev. D **88**, 034017 (2013).
[71] R. L. Workman *et al.* (Particle Data Group), Review of particle physics, Prog. Theor. Exp. Phys. **2022**, 083C01 (2022).
[72] F. Bernardoni, J. Bulava, M. Donnellan, and R. Sommer (ALPHA Collaboration), Precision lattice QCD computation of the $B^*B\pi$ coupling, Phys. Lett. B **740**, 278 (2015).

[73] S. Fleming, M. Kusunoki, T. Mehen, and U. van Kolck, Pion interactions in the $X(3872)$, Phys. Rev. D **76**, 034006 (2007).
[74] R. Machleidt and D. R. Entem, Chiral effective field theory and nuclear forces, Phys. Rep. **503**, 1 (2011).
[75] P. Reinert, H. Krebs, and E. Epelbaum, Semilocal momentum-space regularized chiral two-nucleon potentials up to fifth order, Eur. Phys. J. A **54**, 86 (2018).
[76] X.-K. Dong, V. Baru, F.-K. Guo, C. Hanhart, A. Nefediev, and B.-S. Zou, Is the existence of a $J/\psi J/\psi$ bound state plausible?, Sci. Bull. **66**, 2462 (2021).
[77] M.-L. Du, V. Baru, X.-K. Dong, A. Filin, F.-K. Guo, C. Hanhart, A. Nefediev, J. Nieves, and Q. Wang, Coupled-channel approach to T_{cc}^+ including three-body effects, Phys. Rev. D **105**, 014024 (2022).
[78] L. Meng, E. Ortiz-Pacheco, V. Baru, E. Epelbaum, M. Padmanath, and S. Prelovsek, Doubly charm tetraquark channel with isospin 1 from lattice QCD, arXiv:2411.06266.
[79] H.-X. Chen, W. Chen, X. Liu, and S.-L. Zhu, The hidden-charm pentaquark and tetraquark states, Phys. Rep. **639**, 1 (2016).
[80] T. Whyte, D. J. Wilson, and C. E. Thomas, Near-threshold states in coupled $DD^* - D^*D^*$ scattering from lattice QCD, arXiv:2405.15741.
[81] Y. Lyu, S. Aoki, T. Doi, T. Hatsuda, Y. Ikeda, and J. Meng, Doubly charmed tetraquark T_{cc}^+ from lattice QCD near physical point, Phys. Rev. Lett. **131**, 161901 (2023).
[82] S. Weinberg, Effective chiral Lagrangians for nucleon—pion interactions and nuclear forces, Nucl. Phys. **B363**, 3 (1991).
[83] N. Kaiser, R. Brockmann, and W. Weise, Peripheral nucleon-nucleon phase shifts and chiral symmetry, Nucl. Phys. **A625**, 758 (1997).
[84] S. L. Krug and C. Hanhart, The complete next-to-leading order potential of $\mathbf{B}^{(*)}\bar{\mathbf{B}}^{(*)} \to \mathbf{B}^{(*)}\bar{\mathbf{B}}^{(*)}$, Bull. Lebedev Phys. Inst. **47**, 334 (2020).